TECHNISCHE
UNIVERSITÄT
WIEN

ESEA

Institut für Energiesysteme
und Elektrische Antriebe

Volt/var behaviour of low voltage Grid-Link in European grid type

Master Thesis

In partial fulfillment of the requirements for the degree

Diplom-Ingenieur (Dipl.-Ing.)

committed by

Univ.-Prof. Dr. ing. W. Gawlik
Ass.-Prof. Dr. techn. A. Ilo

of the

Technische Universität Wien

Faculty of Electrical Engineering and Information Technology
Institute of Energy Systems and Electrical Drives

by
Daniel-Leon Schultis 01131268
Gerlgasse 16
1030 Vienna
Austria

Vienna, November 2017

Acknowledgement

With this thesis I finish my studies in electrical engineering, so I want to sincerely thank those people who supported me during my studies and my master thesis. Especially, I want to express my thanks to Dr. Albana Ilo, who supported me with advice during writing this thesis and who inspired me to see the European power system from a more holistic point of view. Thanks for the large amount of time you invested to guide me through this broad topic. Furthermore, I want to thank Christian Schirmer for providing the network data I used for the simulations and for his advice on how to understand their components. I also want to thank Professor Wolfgang Gawlik who enabled me to write my thesis about this topic.

Kurzfassung

Der Trend hin zur dezentralen Erzeugung erneuerbarer elektrischer Energie bringt neue Herausforderungen für die Netzbetreiber mit sich, da die fluktuierende Wirkleistungseinspeisung zu Überschreitungen der maximal zulässigen Strom- und Spannungswerte führen kann. Insbesondere die gesetzlich geforderten Spannungsbeschränkungen sind häufig der begrenzende Faktor für die Integration fluktuierender Erzeuger in die Verteilnetze. Um den Spannungsüberhöhungen auch ohne einen Netzausbau entgegen wirken zu können, werden die Stromrichter, über welche Erzeugungsanlagen wie z.B. Photovoltaik an das Verteilnetz angebunden sind, häufig mit lokalen Regelungen wie der $P(U)$-, der $Q(U)$- oder der $cos\varphi(P)$-Regelung ausgestattet. Diese Regelungen beeinflussen den Wirk- bzw. Blindleistungsaustausch der Erzeugungsanlagen mit dem Netz mit dem Ziel der Spannungshaltung. Außerdem könnte bei lokaler Überspannung die Wirkleistungseinspeisung einer Erzeugungsanlage durch einen Überspannungsschutz zur Gänze unterbunden werden. Ein weiteres denkbares, jedoch bisher wenig beachtetes Spannungsregelungskonzept ist es lokal geregelte Blindleistungssenken mit Spannungssollwerten nahe der maximal zulässigen Netzspannung an den Enden der betroffenen Stichleitungen zu betreiben und die Stromrichter der Kunden zu verwenden um deren eigenen Blindleistungsbedarf zu decken. Dieses Konzept wird hier als $L(U)$-Regelung mit Q-autarken Kunden bezeichnet.

In dieser Masterarbeit werden die Einflüsse der genannten Regelungskonzepte auf die betriebliche Performance eines theoretischen Niederspannungsnetzes unter verschiedenen Last/Erzeugungs-Szenarien anhand von Lastflusssimulationen miteinander verglichen. Zur Bewertung der Performance des Netzes werden dabei die Netzverluste, die Auslastung des Transformators, der Blindleistungsaustausch zwischen dem Nieder- und dem Mittelspannungsnetz, die eventuell verbleibenden Spannungsbandverletzungen und die eventuell abgeregelte Wirkleistungseinspeisung herangezogen. Zusätzlich wird bewertet, welche dieser Regelungskonzepte zu einer Diskriminierung einzelner Netzkunden führt, und welche Konzepte einen Datenaustausch zwischen Kunden und Netzbetreiber erfordern um eine *koordinierte* Blindleistungsregelung des Niederspannungsnetzes zu ermöglichen. Außerdem wird die $L(U)$-Regelung mit und ohne Q-autarken Kunden unter verschiedenen realen Netzbedingungen simuliert.

Nach den Ergebnissen der wirkleistungsbasierten Regelungskonzepte spart die teilweise Abregelung der Wirkleistungseinspeisung durch eine $P(U)$-Regelung gegenüber einer vollkommenen Unterbindung der Wirkleistunseinspeisung durch einen Überspannungsschutz Wirkleistung ein und verhindert trotzdem zuverlässig Überschreitungen der Maximalspannung. Nach den Ergebnissen der blindleistungsbasierten Regelungskonzepte schneidet die $cos\varphi(P)$-Regelung bezüglich aller betrachteten Kriterien durchschnittlich am schlechtesten ab, während die $L(U)$-Regelung mit Q-autarken Kunden bezüglich aller betrachteten Kriterien durchschnittlich am besten abschneidet. Die $L(U)$-Regelung mit und ohne Q-autarken Kunden verhindert auch unter realen Netzbedingungen zuverlässig Überschreitungen der oberen Spannungsgrenze und erhöht damit entsprechend stark die Aufnahmekapazität der Niederspannungsnetze für verteilte Energieerzeuger. Weiters hat sich herausgestellt, dass ausschließlich die Regelungskonzepte, welche die Stromrichter der Kunden zur Spannungshaltung verwenden, zu einer Diskriminierung der Kunden führen und einen Datenaustausch zwischen Kunden und Netzbetreiber benötigen um eine koordinierte Blindleistungsregelung des Niederspannungsnetzes zu ermöglichen.

Abstract

The trend towards the decentralised production of renewable electrical energy entails new challenges for the network operators, since the fluctuating active power infeed may lead to exceedances of the maximum permissible current and voltage values. In particular, the legally stipulated voltage limitations are often the limiting factor for the integration of fluctuating producers into distribution networks. To counteract the voltage rise also without grid reinforcements, local $Q(U)$-, $P(U)$- and $cos\varphi(P)$-controls are often implemented into the inverters which couple decentralised producers, like photovoltaic arrays for instance, with the distribution grid. These controls influence the active or reactive power exchange between the producers and the grid in order to improve the grid's voltage profile. Furthermore, the active power injection of a producer could be completely prevented during overvoltage conditions by an overvoltage protection. Another conceivable, but so far barely considered voltage control concept is to operate locally controlled reactive power sinks with voltage set-points close to the maximum permissible voltage limitation at the ends of the affected feeders, and to simultaneously use the customers' inverters to cover their own reactive power demand. This concept is called $L(U)$-control with Q-autarkic customers in this thesis.

Based on load flow simulations, the impacts of the above-mentioned control concepts on the performance of a theoretical low voltage network are analysed under different load/production scenarios and compared with each other. The performance of the low voltage grid is evaluated by means of the network losses, the transformer loading, the reactive power exchange between the low and the medium voltage grid, the possibly remaining voltage limit violations and the possibly curtailed active power. In addition, it is assessed which of these control concepts leads to a discrimination of individual customers and which concepts require a data exchange between the customers and the network operators in order to enable a *coordinated* reactive power control of the low voltage network. Furthermore, the $L(U)$-control with and without Q-autarkic customers is simulated under different real network conditions.

The results of the active power based control concepts show that the partial curtailment of the producers' active power injection by $P(U)$- controls waste less active power than the disconnection of the producers from the grid by their overvoltage protections, while it still reliably prevents upper voltage limit violations. For each of the evaluation criteria, the results of the reactive power based control concepts show that the $cos\varphi(P)$-controls averagely lead to the worst grid performance, while the $L(U)$-controls with Q-autarkic customers averagely lead to the best grid performance. Also under realistic network conditions, the $L(U)$-controls with and without Q-autarkic customers reliably prevent violations of the upper voltage limitation and thus increase the networks' hosting capacities for distributed electricity production. Furthermore it turned out that exclusively those voltage control concepts, which require customer-owned inverters for voltage control, lead to a discrimination of individual customers and requires a data exchange between the customers and the DSO in order to enable a coordinated reactive power control of the low voltage grid.

Contents

1. Introduction

1.1. Background

The European Commission, EC, follows an ambitious energy strategy in order to combat climate change and air pollution, to decrease the European Union's dependency on imported fuels and to keep energy affordable for consumers and businesses also in the long-term. These efforts already led to an increasing capacity of diverse renewable energy sources for electricity, RES-E, connected to the European power system. Figure 1.1 illustrates the renewable electricity production by these RES-E from 2004 to 2015. The
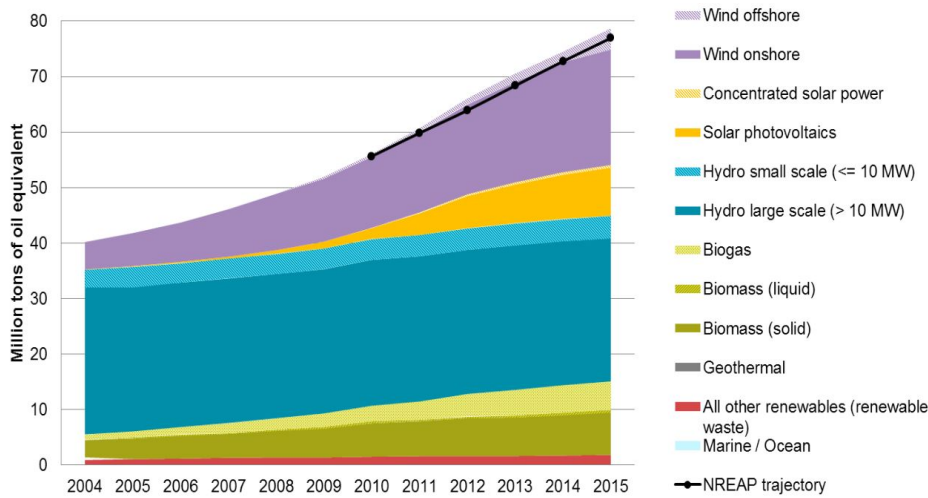
Figure 1.1.: EU-28 renewable electricity production by source [1]

installed capacity of RES-E will likely further increase in order to achieve the EC's 2030 and 2050 targets. In particular, photovoltaic, PV, is one of the most promising technologies to meet the EC's medium- and long-term renewable energy targets [2]. In contrast to conventional power plants, a significant portion of these renewable energy sources is connected to distribution grids [3]. Furthermore, the increasing installed capacity of these distributed generators, DGs, leads to an increasing replacement of large fossil-fueled power plants, which are conventionally employed by transmission system operators, TSOs, for system service provision like "voltage maintenance" for instance [3, 4]. These system services, also called "ancillary services", are required by the TSOs to ensure a safe and reliable grid operation. Hence, the increasing share of distributed generation confronts the distribution system operators, DSOs, and also the TSOs with new challenges and opportunities. More precise, the DSOs will have to manage various operational challenges like aggravated voltage maintenance due to fluctuating DG infeed, malfunction of protection devices due to reverse power flows and equipment overloading during high infeed periods for instance [5] while the TSOs will have to obtain an increasing share of their required system services from other "ancillary service sources" than conventional power plants [3]. A conceivable part of the solution is to integrate the DGs into the grid operation, so that they are able to actively provide system services to the responsible DSOs. These so called "active distribution grids" enable the DSOs to optimise their grids' performances in terms of voltage control and loss minimisation and also to offer system services to the overlaid transmission grid's operator. With this measure, the existing potential for ancillary service provision of distribution grids will be utilised for the (sub)transmission grids, instead of cost-intensively installing and operating other ancillary service sources, like switchable capacitor banks for instance, within the (sub)transmission grids. As shown later, this potential is not only constituted by DGs, but also by consumers and electrical

equipment located within the distribution grid, since their voltage-dependent active and reactive power consumption can theoretically be influenced and thus also be utilised for ancillary service provision by the responsible DSO.

Some of the European TSOs already employ distribution grids for voltage maintenance within their transmission grids. For instance, the Swiss TSO "Swissgrid" implemented a payment structure for a reactive power support (Q-support) of subordinated distribution grids and directly connected bulk buyers. Within this framework, the DSOs and directly connected bulk buyers can choose for each of their connection points to the (sub)transmission grid between being treated as a passive or an active customer. In passive mode, the customer, is it a DSO or a directly connected bulk buyer, is requested to limit his reactive power exchange with the overlaid grid in dependency of his active power exchange[1]. In active mode, the customer is requested to follow a predefined day-ahead voltage schedule he daily receives from Swissgrid. [6]

1.2. Motivation

As already mentioned in the previous section, the increasing amount of distributed electricity production brings along a variety of new challenges to the DSOs. The hosting capacities of their networks, which is defined as "the maximum distributed generation penetration for which the power system still operates satisfactorily" [2], are restricted by voltage limitations (legally stipulated voltage range) and current limitations (rating of the electrical equipment). Previous simulations and projects identified especially the voltage rise [7, 8, 9, 10] but also transformer overloading [8] as the most restrictive limitations for PV grid integration under usual network conditions. However, the DSOs are legally committed to optimise, strengthen and expand their networks according to the state-of-the-art to ensure the acceptance, transmission and distribution of electricity from renewable energy sources, as long as this is economically reasonable for them [11]. The conventional measure to increase the hosting capacity of a distribution network is to cost-intensively reinforce the grid, but since photovoltaic systems reach their peak production just for a few hours per year (see figure 2.10) it is economically inefficient to dimension the grid according to that peak. Instead, smart appliances like demand side management, storage operation, on load tap changing, active power curtailment of DGs and reactive power control strategies can be used to relieve local network bottlenecks and thus to better utilise the existing grid infrastructure. A reliable voltage control strategy is required to ensure the compliance with the EN 50160 voltage limits and to postpone cost-intensive grid reinforcements while integrating more distributed electricity production.

1.3. Objectives

This thesis shall provide a fundamental understanding of the impacts of local active and reactive power controls on a LV-grid's performance in terms of its voltage profile, the active power losses, the equipment loading and the reactive power exchange with the overlaid MV-grid. Additionally to the commonly known $P(U)$-, $Q(U)$- and $cos\varphi(P)$-controls of photovoltaic inverters, another local voltage control concept based on DSO-owned control-coils, called $L(U)$-control in the following, with and without Q-autarkic customers is proposed in this thesis. The objective is to compare the impacts of all these control strategies on the LV-grid's performance based on simulations with a theoretical LV-grid. Thereby also the different behaviour of each control for cable- and overhead line-feeders is investigated. Furthermore, the behaviour of the $L(U)$-control with and without Q-autarkic customers is investigated by simulating real low voltage grids, including two urban, one rural and one industrial LV-grid.

---

[1]Look at figure 2.9 "Limitation of Q-exchange by active power" to better understand this strategy.

1.4. Scope

This thesis focuses on the behaviour of European low voltage grids in presence of P- or Q-controlled distributed generators and $L(U)$-controlled coils. Although European low voltage networks are commonly unbalanced, they are assumed to be balanced and thus only one phase is calculated in the static load flow simulations.

1.5. Thesis Structure

Chapter 2 presents the theoretical background which is required to understand the functionalities of the investigated local active and reactive power controls and their impacts on the performance of the low voltage grid and the overlaid grids. Furthermore, the voltage dependency of loads is discussed and the Grid-Link concept is introduced. Chapter 3 describes the models which are used for the simulations, including the network, load, generator, line and transformer models. Chapter 4 describes the load/production scenarios and the corresponding primary voltages of the distribution transformer which are used for the simulations. Chapter 5.1 describes how the simulation results are summarised to attain a clear overview of the behaviour of the simulated low voltage grid. Chapter 6 describes the simulation results (summarised according to chapter 5.1) of the scenarios (defined in chapter 4) for different active and reactive power control strategies. Chapter 7 concludes the findings of chapter 2 and 6.

2. Theoretical background

Section 2.1 gives an overview of the European power system, i.e. of its general structure and the nowadays established voltage control schemes. Section 2.2 focuses on distribution grids and explains the impacts of power flows on the performance of these grids as well as the possibilities to optimise their performances by manipulating reactive power flows. Section 2.3 explains how the existing potential of customer-owned PV-inverters can be utilised for voltage control within low voltage networks and how DSO-owned reactive power devices can be used for voltage control. More precise, different active power curtailment strategies and reactive power control strategies are introduced and compared with each other. Finally, section 2.4 describes the behaviour of loads, like residential customers for instance, connected to a low voltage grid, i.e. the dependency of their active and reactive power consumption on their local network voltages. Section 2.5 introduces the *LINK*-Solution, based on the *LINK*-Paradigm described in [12], as a possible Smart Grid solution which enables a reliable large-scale integration of distributed and renewable energy resources into the existing grid infrastructure.

2.1. Overview of the European power grid

The European power grid and especially its distribution grids generally differ from American grids in terms of symmetry, balance, cable share, geographical extension, number of distribution transformers and operating frequency, for instance. This thesis focuses on the European grid style.

2.1.1. Structure of the European power grid

The European power grid consists of transmission (including very high voltage level, VHV), subtransmission (including high voltage level, HV) and distribution grids (including medium and low voltage level, MV, LV), connected by transformers to each other, whereby the transmission grids are operated by transmission system operators and the subtransmission and distribution grids are operated by distribution system operators [12]. While the MV/LV-transformers have a fixed tap position, the HV/MV-transformers usually have an on load tap changer [13]. The European transmission grid is separated into several control zones which are horizontally connected to each other and controlled by their individual transmission system operators. It is highly meshed, consists mainly of overhead lines, allows bidirectional power flows and is able to transmit power over long distances with low losses. The transmission grid conventionally forward the power received from large scale power plants to its subordinated subtransmission grids. These subtransmission grids distribute the power received from the overlaid transmission grid to the regionally spread medium voltage grids. In normal operation, they are galvanically isolated from each other, but in contingency cases they can be connected to each other horizontally, either directly or at medium voltage level [14]. The distribution grids, namely the medium and low voltage grids, are generally operated by DSOs and have usually radial topologies. The medium voltage grids forward the power received from the subtransmission grid cost-effectively to the secondary substations and directly connected bulk buyers [14]. Those grids are symmetrical and balanced [13]. The low voltage grids further forward the power received from their overlaid medium voltage grid to the final customers. These grids are symmetrical and unbalanced. Figure 2.1 presents an overview of the European power grid. This figure illustrates the different network levels and the corresponding voltages, the transformers between these network levels, the final customers connected to the low voltage grids and the area of the TSO's and DSO's responsibility.
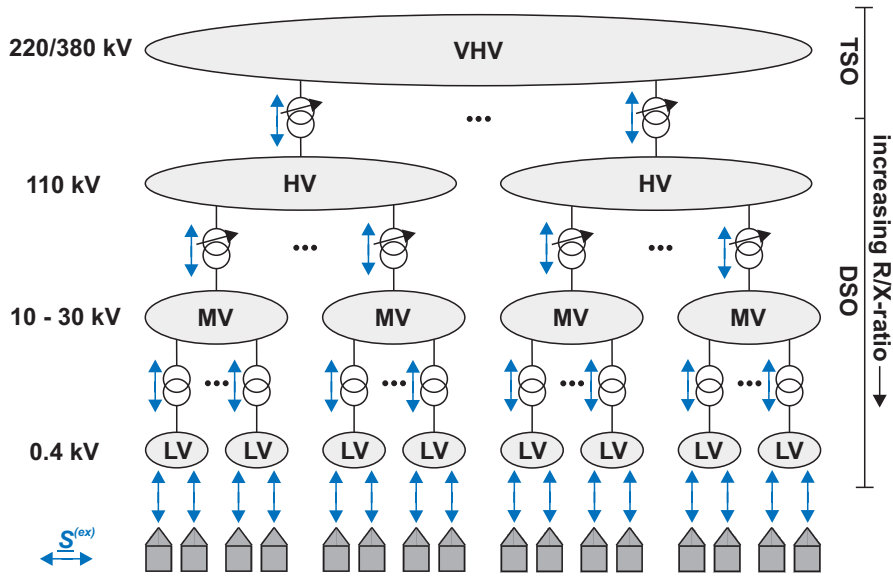
Figure 2.1.: Structure of the European power grid

2.1.2. Voltage control in the European power system

Conventionally, the large-scale power plants connected to the transmission grid supply consumers which are located in the distribution grids, so that active and reactive power flows unidirectionally from the VHV-grid through the distribution grids to the customers. The synchronous generators of these large-scale power plants control their output voltages by manipulating (usually injecting) reactive power via their excitation systems [15]. If the power plants' Q-provision isn't sufficient to maintain acceptable voltages within the corresponding transmission grid, the TSO can cost-intensively install static compensation elements like switchable shunt capacitor-banks to make additional reactive power sources available for voltage control [4]. Furthermore, the TSO can utilise topology measures for voltage maintenance [4]. In distribution grids, the voltage is conventionally controlled by an OLTC at the substation [2, 15]. If required, the DSO can additionally install compensation elements in order to maintain voltages also in remote parts of his distribution grid [15]. In a future smart grid, the potential Q-provision of inverter coupled DGs could also be utilised for voltage control. Table 2.1 contains for each voltage level the typically available possibilities of a network operator, called Q-variables in the following, to influence the Q-balance of his network.

Typical availability	Q-variable
VHV/HV	Q-provision of conventional power plants
VHV/HV/MV	Q-provision of reactive power devices
HV/MV/LV	Q-provision of distributed generators
VHV/HV/MV	Tap position of transformers
VHV/HV	Network topology measures

Table 2.1.: Q-variables of network operators

2.2. Behaviour of distribution networks

This section discusses the impacts of active and reactive power flows on the performance of radial distribution grids. A distribution grid consists of its electrical equipment, i.e. its supplying transformer (HV/MV for medium voltage grids and MV/LV for low voltage grids), its lines (overhead lines or cables) and its reactive power devices (e.g. capacitors or coils). In this thesis, the performance of such a distribution grid is assessed for a certain load/production situation by its voltage profile, the emerging active power losses and the loading of its electrical equipment. This performance is ideal if no active and reactive power flows through the distribution grid, since in this case all node voltages equal to the supplying transformer's secondary open circuit voltage, no active power losses occur and the electrical equipment isn't loaded at all. If the electrical equipment's capacitances are neglected[1], this ideal performance is achieved during an open-circuit operation, i.e. if no loads and producers are connected. But if producing and/or consuming elements (DGs, loads, subordinated grids, ...) are connected, active and reactive power flows through the distribution grid. These power flows impair the distribution grid's performance since they influence the grid's voltage profile, cause active power losses and load the grid's electrical equipment. For certain P- and Q-flows, the extent of these impacts differ in each network level, since these network levels imply different equipment impedances and operating voltages. In general it can be stated, that the higher the operating voltage is and the lower the equipment impedances are, the lower are the impacts of given P- and Q-flows on the grid's performance. Additionally to these impacts, the reactive power exchange with the overlaid grid is discussed in section 2.2.4 since it influences the overlaid grids' performances. Section 2.2.5 discusses the Q-flows which are required to optimise each performance criterion. For simplicity, only single-phase systems are regarded for all derivations in this section and all voltages within these systems are assumed to be in-phase[2].

However, firstly the frequently used variables are introduced to maintain clear and consistent relations. Figure 2.2 shows a single-phase network element with an impedance $\underline{Z}^{(emt)}$, which may represent a transformer[3], a line segment and a reactive power device, respectively. The active and reactive power flows at
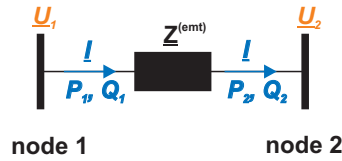

Figure 2.2.: Simplified single-phase network element

both sides of this element can be calculated according to equations (2.1) and (2.2).

$$\underline{S}_1 = \underline{I}^* \cdot \underline{U}_1 \tag{2.1}$$

$$\underline{S}_2 = \underline{I}^* \cdot \underline{U}_2 \tag{2.2}$$

Figure 2.3 shows a simplified single-phase multi-feeder radial distribution network where $\underline{Z}^{(tr)}$ represents the transformer's impedance and $\underline{Z}_{f,n}^{(sgm)}$ the line segments' impedances. This general structure of a radial distribution network includes F feeders and N_f nodes within each feeder f. A lumped load is located at each node (f, n) represented by its aggregated power infeed $\underline{S}_{f,n}^{(lpd)}$. In case of a medium voltage grid, this lumped load may be a low voltage grid, a directly connected load, storage and producer, a facility owned reactive power device and a whole sub branch of the medium voltage network itself, respectively. In case of a low voltage grid, it may be a prosumer, a consumer, a directly connected storage and producer, a facility owned reactive power device and a whole sub branch of the low voltage network itself, respectively. Since power can be injected or absorbed at each node, the power flows $\underline{S}_{f,n}^{(sgm)}$ through the line segments

---

[1]In low voltage grids the electrical equipment's capacitances inject only a very small amount of reactive power due to the low operating voltage.

[2]$\angle \underline{U}^{(tr,p)} = \angle \underline{U}^{(tr,s)} = \angle \underline{U}_{f,n}$ $\quad \forall f \in [1, F], \quad n \in [1, N_f]$ $\quad$ according to figure 2.3.

[3]The electrical quantities have to be normalised if figure 2.2 shall describe a transformer.
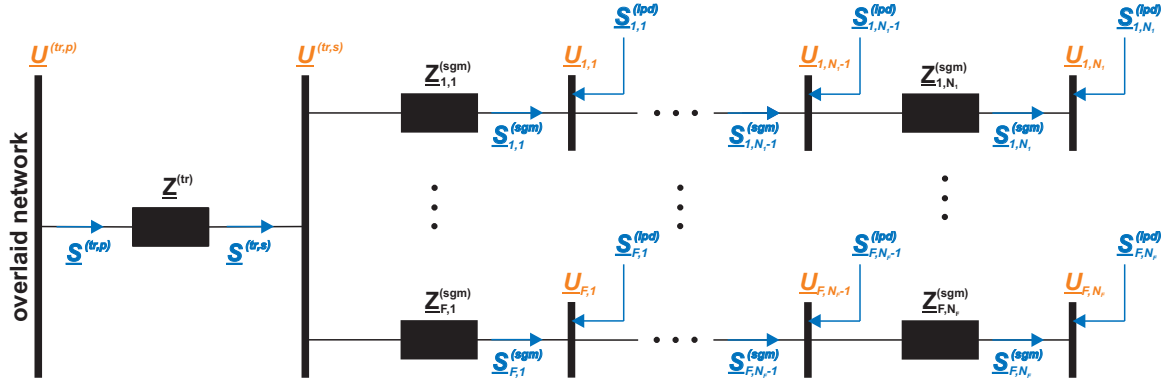
Figure 2.3.: Structure of a radial distribution network

generally differ from each other. If the injection/absorption at each node is known, they can be calculated with equation (2.3).

$$\underline{S}_{f,n}^{(sgm)} \approx -U_{f,n} \cdot \sum_{j=n}^{N_f} \frac{\underline{S}_{f,j}^{(lpd)}}{U_{f,j}} \tag{2.3}$$

The power flow at the transformer's primary side can be calculated with equation (2.4).

$$\underline{S}^{(tr,p)} \approx -U^{(tr,p)} \cdot \sum_{i=1}^{F} \sum_{j=1}^{N_i} \frac{\underline{S}_{i,j}^{(lpd)}}{U_{i,j}} \tag{2.4}$$

Figure 2.4 illustrates the structure of a prosumer connected to node (f, n) of a low voltage grid. In this thesis, such a prosumer is assumed to consist of a producer and a consumer, whereby the producer consists of a photovoltaic array, an inverter and an overvoltage protection, and the consumer corresponds to a (voltage dependent) load. The overvoltage protection is assumed to be located between the photovoltaic
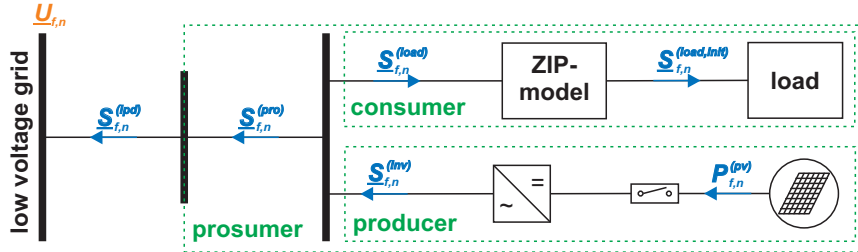
Figure 2.4.: Structure of a prosumer

array and the inverter since in this case the protection prevents the inverter from injecting active power during overvoltages but not from absorbing reactive power in order to decrease its local network voltage. The aggregated power injection of a single prosumer connected to a node (f, n) can be calculated with equation (2.5).

$$\underline{S}_{f,n}^{(pro)} = \left(P_{f,n}^{(inv)} - P_{f,n}^{(load)} \right) + j \left(Q_{f,n}^{(inv)} - Q_{f,n}^{(load)} \right) \tag{2.5}$$

The aggregated power injection of all prosumers connected to a single low voltage grid can be calculated with equation (2.6).

$$\underline{S}^{(pro)} = \sum_{i=1}^{F} \sum_{j=1}^{N_i} \underline{S}_{i,j}^{(pro)} \tag{2.6}$$

Figure 2.5 shows the lumped load at a node (f, n) of a distribution grid, to which only a reactive power device is connected. In figure 2.5 such a reactive power device is assumed to be a coil and capacitor,

13

Figure 2.5.: Structure of a reactive power device

respectively, but actually such a reactive power device can also be realised by a power electronic device. Its power absorption can be calculated with equation (2.7).

$$\underline{S}_{f,n}^{(rct)} = \frac{U_{f,n}^2}{\left(R^{(rct)}\right)^2 + \left(X^{(rct)}\right)^2} \cdot \left(R_{f,n}^{(rct)} + j \cdot X_{f,n}^{(rct)}\right) \tag{2.7}$$

Since these reactive power devices are usually used for voltage control, their reactances are variable, either continuously or in discrete steps. The term "reactive power device" is used in this thesi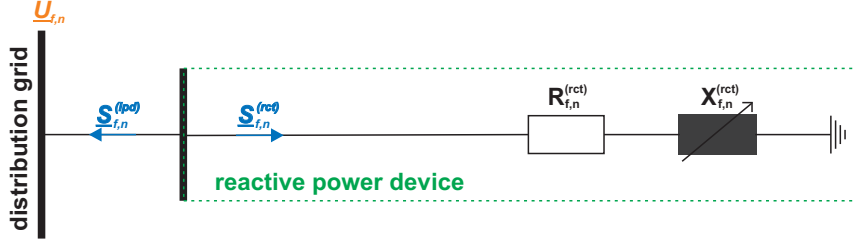s only for reactive power sources/sinks which are under the responsibility of the DSO, i.e. the customers photovoltaic inverters are not included.

2.2.1. Voltage profile

The voltage profile of a distribution grid or a single feeder is a diagram which shows all node-voltages of the grid or the feeder in dependenrecy of their distance[4] to the supplying transformer's secondary side. Following the EN 50160, all customers connected to a distribution grid have to be supplied with a voltage of ±10% around rated voltage. Usually the MV-grid's supplying transformer possesses an on load tap changer [13] and thus its secondary voltage can be kept close to a predefined set point. Starting from this voltage, the power flows through the MV- and LV-grid's line impedances and the MV/LV-transformer's impedances cause voltage variations which may lead to local limit violations in critical load/production situations. To get an impression of the voltage variations due to power flows, equation (2.8) can be formulated[5] based on the simplified single-phase network element shown in figure 2.2.

$$U^{(emt)} \approx -\frac{P_1 \cdot R^{(emt)} + Q_1 \cdot X^{(emt)}}{U_1} \approx -\frac{P_2 \cdot R^{(emt)} + Q_2 \cdot X^{(emt)}}{U_2} \tag{2.8}$$

With $\Delta U = U_2 - U_1 = U^{(emt)}$. It can be seen that the difference in voltage ΔU depends on the power flow and the impedance between both nodes. The influence of the active and reactive part of the power flow on that voltage difference is predetermined by the active and reactive part of the impedance between both nodes, respectively its R/X ratio. For a highly resistive impedance, the active power part is more influential; for a highly inductive impedance, the reactive power part is more influential. Because of the different nominal voltages at both sides of the transformer, normalised quantities according to equations (2.9), (2.10) and (2.11) are used in this section to describe the voltage variations.

$$u^{(tr,p)} = \frac{U^{(tr,p)}}{U^{(r,mv)}} \qquad u^{(tr,s)} = \frac{U^{(tr,s)}}{U^{(r,lv)}} \qquad u_{f,n} = \frac{U_{f,n}}{U^{(r,lv)}} \tag{2.9}$$

$$\underline{s}^{(tr,p)} = \frac{\underline{S}^{(tr,p)}}{S_{ref}} \qquad \underline{s}^{(tr,s)} = \frac{\underline{S}^{(tr,s)}}{S_{ref}} \qquad \underline{s}^{(sgm)} = \frac{\underline{S}^{(sgm)}}{S_{ref}} \tag{2.10}$$

$$\underline{z}^{(tr)} = \frac{\underline{Z}^{(tr)}}{Z_{ref}} \qquad \underline{z}_{f,n}^{(sgm)} = \frac{\underline{Z}_{f,n}^{(sgm)}}{Z_{ref}} \qquad Z_{ref} = \frac{\left(U^{(r,lv)}\right)^2}{S_{ref}} \tag{2.11}$$

---

[4]Line length (in meters) between the corresponding node and the supplying transformer's secondary side.
[5]Assuming $\angle \underline{U}_1 \approx \angle \underline{U}_2$.

Where $U^{(r,mv)}$ is the medium and $U^{(r,lv)}$ the low voltage grid's rated voltage. The selected values of the reference quantities (Z_{ref}, S_{ref}) don't impact the following derivations. Regarding the structure of a radial distribution grid according to figure 2.3, two fundamentally different types of voltage variations can be distinguished: The transformer caused and the line segment caused voltage variations.

$$\Delta u^{(tr)} = u^{(tr,s)} - u^{(tr,p)} \tag{2.12}$$

$$\Delta u_{f,n}^{(sgm)} = u_{f,n} - u_{f,n-1} \tag{2.13}$$

The transformer caused voltage variation $\Delta u^{(tr)}$ is generally caused by two different effects, the power flows through the transformer's impedance and its gear ratio if it differs from the ratio of the over- and underlaid networks' nominal voltages. Such gear ratios typically occur if the transformer is operated with its tap changer not in mid-position. To analyse both effects equation (2.12) can be reformulated into equation (2.14), wherein $u^{(tr,soc)}$ is the transformer's normalised secondary open circuit voltage.

$$\Delta u^{(tr)} = \Delta u^{(tr,pf)} + \Delta u^{(tr,tap)} = \left(u^{(tr,s)} - u^{(tr,soc)} \right) + \left(u^{(tr,soc)} - u^{(tr,p)} \right) \tag{2.14}$$

The transformer's gear ratio $t^{(tr)}$ and the ratio of the over- and underlay network's nominal voltages $t^{(grid)}$ are defined as follows:

$$t^{(tr)} = \frac{U^{(r,tr,p)}}{U^{(r,tr,s)}} \qquad\qquad t^{(grid)} = \frac{U^{(r,mv)}}{U^{(r,lv)}}$$

Whereby $t^{(grid)}$ does not change throughout the grid operation, $t^{(tr)}$ changes if the transformer's tap position changes[6]. The normalised voltage variation caused by the transformer's gear ratio $\Delta u^{(tr,tap)}$ can be determined with equation (2.15).

$$\Delta u^{(tr,tap)} = u^{(tr,soc)} - u^{(tr,p)} = \left(\frac{t^{(grid)}}{t^{(tr)}} - 1 \right) \cdot u^{(tr,p)} \tag{2.15}$$

Applying equation (2.8) to the transformer's impedance from figure 2.3, the power flow caused voltage variation along the transformer $\Delta u^{(tr,pf)}$ can be determined with equation (2.16).

$$\Delta u^{(tr,pf)} = u^{(tr,s)} - u^{(tr,soc)} = -\frac{r^{(tr)} \cdot p^{(tr,p)} + x^{(tr)} \cdot q^{(tr,p)}}{u^{(tr,p)}} \tag{2.16}$$

Hence, the entire voltage variation caused by the transformer can be calculated with equation (2.17).

$$\Delta u^{(tr)} = \left(\frac{t^{(grid)}}{t^{(tr)}} - 1 \right) \cdot u^{(tr,p)} - \frac{r^{(tr)} \cdot p^{(tr,p)} + x^{(tr)} \cdot q^{(tr,p)}}{u^{(tr,p)}} \tag{2.17}$$

The voltage variation along a line segment $\Delta u_{f,n}^{(sgm)}$ is caused by the power flows through its impedance. Applying equation (2.8) to the impedance of a line segment from figure 2.3, the corresponding voltage variation can be calculated with equation (2.18).

$$\Delta u_{f,n}^{(sgm)} = u_{f,n} - u_{f,n-1} = -\frac{r_{f,n}^{(sgm)} \cdot p_{f,n}^{(sgm)} + x_{f,n}^{(sgm)} \cdot q_{f,n}^{(sgm)}}{u_{f,n}} \tag{2.18}$$

This equation only describes the voltage variation caused by a single line segment, i.e. between two adjacent nodes. All these segment-wise voltage variations have to be added up according to equation (2.19) to attain the overall feeder impedance caused voltage variation $\Delta u_{f,n}^{(fdr)}$ of a node (f, n).

$$\Delta u_{f,n}^{(fdr)} = u_{f,n} - u^{(tr,s)} = \sum_{j=1}^{n} \Delta u_{f,j}^{(sgm)} \tag{2.19}$$

---

[6]Only possible if the transformer possesses an OLTC.

The resulting difference in voltage between a node (f, n) and the transformer's primary side $\Delta u_{f,n}^{(total)}$ can be calculated according to equation (2.20) by superimposing the transformer's and the related feeder's voltage variation.

$$\Delta u_{f,n}^{(total)} = u_{f,n} - u^{(tr,p)} = \Delta u^{(tr)} + \Delta u_{f,n}^{(fdr)} \tag{2.20}$$

Both effects fundamentally differ in their emergence and their impact on the network's overall voltage profile. According to equation (2.17), the transformer's voltage variation is caused by the power flows through its impedance, regardless the exact location of the loads and producers these power flows are related to. Theoretically, this voltage variation can be (partly) compensated by setting an appropriate tap position. Starting from the transformer's secondary voltage, another voltage variation occurs along each feeder in dependency of the node's electrical distance to the supplying transformer and the power flows through the involved line segments, as equations (2.18) and (2.19) show. While the voltage variation along the transformer influences the voltage profiles of all feeders equally[7], the voltage variation along a line only influences the voltage profile of the related feeder. Assuming $R^{(tr)}/X^{(tr)} = 1/4$, which is a usual value for European MV/LV-transformers [16], the reactive power flows through the transformer exert a greater impact on the transformer's voltage variation than the active ones. For a line's voltage variation, it depends on the line's R/X-ratio which part of the power flow exerts a greater impact. For a mainly inductive line, the reactive part is more influential; for a mainly resistive line, the active part is more influential. Noting that the first case tendentially applies for overhead lines, and the second case for cables (compare table 7.6), it follows that the reactive power flows are more crucial concerning voltage variations for feeders consisting of overhead lines. If the overlaid network's impedance is neglected, the local R/X-ratio of a prosumer located at node (f, n) depends on the impedances of all line segments between this prosumer and the transformer's secondary side as well as on the transformer's impedance. Figure 2.6 shows a prosumer which is supplied by an ideal source, a transformer and a single line segment. If the

Figure 2.6.: Prosumer supplied by an ideal source, a transformer and a single line segment

overlaid networks' impedances are neglected, this (distance dependent) impedance can be determined with equation (2.21).

$$\frac{R}{X}(l) = \frac{R^{(tr)} + R^{(sgm)'} \cdot l}{X^{(tr)} + X^{(sgm)'} \cdot l} \tag{2.21}$$

Where l is the line's length and $R^{(sgm)'} + j \cdot X^{(sgm)'}$ the line's specific impedance. At the transformer's secondary side ($l = 0\,\mathrm{m}$), the local R/X-ratio corresponds to the transformer's R/X-ratio and in infinite distance, the local R/X-ratio converges to the line's R/X-ratio, as equations (2.22) and (2.23) show.

$$\lim_{l \to 0} \frac{R}{X}(l) = \frac{R^{(tr)}}{X^{(tr)}} \tag{2.22}$$

$$\lim_{l \to \infty} \frac{R}{X}(l) = \frac{R^{(sgm)}}{X^{(sgm)}} \tag{2.23}$$

Figure 2.7 illustrates relation (2.21) for both feeders of the theoretical grid described in section 3.1.1. One of these feeders consists solely of overhead lines and one feeder solely of cables. It can be seen that the R/X-ratio increases along the feeder, especially in case of a cable-feeder.

The voltage spreading $\Delta u^{(sdg)}$ of a distribution grid represents the maximum voltage difference within the distribution grid, according to equation 2.24. Neglecting voltage dependencies of loads and generators, this voltage spreading cannot be influenced by using the tap changer, but only by influencing the power flows through the corresponding feeders.

$$\Delta u^{(sdg)} = max\left(u^{(tr,s)}, u_{f,n}\right) - min\left(u^{(tr,s)}, u_{f,n}\right) \tag{2.24}$$

---

[7]Neglecting the loads', line segments' and generators' voltage dependency.
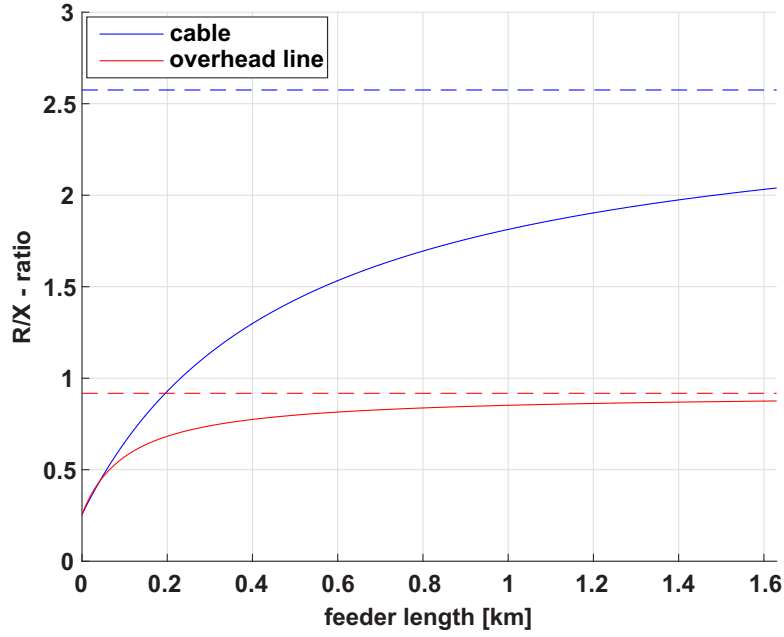
Figure 2.7.: R/X-ratio of the cable- and overhead line-feeders of the theoretical Link-Grid in dependency of the feeder length

Figure 2.8 illustrates the voltage profile for one load flow situation of one of the later on simulated low voltage networks. This diagram shows the transformer's open circuit secondary voltage as a black cross at feeder length 0 m and the voltage profiles of all feeders, whereby the colors of the feeders comply with those from figures 3.1 to 3.5 and 7.1 to 7.5, respectively. The simulation results contain one voltage value for each network-node. In figure 2.8 these values are market with dots in the same color as their related feeder. The lines between the dots do not represent any simulations results, they are just inserted to clarify the feeders' topologies. For a better understanding, some of the different types of voltage variations defined above are also included in the diagram.
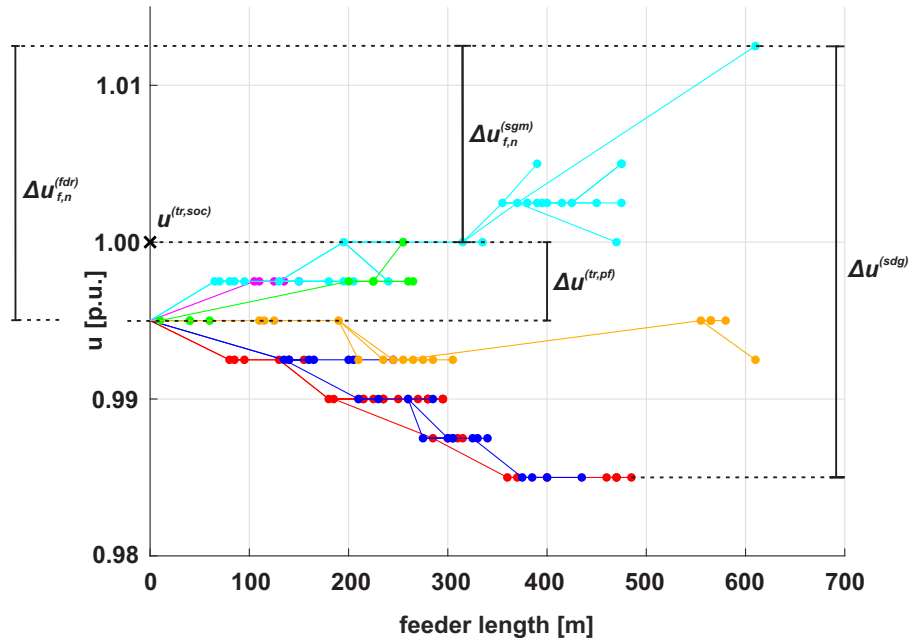

Figure 2.8.: Exemplary voltage profile

17

2.2.2. Loading of the electrical equipment

In general, power flows thermally strain the electrical equipment of a distribution grid, like overhead lines, cables, transformers and reactive power devices. This strain doesn't substantially impair the grid performance as long as these power flows do not lead to an exceedance of the equipment's ratings. But otherwise, if their ratings are exceeded for a considerable time, the electrical equipment is subject to a faster aging. This should be avoided in order to afford an economical grid operation also in the long-term. Regarding the simplified single-phase network element from figure 2.2, the loading of a network element $\mathcal{L}^{(emt)}$ is defined according to equation (2.25) as the ratio of the actual current I through the element and its rated current $I^{(r,emt)}$. For a line, is it a cable or an overhead line, usually a thermal limiting current $I^{(th,sgm)}$ is reported in its data sheet instead of a rated current.

$$\mathcal{L}^{(emt)} = \frac{|\underline{I}|}{I^{(r,emt)}} \tag{2.25}$$

Expressing the current by active and reactive power flows, equation (2.25) can be reformulated into equation (2.26).

$$\mathcal{L}^{(emt)} \approx \frac{\sqrt{\left(P_1^2 + Q_1^2\right)}}{U_1 \cdot I^{(r,emt)}} \approx \frac{\sqrt{\left(P_2^2 + Q_2^2\right)}}{U_2 \cdot I^{(r,emt)}} \tag{2.26}$$

Regarding the simplified distribution grid from figure 2.3, the transformer's and line segments' loading can be determined with equations (2.27) and (2.28), respectively.

$$\mathcal{L}^{(tr)} = \frac{\sqrt{\left(P^{(tr,p)}\right)^2 + \left(Q^{(tr,p)}\right)^2}}{U^{(tr,p)} \cdot I^{(r,tr,p)}} = \frac{\sqrt{\left(P^{(tr,s)}\right)^2 + \left(Q^{(tr,s)}\right)^2}}{U^{(tr,s)} \cdot I^{(r,tr,s)}} \tag{2.27}$$

$$\mathcal{L}_{f,n}^{(sgm)} = \frac{\sqrt{\left(P_{f,n}^{(sgm)}\right)^2 + \left(Q_{f,n}^{(sgm)}\right)^2}}{U_{f,n} \cdot I^{(th,sgm)}} \tag{2.28}$$

The nominal current of three-phase transformers can be calculated with equation (2.29) by using the data from table 7.7.

$$I^{(r,tr,p)} = \frac{S^{(r,tr)}}{\sqrt{3} \cdot U^{(r,tr,p)}} \qquad\qquad I^{(r,tr,s)} = \frac{S^{(r,tr)}}{\sqrt{3} \cdot U^{(r,tr,s)}} \tag{2.29}$$

The loading of a reactive power device according to figure 2.5 can be calculated with equation (2.30).

$$\mathcal{L}_{f,n}^{(rct)} = \frac{\sqrt{\left(P_{f,n}^{(rct)}\right)^2 + \left(Q_{f,n}^{(rct)}\right)^2}}{U_{f,n} \cdot I^{(r,rct)}} \tag{2.30}$$

2.2.3. Power consumption of the electrical equipment

The power flows also cause an active and reactive power consumption of the network's electrical equipment. Regarding the network element from figure 2.2, its power consumption $\underline{S}^{(loss,emt)}$ can be calculated with equation (2.31).

$$\underline{S}^{(loss,emt)} = \underline{I}^* \cdot (\underline{U}_1 - \underline{U}_2) = I^2 \cdot \underline{Z} \tag{2.31}$$

The equipment's active power consumption, called active power losses in the following, should be kept low in energy systems for economical and environmental reasons. Derived from equation (2.31), the active power consumption of a network element $P^{(loss,emt)}$ can be determined with equation (2.32).

$$P^{(loss,emt)} \approx R^{(emt)} \cdot \frac{P_1^2 + Q_1^2}{U_1^2} \approx R^{(emt)} \cdot \frac{P_2^2 + Q_2^2}{U_2^2} \tag{2.32}$$

The equipment's reactive power consumption, called reactive power losses in the following, should be kept low, too, since it leads to higher reactive power flows within the grid and thus to a higher equipment loading, to higher voltage variations and to higher active power losses. Derived from equation (2.31), the reactive power consumption of a network element $Q^{(loss,emt)}$ can be determined with equation (2.33).

$$Q^{(loss,emt)} \approx X^{(emt)} \cdot \frac{P_1^2 + Q_1^2}{U_1^2} \approx X^{(emt)} \cdot \frac{P_2^2 + Q_2^2}{U_2^2} \tag{2.33}$$

In this thesis, the power losses of a distribution network include the power losses of the network's complete electrical equipment, i.e. of its supplying transformer, its lines and its reactive power devices. By analogy with equation (2.32), the active power losses of the transformer and the line segments can be determined with equations (2.34) and (2.35), respectively.

$$P^{(loss,tr)} = R^{(tr)} \cdot \frac{\left(P^{(tr,p)}\right)^2 + \left(Q^{(tr,p)}\right)^2}{\left(U^{(tr,p)}\right)^2} \tag{2.34}$$

$$P_{f,n}^{(loss,sgm)} = R_{f,n}^{(sgm)} \cdot \frac{\left(P_{f,n}^{(sgm)}\right)^2 + \left(Q_{f,n}^{(sgm)}\right)^2}{\left(U_{f,n}\right)^2} \tag{2.35}$$

By analogy with equation (2.33), the reactive power losses of the transformer and the line segments can be determined with equations (2.36) and (2.37), respectively.

$$Q^{(loss,tr)} = X^{(tr)} \cdot \frac{\left(P^{(tr,p)}\right)^2 + \left(Q^{(tr,p)}\right)^2}{\left(U^{(tr,p)}\right)^2} \tag{2.36}$$

$$Q_{f,n}^{(loss,sgm)} = X_{f,n}^{(sgm)} \cdot \frac{\left(P_{f,n}^{(sgm)}\right)^2 + \left(Q_{f,n}^{(sgm)}\right)^2}{\left(U_{f,n}\right)^2} \tag{2.37}$$

The structure of equations (2.32) and (2.33) is not expedient to describe the active and reactive power consumption of a reactive power device, since in this case its self-consumption equals to the complete[8] incoming power flow according to figure 2.5 and equation (2.38).

$$\underline{S}_{f,n}^{(loss,rct)} = \underline{S}_{f,n}^{(rct)} \tag{2.38}$$

Instead, equation (2.7) can be used to determine the active and reactive power consumption of a reactive power device in dependency of the local voltage. The active power losses of a distribution network $P^{(loss)}$ can be determined according to equation (2.39) by adding up the active power losses of the networks supplying transformer, all line segments and all reactive power devices.

$$P^{(loss)} = P^{(loss,tr)} + \sum_{i=1}^{F} \sum_{j=1}^{N_i} \left(P_{i,j}^{(loss,sgm)} + P_{i,j}^{(loss,rct)} \right) \tag{2.39}$$

The reactive power losses of a distribution network $Q^{(loss)}$ can be determined according to equation (2.40) by adding up the reactive power losses of the supplying transformer, all line segments and all reactive power devices.

$$Q^{(loss)} = Q^{(loss,tr)} + \sum_{i=1}^{F} \sum_{j=1}^{N_i} \left(Q_{i,j}^{(loss,sgm)} + Q_{i,j}^{(loss,rct)} \right) \tag{2.40}$$

---

[8]Since the voltage at the reactive power device's grounded side is zero, no power is flowing out of the device and thus the whole power is consumed by the device itself.

2.2.4. Reactive power exchange with the overlaid network

The reactive power which is consumed by Q-sinks has to be provided by Q-sources. In the European power grid, these Q-sources and -sinks are spread over the different voltage levels so that reactive power flows from the Q-sources through the different grid parts to the Q-sinks. The resulting reactive power flows impact the voltage profiles of the involved grid parts and cause additional active power losses and equipment loadings. Regarding a distribution grid, the Q-sinks may be inductive loads (consumers), Q-controlled inverters and the electrical equipment's reactive power consumption, for instance. Usually, this Q-demand cannot be covered locally so that reactive power has to be provided by the overlaid grid(s), resulting in a Q-exchange between the distribution and transmission grid.

With a further increasing capacity of distributed generation, more reactive power will be required by the distribution grids for voltage control, while less conventional power plants will be available to provide reactive power within the transmission grid. The shortage of Q-sources in the European transmission grid and the increasing Q-demand of the connected distribution grids will jeopardise the system security by violations of the admissible voltage range within the transmission grid. Cost-intensive measures like installing and operating switchable shunt capacitor-banks are conventionally employed to counteract these voltage violations. [4]

Each network operator can theoretically influence the Q-balance of his network with the measures listed in table 2.1. In distribution grids, these Q-variables are commonly used for local voltage control purposes without considering their overall Q-balances. This leads to an uncontrolled and excessive reactive power exchange which has to be managed by the overlaid network. If the DGs inject active power, the resulting Q-demand and P-supply of the distribution grids leads to high power flows within the transmission grid which also increase the reactive power consumption of the transmission grid's overhead lines and transformers and thus further intensify the problem of missing Q-sources within the transmission grid (compare to equations (2.37) and (2.36)). A conflict arises between the DSOs' and TSOs' interests regarding the usage of the available Q-variables. Concepts are required for the future Q-exchange between the transmission and distribution grids to avoid technically and economically inefficient solutions. [4]

In Austria, the TSO and DSOs are legally bound to define minimum requirements concerning their Q-exchanges which have to be satisfied afterwards by the DSOs. Furthermore, the DSOs are obliged to compensate at least the reactive power consumption of their transformers and lines, either by own Q-sources or by contractual arrangements with connected customers. [17]

From a technical point of view the concepts for this Q-exchange may range from no Q-limitations or specific (P-dependent) Q-limits to use case dependent target values for the reactive power exchange. Figure 2.9 shows these reactive power control concepts. They can be theoretically applied between any voltage levels. If there are no Q-limitations between the different voltage levels, a large amount of compensation
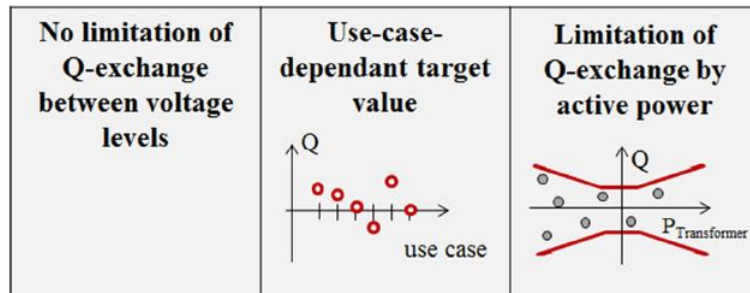

Figure 2.9.: Strategies for a reactive power control concept over all voltage levels [4]

elements is required in the transmission grids, but all the Q-variables are still available to the subordinated grid's operator for loss minimisation and voltage optimisation. If the transmission networks send use case dependent Q-target values to the distribution grids, less compensation elements are required within the transmission grids, but the DSOs are restricted in optimising power losses and voltage profiles. In general it can be stated, that the more restrictive the Q-limitations are, the less reactive power has to be provided,

howsoever, by the TSOs and the more restricted are the DSOs in optimising their networks' power losses and voltage profiles. Consequently, another conflict arises between the TSOs and DSOs which intensifies with an increasing amount of DGs within the distribution grids. [4]

2.2.5. Optimal Q-management

The previous sections discussed the impacts of power flows on the performance of distribution grids. These impacts can be mitigated by increasing the operating voltage and by utilising the available Q-variables for a performance optimisation. The following considerations show which Q-flows are required to minimise each impact, but without influencing the active power flows. The loading of the electrical equipment can by minimised by setting the reactive power flows through each element to zero.

$$Q^{(tr,p)} = Q_{f,n}^{(sgm)} = Q_{f,n}^{(rct)} = 0 \qquad \forall f,n \tag{2.41}$$

The voltage variation along the transformer can be influenced in two ways, by setting an appropriate tap position and by influencing the reactive power flow through the transformer's impedance. This means, that the power flow caused voltage variation can be compensated according to equation (2.42) by an appropriate tap position (but usually the distribution transformer doesn't possess an OLTC).

$$\left(\frac{t^{(grid)}}{t^{(tr)}} - 1 \right) \cdot U^{(tr,p)} = \frac{R^{(tr)} \cdot P^{(tr,p)} + X^{(tr)} \cdot Q^{(tr,p)}}{U^{(tr,p)}} \tag{2.42}$$

If no on load tap changer is available, the reactive power flow through the transformer can theoretically be used to compensate the voltage variation caused by the active power flow.

$$Q^{(tr,p)} = -P^{(tr,p)} \cdot \frac{R^{(tr)}}{X^{(tr)}} \tag{2.43}$$

Both approaches can be combined to minimise the voltage variation along the transformer. The voltage spreading can be influenced by absorbing/injecting reactive power at those feeders with the minimum and maximum node voltages, respectively. This measure is the more effective, the larger the electrical distance between the injection/absorption-point and the transformer's secondary side is. If no voltage spreading shall occur, equation (2.44) must be fulfilled for all line segments.

$$Q_{f,n}^{(sgm)} = -P_{f,n}^{(sgm)} \cdot \frac{R_{f,n}^{(sgm)}}{X_{f,n}^{(sgm)}} \qquad \forall f,n \tag{2.44}$$

The active and reactive power consumption of the transformer, the line segments and the reactive power devices can only be minimised by setting their reactive power flows to zero. This can nearly be achieved if each consumer possesses a reactive power source which covers his Q-demand and no reactive power devices are connected.

$$Q^{(tr,p)} = Q_{f,n}^{(sgm)} = Q_{f,n}^{(rct)} = 0 \qquad \forall f,n \tag{2.45}$$

The optimal reactive power exchange depends on the selected reactive power control concept from figure 2.9. If no target values are specified by the overlaid grid, the reactive power exchange should be set to zero for an optimal performance. This can be achieved if there is an overall reactive power balance in the distribution network.

$$Q^{(tr,p)} = 0 \tag{2.46}$$

But if there are target values specified by the overlaid grid, the reactive power exchange should follow them:

$$Q^{(tr,p)} = Q_0^{(tr,p)} \tag{2.47}$$

As equations (2.41), (2.43), (2.44) and (2.45) show, there is a goal conflict between voltage profile optimisation and loss and loading minimisation, respectively, since the reactive power which is required for voltage profile optimisation causes additional power losses and additionally loads the electrical equipment. Setting the reactive power exchange to zero also minimises the transformer losses, but restricts the capabilities for voltage profile optimisation. If use-case dependent target Q-values are defined by the overlaid network, the capabilities for voltage profile optimisation are again restricted and additional losses occur. From a holistic system view, a promising approach may be to dynamically optimise power losses while considering Q-target values from adjacent grids as dynamic and voltage limitations, equipment loading, PQ-diagrams of generators, DGs and inverters, maximal step numbers of transformers as well as installed ratings of reactive power devices as static constraints.

2.3. Voltage control in low voltage networks

If the photovoltaic generation of a prosumer according to figure 2.4 exceeds his active power consumption $(P_{f,n}^{(inv)} > P_{f,n}^{(load)})$, the resulting active power infeed increases his local voltage. As already mentioned in section 1.2, these increased voltages are often the most restrictive limitations for PV grid integration. Different measures can be taken to increase a network's hosting capacity. According to equation (2.8), the rise in voltage can be reduced by reducing the line impedances, i.e. by reinforcing the grid. Another possibility to counteract the rise of voltage is to influence the P- and Q-flows within the grid. In a Smart Grid, the P- and Q-flows can be influenced by smart storage operation, demand side management, active power curtailment of distributed generators and reactive power control of DG-inverters and reactive power devices, for instance. All these measures can be performed as a local control, where only locally available data and thus no data exchange between different market players is required to perform voltage control, and as a coordinated control, where data is exchanged between different devices through a communication system to optimally control the overall system. As a conclusion of the project "MorePV2Grid", local volt/var and volt/watt controls can significantly increase the hosting capacity of low voltage grids at particularly low costs [18]. Furthermore, the additional benefits of a coordinated approach may be negated by additional system vulnerability due to reliance on communication and latency in communication [15], as well as in terms of data privacy and cyber-security. However, volt/var based local voltage control concepts lead to an uncontrolled and excessive reactive power demand of the corresponding low voltage grids. Despite the previously mentioned disadvantages of a coordinated control approach, a coordinated reactive power based control concept enables the LV-grid to provide a Q-support to its overlaid MV-grid and in further consequence it enables also the MV-grid to provide a Q-support to its overlaid HV-grid.

The customer owned PV-inverters can be locally controlled to support the grid with reactive power injection/absorption and to curtail their active power injection in order to avoid voltage limit violations. If the curtailed active power or the injected/absorbed reactive power depends on the local network conditions, this kind of local control leads to a discrimination between customers since they are differently located within the grid and thus provide system services to a different extent, in fact without remuneration. A coordinated voltage control concept based on PV-inverters requires a data exchange between the customers and the DSO which jeopardises the customers' data privacy.

The DSO owned reactive power devices can be locally controlled to inject/absorb reactive power at their connection points in order to control their local voltages. With this voltage control concept the customers aren't requested to provide system services and thus they are prevented from being discriminated. A coordinated voltage control concept based on reactive power devices doesn't require a data exchange between the customers and the DSO and thus maintains the customers data privacy.

Combining both previously explained voltage control concepts, another possible concept is to use each customer's inverter to compensate his own reactive power demand $(Q_{f,n}^{(pro)} = 0)$ and to use the DSO's reactive power devices for a local voltage control. This kind of local voltage control may be beneficial in terms of loss reduction and it also prevents customers from being discriminated. Furthermore, as a coordinated approach, this concept enables the low voltage grid to offer Q-support to a certain extent to its overlaid medium voltage grid without requiring a data exchange between the DSO and the customers,

since the DSO has the complete control over the LV-grid's reactive power behaviour.

Section 2.3.1 presents and discusses different local active power curtailment strategies for PV-inverters, while section 2.3.2 presents and discusses different local reactive power control strategies for PV-inverters and for reactive power devices. Section 2.3.3 presents parts of the Austrian grid code which are relevant for PV-inverters connected to Austrian low voltage grids.

2.3.1. Active power curtailment

This voltage control concept curtails the active power injection of a distributed generator in order to reduce the rise in voltage at its connection point to the low voltage grid. In contrast to a volt/var based control strategy, active power curtailment can be used not only to avoid voltage violations, but also to avoid equipment overloading. However, curtailing active power also means to reduce the earnings of the DGs' owners and to waste renewable energy. Figure 2.10 illustrates the power/time distribution of solar-, wind- and hydro-based generators. It can be seen that photovoltaic systems reach their peak production just for a few hours per year and thus active power curtailment is particularly interesting for this kind of distributed generators. More precise, network bottlenecks can be relieved by active power curtailment of distributed photovoltaic generators without reducing their yearly produced energy significantly [19]. According to [19], four active power curtailment strategies have been demonstrated a good potential:
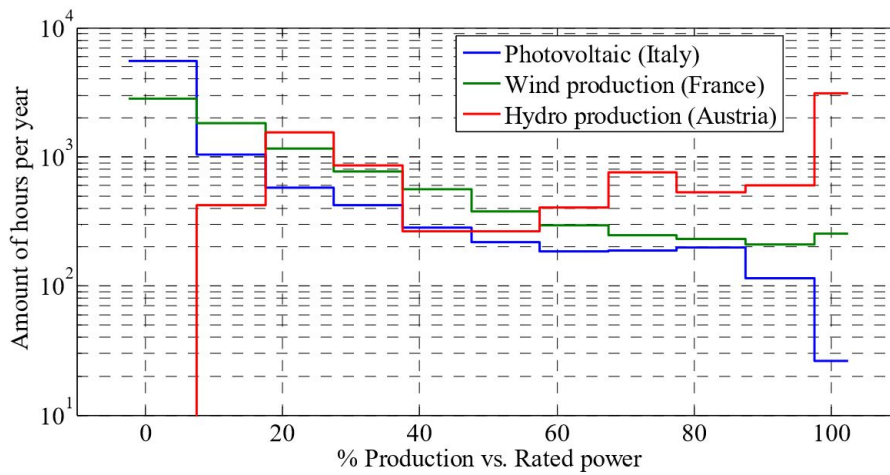

Figure 2.10.: Time occurrence/duration of the generated power from a three actual renewable generators – one-year time window [19]

"Disconnection of the generation units in case of overvoltage", "fixed power curtailment", "volt/watt droop control" and "generation of a fixed portion of the available production". Figure 2.11 illustrates their functionalities and impacts on their local voltages. In figure 2.11a, the photovoltaic array is disconnected from the grid by its overvoltage protection, if its local voltage exceeds the maximum allowed voltage value (1.1 p.u. in this thesis). With this control strategy a large amount of energy is curtailed, since overvoltages typically occur during peak production periods and the photovoltaic array cannot inject any active power if its disconnected from the grid. The voltage drops down immediately since no active power is injected any more and rises again when the photovoltaic system is reconnected. According to [20], this may result in a cyclic behaviour of disconnection, automatic reclosing and further disconnection of the inverter. In figure 2.11b, the photovoltaic system's active power injection is limited to a maximum value by its inverter. The active power limitation has to be chosen carefully in accordance with the local network conditions and the photovoltaic array's rating. Figure 2.11c shows a voltage dependent active power curtailment strategy, called P(U)-control in the following. This control scheme only curtails the amount of active power which causes the overvoltage, while the remaining active power is still injected into the grid. Only a small portion of the injected energy is curtailed and the local voltage stays slightly below its upper limit. In figure 2.11d, a fixed percentage of the active power infeed is curtailed regardless the current active power injection and the local voltage. According to simulations from [19], this control strategy curtails the
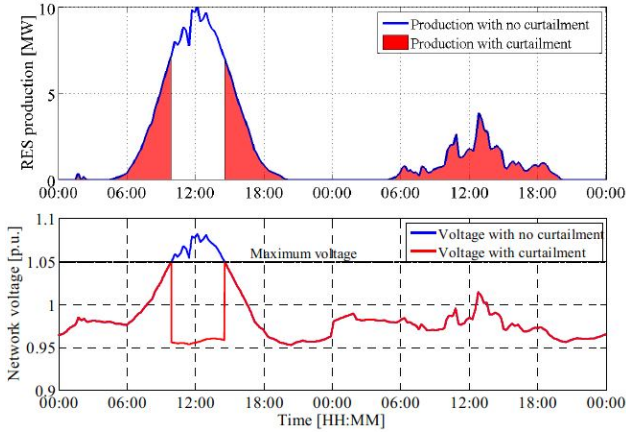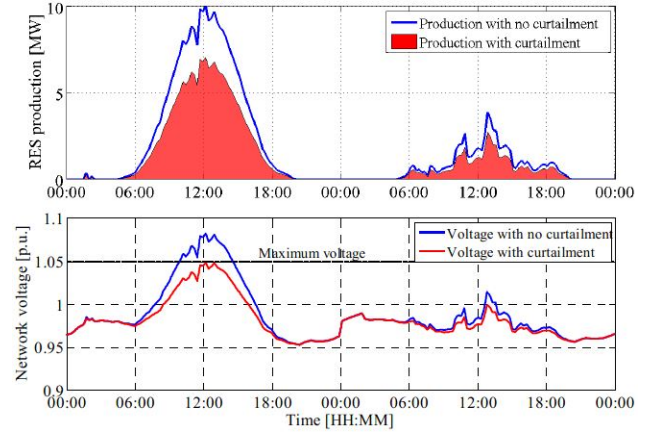
(a) Disconnection of the generation units in case of overvoltage. Active power and voltage profiles.
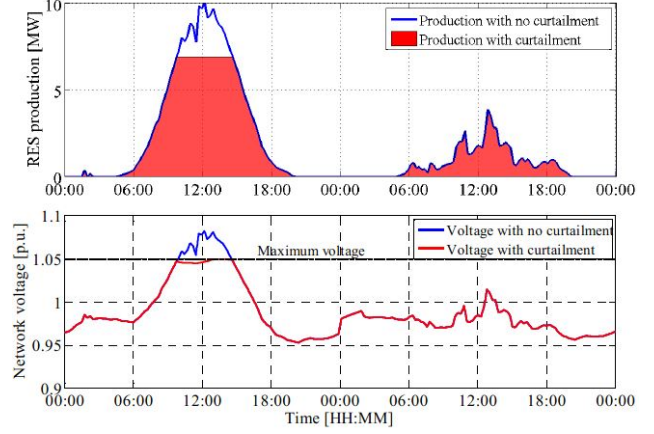
(b) Fixed power curtailment. Active power and voltage profiles.
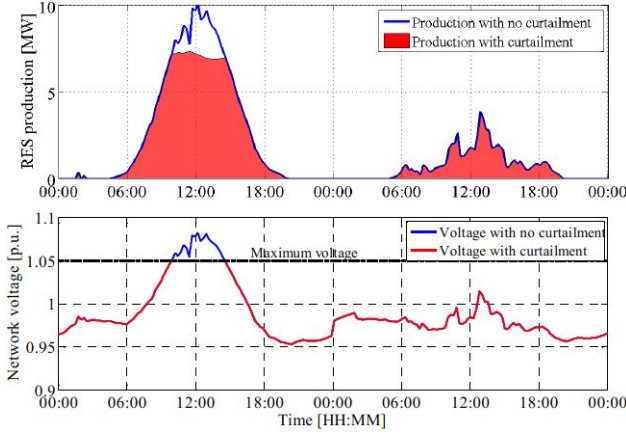
(c) Volt/watt droop control. Active power and voltage profiles.

(d) Generation of a fixed portion of the available production. Active power and voltage profiles.

Figure 2.11.: Effects of different active power curtailment strategies on the active power injection and the local network voltage of distributed generators connected to a low voltage grid [19]

largest amount of energy compared to the three previously explained ones. The simulations from [19] also state that the hosting capacity of a low voltage grid can be increased by a volt/watt based control scheme, while only a small portion of the renewable energy is curtailed. Particularly the $P(U)$-control shows a good performance in terms of avoiding voltage limit violations and increasing the network's hosting capacity. This control concept may increase the network's hosting capacity by $30\,\%$ to $60\,\%$, with respect to the operation without curtailment [19]. Furthermore, if the $P(U)$-characteristic sets the photovoltaic systems' active power output to zero at their maximum allowed local voltage, voltage rises are no longer restricting the network's hosting capacity [18]. Due to its simplicity and marginal impacts on energy efficiency, volt/watt controls can be seen as competitive to conventional grid reinforcement for increasing a distribution network's hosting capacity [19].

2.3.2. Reactive power control

With this control concept the voltage profile of a low voltage grid is influenced by injecting/absorbing reactive power by the connected Q-sources/sinks. These Q-sources/sinks can be DSO-owned reactive power devices and customer-owned inverters, respectively. In contrast to active power curtailment, reactive power control strategies cannot only be used to decrease but also to increase the node-voltages of a network. Reducing the network's node-voltages by absorbing reactive power typically cause additional grid losses and equipment loading, since in this case the consumers and the Q-sinks are both consuming reactive power. But according to [18], the control-related Q-flows do only insignificantly increase the grid's active power losses and makes them a subordinated constraint of utilising reactive power for voltage control. According to equations (2.48) and (2.49), the Q-provision of a PV-system is restricted by the inverter's rated apparent power and its actual active power injection while the Q-provision of a reactive power device is only restricted by its rated apparent power[9].

$$\left| Q_{f,n}^{(max,inv)} \right| = \sqrt{\left(S_{f,n}^{(r,inv)} \right)^2 - \left(P_{f,n}^{(inv)} \right)^2} \tag{2.48}$$

$$\left| Q_{f,n}^{(max,rct)} \right| = S_{f,n}^{(r,rct)} \tag{2.49}$$

A. Local control of PV-inverters

Additionally to its active power injection, a PV-inverter may absorb or inject reactive power in order to influence its local voltage. According to [2], four different reactive power control strategies are commonly used to locally control distributed generators: "Fixed power factor $(cos(\varphi) = cos(\varphi_0))$", "fixed reactive power $(Q = Q_0)$", "power factor as a function of the injected active power $(cos\varphi = f(P))$" and "reactive power as a function of the connection voltage $(Q = f(U))$". However, firstly the question is investigated how much reactive power a prosumer has to absorb/inject to compensate the voltage rise/drop caused by his active power injection/absorption. Regarding a prosumer supplied by an ideal power source, a transformer and a line segment according to figure 2.6, the relative compensation ξ of his active power injection/absorption caused voltage rise/drop by absorbing/injecting reactive power depends on his local R/X-ratio. This relative compensation can be determined with equation (2.50).

$$\xi = \frac{\left(X^{(tr)} + X^{(sgm)'} \cdot l \right) \cdot Q^{(pro)}}{\left(R^{(tr)} + R^{(sgm)'} \cdot l \right) \cdot P^{(pro)}} = \frac{X}{R}(l) \cdot \tan\left(\varphi^{(pro)} \right) \tag{2.50}$$

Figure 2.12 shows the power factor of a prosumer which is required to compensate certain portions of his active power injection/absorption caused voltage rise/drop in dependency of his local R/X-ratio. The higher the local R/X-ratio is, the lower the prosumer's power factor must be to achieve a certain relative compensation of his active power injection/absorption caused voltage rise/drop. Since the R/X-ratio typically increases along a feeder, prosumer's located at the end of a feeder have to inject/absorb active

---

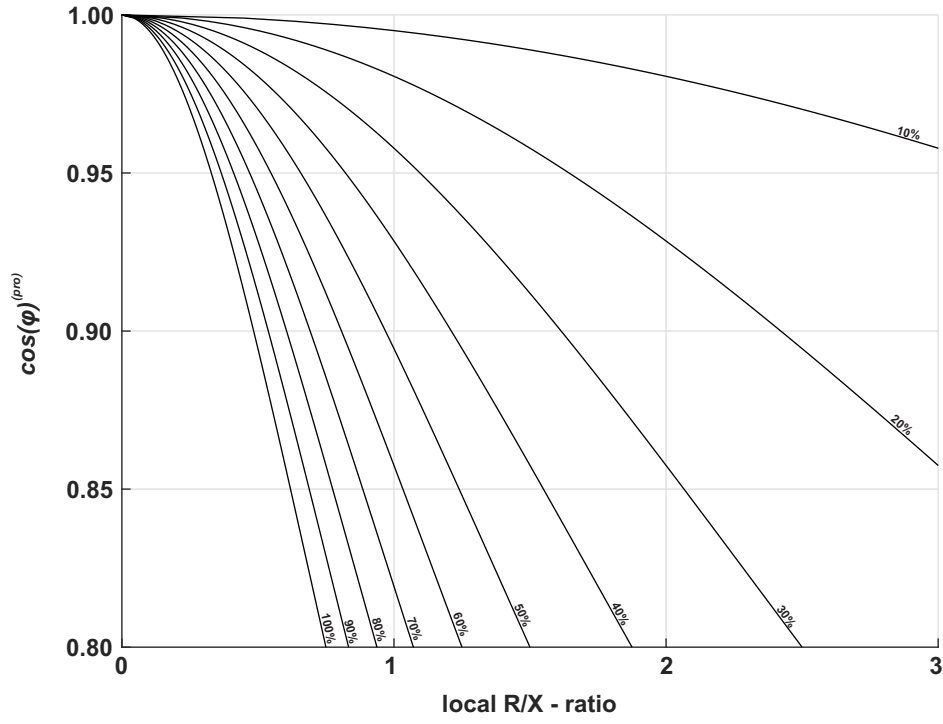[9]If it doesn't absorb any active power $(R_{f,n}^{(rct)} = 0)$.

Figure 2.12.: Power factor of a prosumer which is required to compensate certain portions ξ of his active power injection/absorption caused voltage rise/drop in dependency of his local R/X-ratio

power with a lower power factor to achieve the same relative voltage rise/drop compensation. As shown in figure 2.7, the local R/X-ratio of a prosumer connected to one of the theoretical Link-Grid's feeders depends on the line length between him and the distribution transformer. Figure 2.13 shows the power factor of a prosumer connected to a cable- and a overhead line-feeder of the theoretical Link-Grid which is required to compensate certain portions of his active power injection/absorption caused voltage rise/drop in dependency of the line length between him and the distribution transformer. It can be seen that the power
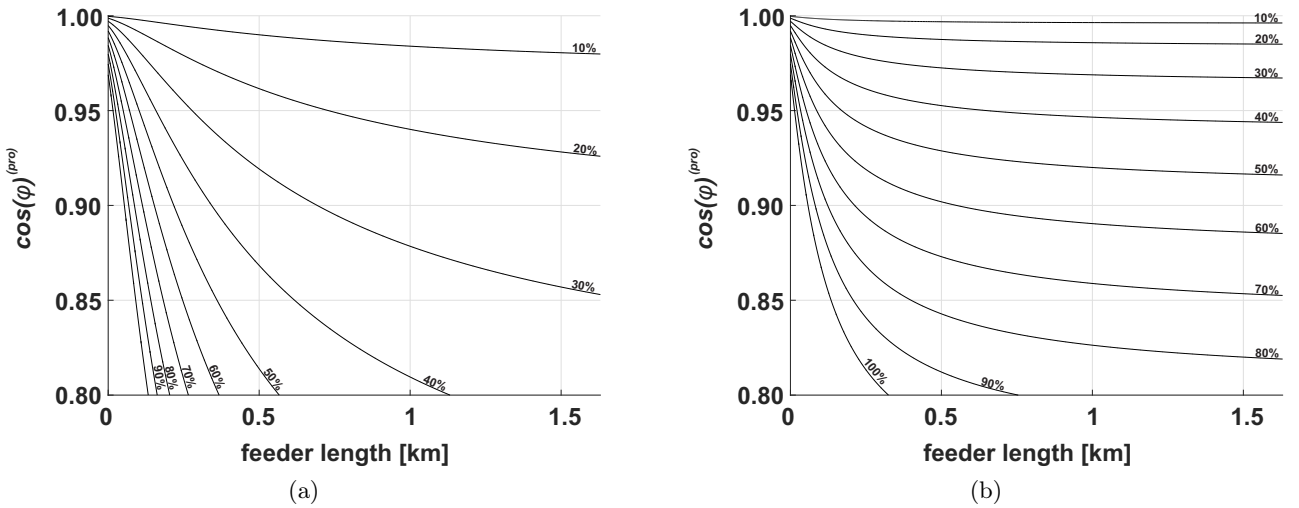

Figure 2.13.: Power factor of a prosumer which is required to compensate certain portions ξ of his active power injection/absorption caused voltage rise/drop in dependency of the line length between him and the distribution transformer for the feeders of the theoretical Link-Grid: (a) Cable feeders (C1 and C2), (b) Overhead line feeders (L1 and L2)

factor which is required to compensate certain portions of a prosumer's active power injection/absorption

26

caused voltage rise/drop varies along the feeder, especially in case of a cable-feeder. However, conclusions of the project "MorePV2Grid" show that the feasible relative compensation[10] of the PV-induced voltage rise by local reactive power control of the PV-inverters ranges from 20 % to 80 %, and 30 % compensation (i.e. 30 % more hosting capacity) can be seen as typical for state-of-the-art low voltage grids with a high cable share [18].

From the four previously mentioned reactive power control strategies, this thesis only investigates the $cos\varphi = f(P)$-control, called $cos\varphi(P)$-control in the following, and the $Q = f(U)$-control, called $Q(U)$-control in the following. A $cos\varphi(P)$-controlled PV-inverter absorbs reactive power depending on its active power injection according to a predefined characteristics (compare to fig. 2.15b) in order to reduce its active power injection caused voltage rise. This control strategy doesn't consider the actual network situation and thus leads to unfavourable Q-flows in some load/production situations. For instance, if a prosumer simultaneously produces and consumes a large amount of active power, he doesn't increase his local voltage and thus no reactive power has to be consumed by the inverter to reduce his local voltage. But anyway, a $cos\varphi(P)$-controlled inverter consumes reactive power and thus causes additional power losses and equipment loading. A $Q(U)$-controlled PV-inverter injects and absorbs reactive power in dependency of its local voltage according to a predefined characteristic (compare to fig. 2.15a). With this control the inverter not only decreases its local voltage during high voltage conditions, but also increases its local voltage during low voltage conditions. A dead band is usually applied to the characteristic in order to avoid reactive power flows at local voltages close to nominal voltage.

B. Local control of reactive power devices

In general, a reactive power device may absorb (e.g. a coil) or inject (e.g. a condenser) reactive power and thus may decrease or increase its local voltage. Since this thesis proposes the $L(U)$-control as a voltage control concept to increase the hosting capacity of a low voltage grid, only Q-absorbing reactive power devices are considered in the following. An obvious approach to locally control the local voltage of such a reactive power device is to use a fixed voltage set point close to the upper voltage limitation for the device's control. If the reactive power device's inductance can be varied continuously and if it is dimensioned sufficiently to absorb the required amount of reactive power it is able to prevent its local voltage from exceeding this set point, regardless the load/production situation within the low voltage grid. Furthermore, such a reactive power device only absorbs reactive power if its local voltage exceeds the defined voltage set point and thus avoids unnecessary control related Q-flows within the grid. This control prevents customers from being discriminated since they aren't forced to provide system services to an individual extent.

---

[10]Average of all prosumers connected to one low voltage grid.

2.3.3. Legal framework

The Austrian grid code requires DGs to be able to provide reactive power and to curtail their active power injection for voltage control purposes. This section gives an overview of the Austrian grid connection rules (from [21]) which are relevant for this thesis. Distributed generators generally have to be able to participate in the static voltage stability of the distribution grid they are connected to. For that purpose, the DGs have to be controlled to comply automatically with the characteristics specified by the responsible DSO. A distributed generator with an inverter bigger than $3.68\,\mathrm{kVA}$ newly connected to an Austrian low voltage grid is legally bound to be able to provide reactive power up to at least $\pm 43.6\,\%$ of the inverter's rated apparent power. This required reactive power support is illustrated in figure 2.14. The inverter's output has to be freely adjustable if its active power output exceeds $90\,\%$ of the inverter's rated apparent power (green area). If the inverter's active power output lies between $20\,\%$ and $90\,\%$ of its rated apparent power, the inverter has to be able to inject and absorb at least $43.6\,\%$ of its rated apparent power, respectively (red framed area). The exact compliance to this minimum requirement is not stipulated any more if the inverter's active power output falls below $20\,\%$ (grey area). This reactive power requirement always takes precedence over the inverter's active power infeed. The participation in
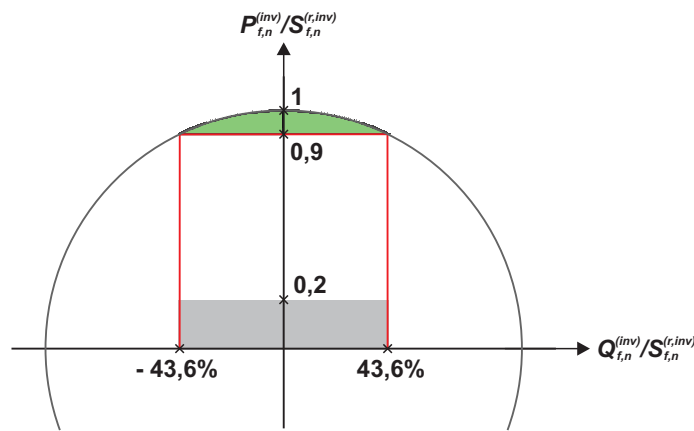

Figure 2.14.: Legally stipulated reactive power range for generating modules with inverters ($S^{(r,inv)} > 3.68\,\mathrm{kVA}$) connected to an Austrian low voltage grid

static voltage stability can be achieved by active power curtailment and by different reactive power control strategies. For distributed generators with inverters with a $S^{(r,inv)} > 3.68\,\mathrm{kVA}$ these reactive power control strategies can be to operate the inverter with a fixed power factor $cos\varphi^{(inv)}$, with a fixed reactive power injection/absorption $Q^{(inv)}$, with an active power output dependent power factor $cos\varphi^{(inv)}(P)$ and with a voltage dependent reactive power injection/absorption $Q^{(inv)}(U)$, respectively. Since the impact of an inverter's control strategy depends on the local network conditions, the responsible DSO is authorised to allocate individual control strategies and characteristics to the different customers, as long they are in scope of the legally stipulated Q-requirements defined in figure 2.14. If no specifications are given by the DSO, the standard setting is a fixed $cos\varphi^{(inv)} = 1$. Figure 2.15a illustrates an exemplary $Q(U)$-characteristic, wherein the four break points (a, b, c and d) have to be freely adjustable within the legally stipulated Q-requirements defined in figure 2.14. Figure 2.15b shows the standard characteristic for the $cos\varphi(P)$ control strategy. Overvoltages can also be prevented by voltage dependent active power curtailment of the injecting generators. Thereby, their active power infeed should only be reduced to the extend which is necessary to prevent their overvoltage protections from disconnecting the generator from the grid. Figure 2.15c shows the standard setting of the $P(U)$-control. Both breaking points can be set differently than proposed in figure 2.15c, if the responsible DSO agrees. The control may not cause oscillations and discontinuities within the output power.
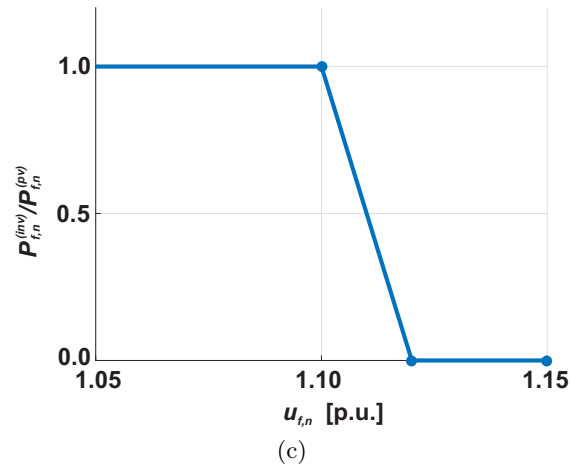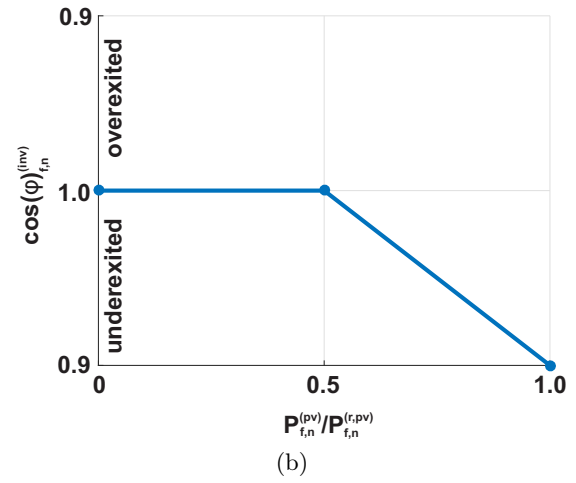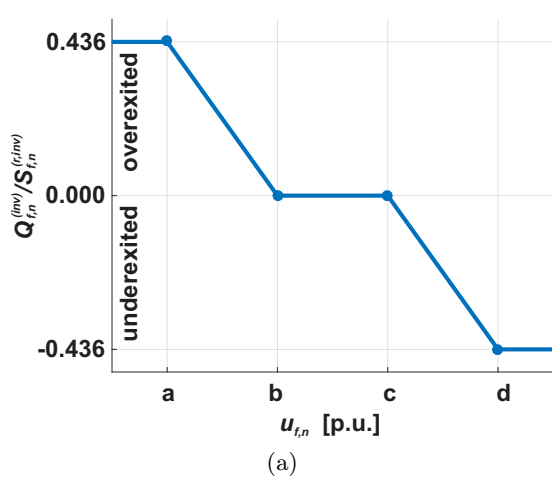
Figure 2.15.: Standard characteristics of the local inverter controls: (a) $Q(U)$-control, (b) $cos\varphi(P)$-control, (c) $P(U)$-control

2.4. Load voltage dependency

In general, the active and reactive power consumption of static loads connected to low voltage grids is a function of their supplying voltage. Different approaches are available to describe the loads' voltage dependency, such as polynomial and exponential load models. In this thesis the polynomial form is used for load modelling. It's also called ZIP model since it comprises constant impedance (Z), constant current (I) and constant power (P) load components. With this approach it is possible to model load compositions embodied by residential, commercial and industrial customers for instance. Mathematically, this approach can be formulated as follows:

$$\frac{P_{f,n}^{(load)}}{P_{f,n}^{(load,init)}} = Z_P \cdot \left(\frac{U_{f,n}}{U^{(r,lv)}} \right)^2 + I_P \cdot \left(\frac{U_{f,n}}{U^{(r,lv)}} \right) + P_P \tag{2.51}$$

$$\frac{Q_{f,n}^{(load)}}{Q^{(load,init)}} = Z_Q \cdot \left(\frac{U_{f,n}}{U^{(r,lv)}} \right)^2 + I_Q \cdot \left(\frac{U_{f,n}}{U^{(r,lv)}} \right) + P_Q \tag{2.52}$$

Whereby $Z_P + I_P + P_P = 1$ and $Z_Q + I_Q + P_Q = 1$. $P_{f,n}^{(load)}$ and $Q_{f,n}^{(load)}$ represent the consumed power at node (f, n) at actual voltage, $P_{f,n}^{(load,init)}$ and $Q_{f,n}^{(load,init)}$ the consumed power at node (f, n) at rated voltage, $U_{f,n}$ the actual voltage and $U^{(r,lv)}$ the rated voltage within the low voltage grid. Z_P and Z_Q describe the load's constant impedance share, I_P and I_Q the load's constant current share and P_P and P_Q the load's constant power share. However, it is difficult to state general applicable ZIP coefficients for specific load classes, since their load compositions change in the short- and long-term as well as regionally. Anyway, [22] presents an experimental determination of the ZIP coefficients of modern residential, commercial and industrial load compositions. Its results are listed in table 7.2 in the appendix and they are used for load modelling in this thesis. Figure 2.16 shows the active and reactive power dependency of a residential customer according to the ZIP coefficients proposed in [22]. It can be seen that especially the customer's reactive power consumption varies with the voltage at his connection point.
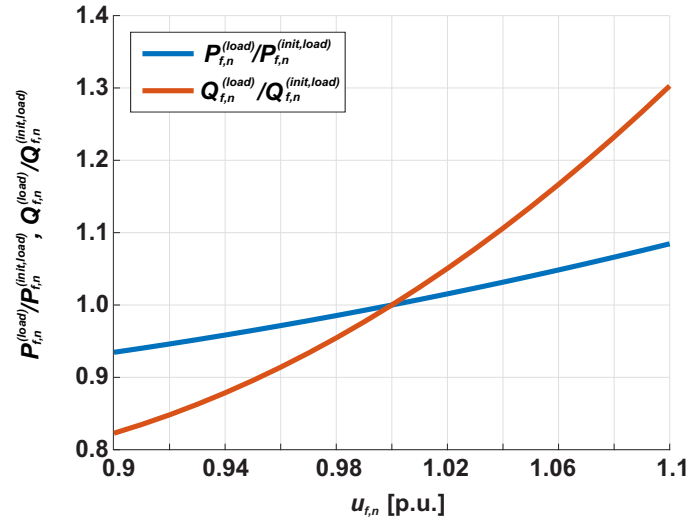

Figure 2.16.: Voltage dependency of a residential customer (type B from table 7.2)

2.5. *LINK*-Solution

LINK-Paradigm is the smart grid paradigm which enables the modelling of the entire power system (i.e. high-, medium-, low voltage levels and the customer plants) and the description of all operation processes (i.e. load - production balance, voltage assessment, demand response, ...) [23]. The *LINK*-Paradigm is defined as a composition of an electrical appliance (be a grid part, producer or storage), the corresponding controlling schema and the Link-Interface. Figure 2.17 shows the components of a Link defined by the *LINK*-Paradigm.
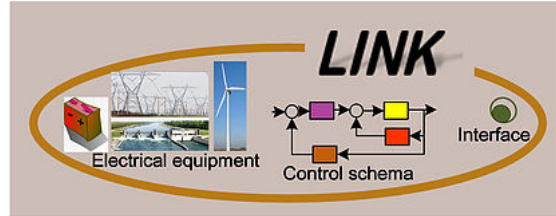

Figure 2.17.: Components of a Link defined by the *LINK*-Paradigm [23]

LINK-Solution is developed based on *LINK*-Paradigm, the resulting holistic model and the unified *LINK*-based architecture, which is supported by *LINK*-technology [23]. It allows a flat business model across the electrical industry and takes into account the electricity market rules and the rigorous cyber security and data privacy requirements. The distributed *LINK*-based architecture reduces in a minimum the amount of exchanged data and enables a secure, reliable and sustainable operation in normal and emergency cases. The *LINK*-based architecture enables the market to flourish and motivates customers to actively participate in the grid operation while maintaining their privacy. [12]

The *LINK*-Paradigm is based on the overall model "The Energy Supply Chain Net" which is defined as follows: An Energy Supply Chain Net is a set of automated power grids, intended for "Chain Links" or "Links", which fit one into another to establish a flexible and reliable electrical connection. Each individual Link or Link-bundle operates independently and has contractual arrangements with other relevant boundary Links, Link-bundles and suppliers which inject directly to their own grid. Each Link or Link-bundle is communicatively coupled with the other relevant neighbour Links or Link-bundles via the usual communication instruments. [12]

Within the "Energy Supply Chain Net Model" each grid part, is it a high voltage grid, a medium voltage grid, a low voltage grid or a customer plant grid, has primary and secondary control for both major quantities, frequency and voltage. Thus, the overall power system is conceived as a set of automated chain links, wherein each grid part represents an independent link on its own.

Based on the *LINK*-Paradigm there are defined three main architecture components: the "Grid-Link", the "Producer-Link" and the "Storage-Link". A Grid-Link consists of three components: A grid part which is called the "Link-Grid", the corresponding secondary control and the "Link-Interfaces". The Link-Grid consists of electrical equipment like overhead lines/cables, transformers and reactive power devices, whereby its transformers and reactive power devices are equipped with their own primary control. The Link-Grid's size is defined from the area, where the secondary control is set up. Each Link-Grid is connected through the corresponding boundary nodes to neighbour Grid-Links and directly connected Producer-Links, Storage-Links and loads. These boundary nodes are called "Boundary Link Node (BLiN)", "Boundary Producer Node (BPN)", "Boundary Storage Node (BSN)" and "Boundary Load Node (BLoN)". The Grid-Link's secondary control sends set points to the Link-Grid's transformers and reactive power devices as well as to its boundary nodes. Figure 2.18a shows a low voltage Link-Grid to which no facility owned reactive power device is connected, while figure 2.18b shows a customer plant Link-Grid to which two loads as well as a Storage- and a Producer-Link are connected. [12]

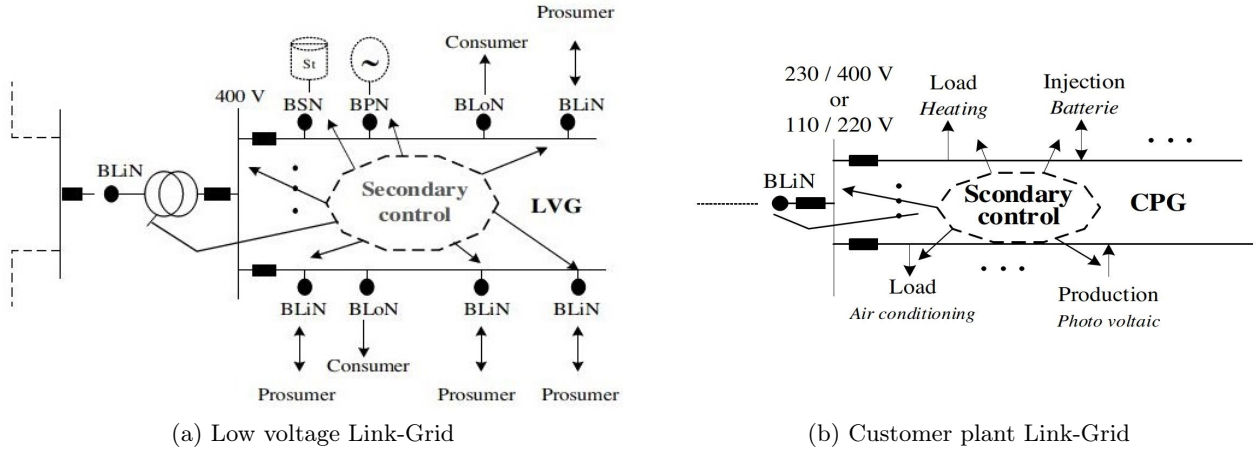(a) Low voltage Link-Grid   (b) Customer plant Link-Grid

Figure 2.18.: Two different types of Link-Grids [12]

Since this thesis focuses on the volt/var behaviour of low voltage Grid-Links the "volt/var secondary control loops", VVSC, are explained in detail in the following. Figure 2.19 schematically presents the resilient volt/var control chain on a typical vertical branch of the European power grid. According to the *LINK*-Paradigm, each Grid-Link has its own VVSC which calculates set points for the Link-Grid's control variables while optimising its own decisions in accordance with its own static constraints and the dynamic constraints imposed by adjacent Links. These dynamic constraints are recalculated in real time dependent on the current situation and thus enable a resilient interaction between adjacent Links. The Link-Grid's control variables include Q-injection/absorption of generators, DGs, inverters and synchronous condensers, switch positions of reactive power devices as well as step positions of transformers. The static constraints include device constraints like PQ-diagrams of generators and inverters, equipment loading, maximal step number of transformers and installed rating of reactive power devices. The Q-exchanges between neighbour Links have a double nature since they can be treated as dynamic constraints and control variables, respectively, depending on the current use-case. More precise, requested Q-values from neighbour Links are treated by the VVSC as dynamic constraints, but it can also use them as control variables to propose new Q-values to neighbour Links. [13]

TSO
Control Center

DSO
Control Center

House Lord
HMU

HV^{Trans}-Link

$HV^{Sub\text{-}Trans}$-Link

MV-Link

LV-Link

CP-Link

(a)

Transmission

Sub transmission

Neighbour
TSO

$\cos f$=const

Static constraint

$CB_{position}$

$VVSC^{HV\text{-}T}$

$Q_{set\ point}$

380.0 kV

$Q_{HV}^{HV^{Trans}}_{Sub\text{-}Trans.}$

Static constraint

Neighbour
DSO

$\cos f$=const

Static constraint

$CB_{position}$

$VVSC^{HV\text{-}S}$

$Q_{set\ point}$

110.0 kV

$Q_{MV}^{HV^{Sub\text{-}Trans.}}$

Dynamic constraint

30.0 kV

$U_{set\ point}$

$Q_{set\ point}$

$Q_{set\ point}$

$VVSC^{MV}$

$Q_{set\ point}$

$Q_{set\ point}$

30.0 kV

Q_{LV}^{MV}

Dynamic constraint

0.4 kV

$U_{set\ point}$

$VVSC^{LV}$

$VVSC^{CP}$

Q_{CP}^{LV}

(b)

External interface between
TSO and DSO control centres

Internal interface
between
applications

Internal interface
between
applications

External interface
between
DSO control centre and
HMU

HV^{Trans}-Link

Q

$HV^{Sub\text{-}Trans}$-Link
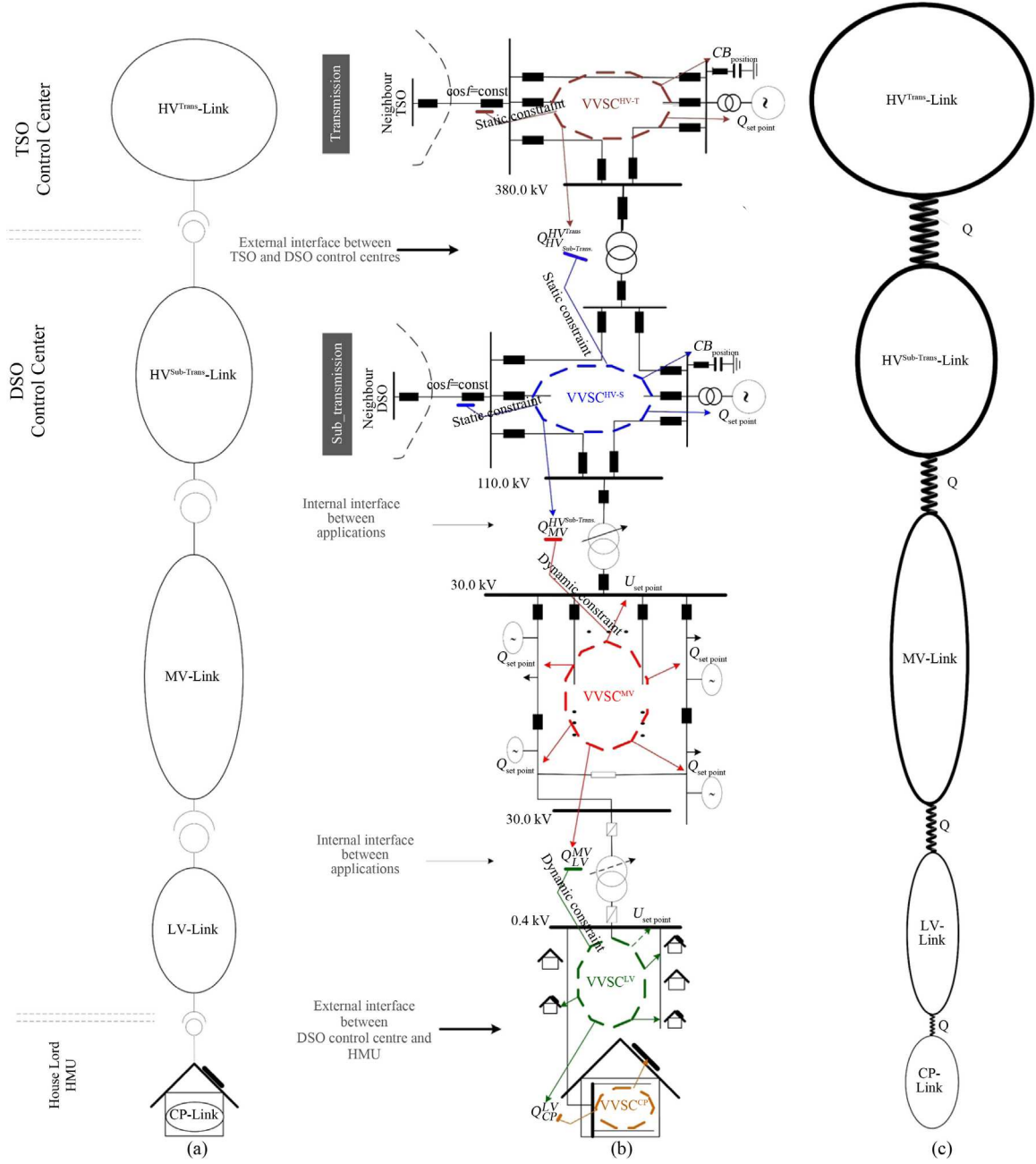
Q

MV-Link

Q

LV-
Link

Q

CP-
Link

(c)

Figure 2.19.: Schematic presentation of the resilient volt/var secondary control chain: (a) Link structure; (b) volt/var control loops; (c) resilient connection over the reactive power [13]

3. Model description

This chapter describes the network-, load-, producer-, line- and transformer models which are used for the simulations. Section 3.1 gives an overview of the used low voltage Link-Grid models, i.e. their topology, customer structure, photovoltaic penetration, cable share and the electrical data of the supplying transformer and the overhead lines and cables. Section 3.2 shows how the customers' native loads are modelled, i.e. the assumed initial power factor for each customer class and the used ZIP-coefficients to model their voltage dependencies. Section 3.3 shows how the customers' photovoltaic systems are modelled, i.e. the assumed inverter ratings, the modelling of their overvoltage protections and the characteristics of the different simulated active power curtailment and reactive power management strategies as well as the modelling of the $L(U)$-control.

3.1. Low voltage test-grids

To get an informative impression of the $L(U)$-control's effectiveness among various network conditions, four European low voltage grids differing in size, transformer rating, customer structure, photovoltaic penetration and cable share are used for the simulations. Three different customer classes occur in these networks: Residential, commercial and industrial customers. For this thesis the complete single-phase network models - including topology, line and transformer data as well as the billing demand, class and location of each customer and the nominal power and location of the installed photovoltaic systems - are provided by the "Institute of Energy Systems and Electrical Drives" of the "Vienna University of Technology". Furthermore, for each network the total annual energy consumption $E_{sec}^{(2016)}$ and the peak active power $P_{sec}^{(2016)}$ occurred throughout the year, measured during 2016 at the transformers' secondary sides, are provided for this thesis. Table 3.1 and 3.2 give a short overview of the simulated networks' properties. Since in this thesis the the low voltage grids' behaviour is evaluated from the holistic point of view proposed by the *LINK*-Paradigm, these test-grids are called Link-Grids in the following.

Link-Grid	$N^{(res)}$	$N^{(com)}$	$N^{(ind)}$	$P^{(r,pv)}$ [kW]	$E_{sec}^{(2016)}$ [kWh]	$P_{sec}^{(2016)}$ [kW]
Theoretical	80	0	0	200	-	-
Large Urban	175	0	0	168	1127040	349
Small Urban	91	0	0	101	990755	242
Rural	61	0	0	20	320165	85
Industrial	7	4	10	30	1022510	455

Table 3.1.: Overview of the Link-Grids' customer structure

Link-Grid	F	cable share [% of km]	total line length [km]	max feeder length [km]	$S^{(r,tr)}$ [kVA]
Theoretical	4	50.00	10.540	1.630	160
Large Urban	9	96.14	12.815	1.270	630
Small Urban	6	81.11	4.975	0.610	400
Rural	4	58.64	6.335	1.630	160
Industrial	3	100.00	2.091	0.715	800

Table 3.2.: Overview of the Link-Grids' size

In addition to the four provided Austrian low voltage grids, a theoretical grid, including two feeders consisting solely of overhead lines and two feeders consisting solely of cables is created. This simplified grid is used to compare the different inverter controls with each other and with the $L(U)$-control. The measured energy consumption $E_{sec}^{(2016)}$ in table 3.1 equates to the superposition of the PV-production, the customers' consumption and the grid losses throughout the whole year. Anyway, for the grids where only residential customers occur, equation (3.1) is used to estimate the annual energy consumption per resident. The resulting energy values are used to assign appropriate ZIP-coefficients to the residents within the different networks. Table 7.3 in the appendix shows the assignment of ZIP-coefficients to the residents connected to the individual Link-Grids.

$$E_{res} = \frac{E_{sec}^{(2016)}}{N_{res}} \tag{3.1}$$

The applied low voltage Link-Grids contain different types of cables and overhead lines. Their electrical data is listed in table 7.6 in the appendix. The cable data comply with the factual data from their producer, but due to a lack of information for the overhead lines a set of data from the PSS SINCAL libraries is used within the network models.

In the appendix, figure 7.1 to 7.5 illustrate detailed information about the networks' topologies and the actually installed PV-systems. Furthermore, table 7.7 provides the data of the Link-Grids' transformers and table 7.8 gives a feeder specific overview of each network model.

3.1.1. Theoretical Link-Grid

The theoretical Link-Grid consists of four feeders, two identical cable-feeders, C1 and C2, and two identical overhead line-feeders, L1 and L2. The topologies of all these feeders equal to that from feeder 1 of the Rural Link-Grid, which is described in section 3.1.2 C. Also the distribution transformer equals to that from the Rural Link-Grid. Table 3.3 shows which cables and overhead lines are used for the feeders' main[1]- and sub[2]-branches. A residential customer with a billing demand of 4 kW is located at the end of each

C1/C2	main branch	C-AL-150
	sub branches	C-AL-50
L1/L2	main branch	OL-AL-95
	sub branches	OL-AL-50

Table 3.3.: Line data of the theoretical Link-Grid

sub-branch. Additionally, a 5 kWp photovoltaic system is located at the end of each sub branch of the feeders C1 and L1. In the simulations, the slack is always located at the distribution transformer's primary side.
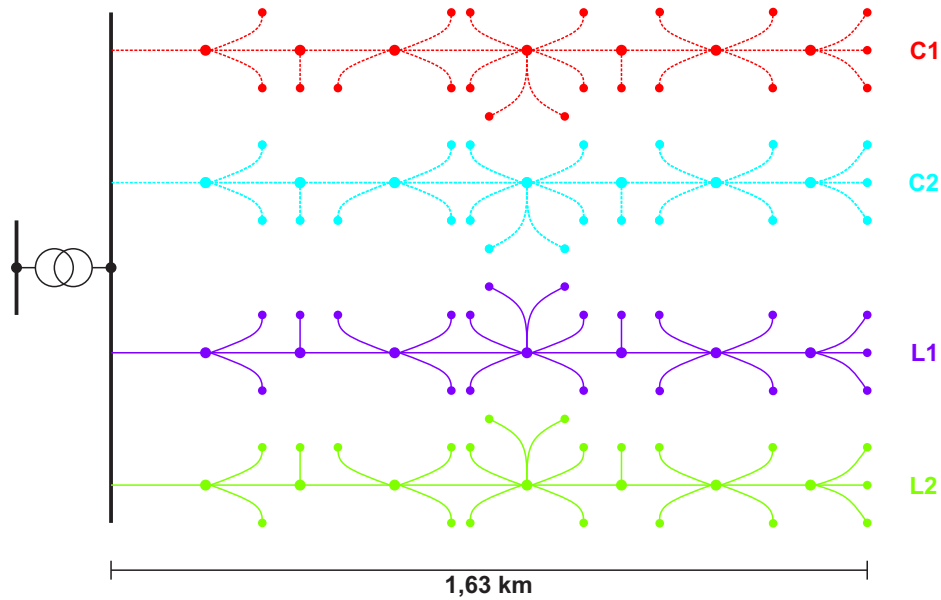
Figure 3.1.: Theoretical Link-Grid

---

[1]Connections between the transformer station and distribution cabinets and between distribution cabinets (in case of a cable feeder).

[2]Connections between the distribution cabinets and the customers (in case of a cable feeder).

3.1.2. Real Link-Grids

A. Large Urban Link-Grid

Figure 3.2 shows an overview of the Large Urban Link-Grid. Only the main-branches of the feeders are shown in this figure. Figure 7.2 in the appendix contains more details of the Large Urban Link-Grid. This relatively large grid with a cable share of about 96% supplies solely urban residential customers.
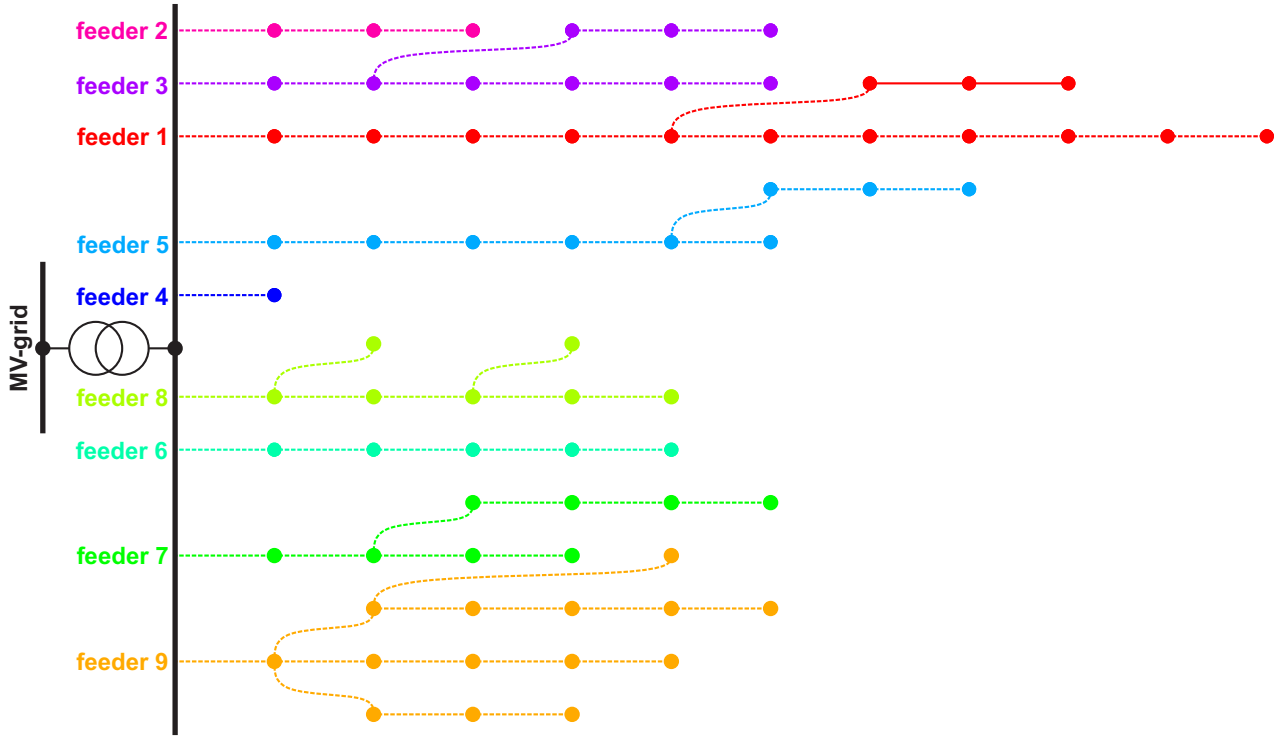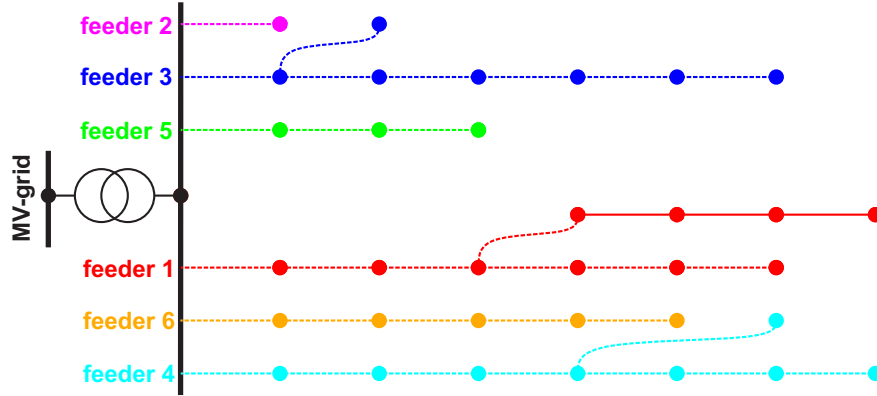

Figure 3.2.: Large Urban Link-Grid (simplified)

Many of these residents are new build single-familiy houses larger than average residents. This results in a relatively[3] high annual energy consumption of about 6.64 MW h per resident, estimated with eq. (3.1). Alltogether, this Link-Grid contains 9 feeders and supplies 175 residential customers. Its distribution transformer is not equipped with an on load tap changer. In the simulations, the slack is always located at the distribution transformer's primary side.

---

[3]According to [24], the annual electric energy consumption per resident is about 4394 kW h in Austria.

B. Small Urban Link-Grid

Figure 3.3 shows an overview of the Small Urban Link-Grid. Only the main-branches of the feeders are shown in this figure. Figure 7.3 in the appendix contains more details of the Small Urban Link-Grid. This

Figure 3.3.: Small Urban Link-Grid (simplified)

relatively small grid with a cable share of about 81% supplies solely urban residential customers. Most of these residents are new build single-family houses larger than average residents. This leads to a very high annual energy consumption of about 10.89 MW h per resident, determined with equation (3.1). Alltogether, this Link-Grid contains 6 feeders and supplies 91 residential customers. Its distribution transformer is not equipped with an on load tap changer. In the simulations, the slack is always located at the distribution transformer's primary side.

C. Rural Link-Grid

Figure 3.4 shows an overview of the Rural Link-Grid. Only the main-branches of the feeders are shown in this figure. Figure 7.4 in the appendix contains more details of the Rural Link-Grid. This relatively small
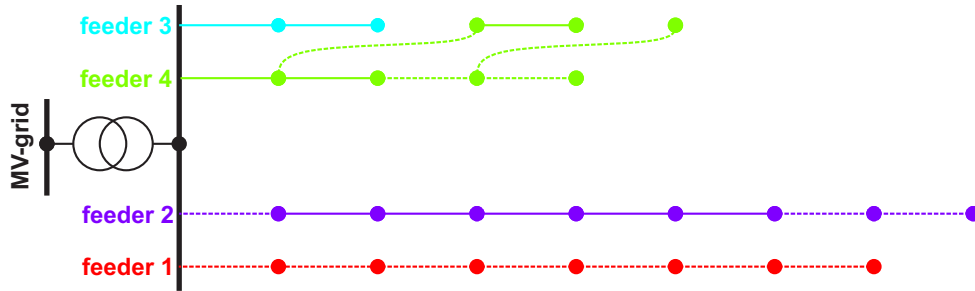
Figure 3.4.: Rural Link-Grid (simplified)

grid with a cable share of about 59% supplies rural residential customers. According to equation (3.1), these residents anually consume about 5248.61 kW h in average. Alltogether, this Link-Grid contains 4 feeders and supplies 61 residential customers. Its distribution transformer is not equipped with an on load tap changer. In the simulations, the slack is always located at the distribution transformer's primary side.

D. Industrial Link-Grid

Figure 3.5 shows an overview of the Industrial Link-Grid. Only the main-branches of the feeders are shown in this figure. Figure 7.5 in the appendix contains more details of the Industrial Link-Grid. This
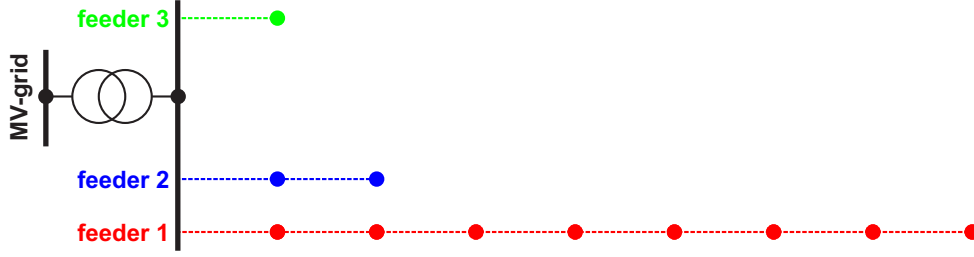

Figure 3.5.: Industrial Link-Grid (simplified)

relatively small grid with a cable share of 100% supplies mainly industrial and a few commercial and residential customers. Due to the large industrial load, the whole main-branch of feeder 1 consist of two parallel cables, whereby its sub-branches constist of just one cable. Feeder 3 also consist of two parallel cables. Because it's not possible to estimate the resident's annual consumption, a consumption of about 4.39 MW h is assumed according to [24]. All together, this Link-Grid contains 3 feeders and supplies 7 residential, 4 commercial and 10 industrial customers. Its distribution transformer is not equipped with an on load tap changer. In this grid, nearly all industrial loads are located at feeder 1, just one, but by far the largest, is located at feeder 3. Feeder 2 supplies solely residential and commercial customers. In the simulations, the slack is always located at the distribution transformer's primary side.

3.2. Load modelling

The customers connected to the Link-Grids are characterised by their active and reactive power consumption. The initial value of a customer's active power consumption $P_{f,n}^{(load,init)}$ is defined by the scenario, whereas the initial value of the reactive power consumption $Q_{f,n}^{(load,init)}$ consequently arises from the assumed power factor. The assumed power factors for each customer class are listed in table 3.4.

	residential	commercial	industrial
$\cos\varphi^{(\mathbf{load,init})}$	0,95	0,90	0,90

Table 3.4.: Power factors of different load classes and generators

All customers are modelled as *PQ*-loads with an inherent ZIP model. The ZIP coefficients used for residential, commercial and industrial customers are summarised in table 7.2 in the appendix and refer to [22]. This paper proposes different sub classes for residential customers depending on their annual energy consumption. For each Link-Grid, one of these sub classes is chosen for all residents within the network according to the above estimated annual consumption per resident. Within the residential sub classes, the annual energy consumption is increasing from type A to type C. The assignment of sub classes to the residential customers in the different networks is listed in table 7.3 in the appendix. [22] also proposes different subclasses for the commercial customers depending on their business fields. Since four commercial customers are located in the Industrial Link-Grid, for each of these customers different ZIP coefficients are chosen from table 7.2. Table 7.4 in the appendix contains the allocation of ZIP coefficients to the commercial customers in the Industrial Link-Grid.

3.3. Generation modelling

Photovoltaic systems include a PV-array, an inverter and an overvoltage protection. The active power output of each PV-array $P_{f,n}^{(pv)}$ is defined in chapter 4. These P-values are influenced by the inverters' voltage control characteristics and the overvoltage protections before they are exchanged with the grid. The inverters are assumed to be over dimensioned according to equation (3.2).

$$S_{f,n}^{(r,inv)} = \frac{1}{0,9} \cdot P_{f,n}^{(r,pv)} \tag{3.2}$$

Figure 3.6 illustrates an inverter's PQ-characteristic, where the nominal power of both, the photovoltaic array and the inverter are included. During peak generation periods, such an inverter can absorb or inject reactive power in the amount of approximately $43.59\,\%$ of its rated apparent power.
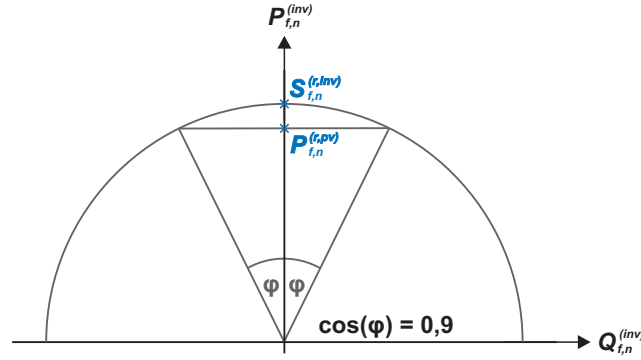
Figure 3.6.: PQ-diagram of the photovoltaic inverters

Furthermore, the inverters are assumed to have an efficiency of $100\,\%$. The inverters' control characteristics used to simulate the different voltage control strategies are explained in detail in the following sections. Table 7.5 in the appendix contains all the break points[4] of the inverter characteristics shown in figures 3.8 to 3.10. The overvoltage protection disconnects the PV-array from the inverter if the local voltage exceeds 1.1 p.u.. Figure 3.7 shows the overvoltage protections' behaviour as a volt/watt curve.
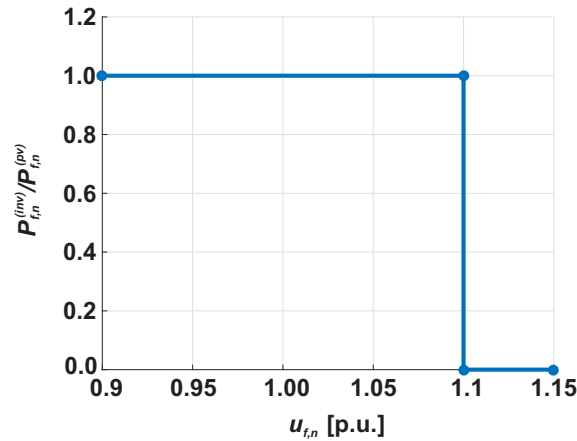

Figure 3.7.: $P(U)$-characteristic of a photovoltaic system's overvoltage protection

---

[4]These break points are marked with blue dots in the figures.

3.3.1. Uncontrolled inverters

For simulating the CP-Producer-Links with uncontrolled inverters, each PV-inverter is modelled as a PQ-producer which injects active power with a $cos(\varphi) = 1$.

3.3.2. *P(U)*-controlled inverters

For simulating the CP-Producer-Links with $P(U)$-controlled inverters, each PV-inverter is modelled as a PQ-producer which injects active power with a $cos(\varphi) = 1$. These inverters are additionally equipped with a $P(U)$-control. The corresponding control characteristic is shown in figure 3.8.
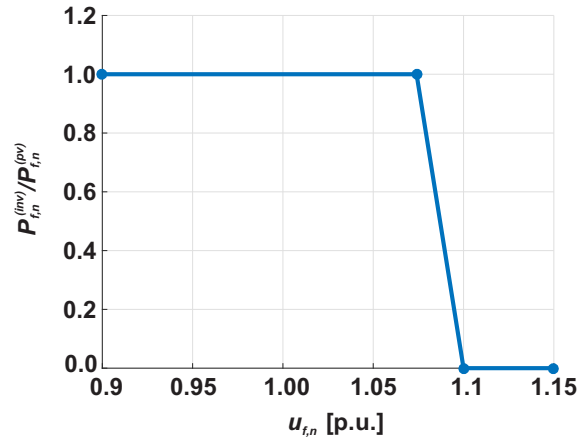
Figure 3.8.: *P(U)*-characteristic of a photovoltaic-inverter

3.3.3. *Q(U)*-controlled inverters

For simulating the CP-Producer-Links with $Q(U)$-controlled inverters, each PV-inverter is modelled as a $Q = f(U)$-producer. While the active power injection of such an inverter is not influenced by the control strategy, its reactive power absorption/injection is a function of its local voltage. The applied control characteristic for the $Q(U)$-control is shown in figure 3.9.
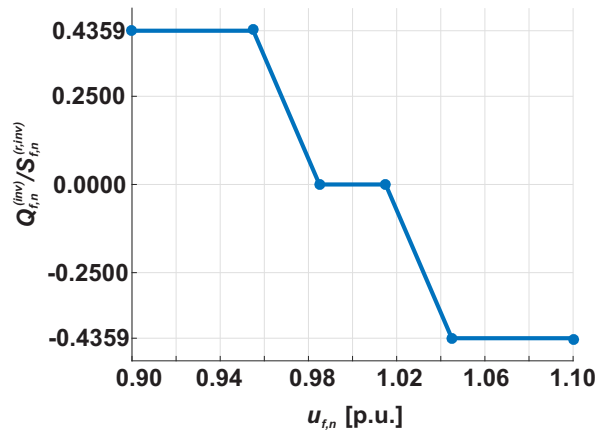
Figure 3.9.: *Q(U)*-characteristic of a photovoltaic-inverter

3.3.4. $cos\varphi(P)$-controlled inverters

For simulating the CP-Producer-Links with $cos\varphi(P)$-controlled inverters, each PV-inverter is modelled as a $cos(\varphi) = f(P)$-producer. While the active power injection of such an inverter is not influenced by the control strategy, its reactive power absorption/injection is a function of the corresponding photovoltaic array's output power. The applied control characteristic for the $cos\varphi(P)$-control is shown in figure 3.10.
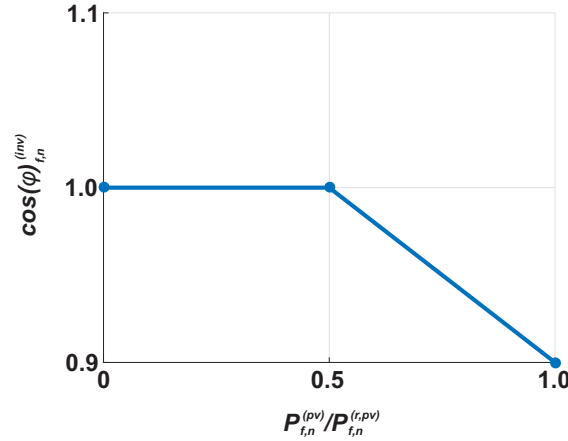

Figure 3.10.: $cos\varphi(P)$-characteristic of a photovoltaic-inverter

3.3.5. $L(U)$-controlled LV-Grid-Link

The exact locations of the control-coils which are connected to the low voltage Link-Grids are shown in figures 7.1 to 7.5 in the appendix. For simulating the LV-Grid-Link operation with $L(U)$-control, the control coils are modelled as continuously variable shunt elements with a voltage set point at 1.09 p.u.. These shunt elements are dimensioned sufficient to absorb any amount of reactive power, but they cannot inject any reactive power. Furthermore, the coils are assumed to have no resistance thus they don't absorb any active power.

3.3.6. Q-autarkic customers

For simulating the Q-autarkic customers, each PV-inverter is modelled as a PQ-producer which injects active power with a $cos(\varphi) = 1$. All customers, even those without a photovoltaic system, are assumed to consume active power with a $cos(\varphi) = 1$.

3.4. Line modelling

All overhead lines and cables are modelled with the equivalent circuit diagram according to figure 3.11. $R^{(sgm)}$, $X^{(sgm)}$ and $B^{(sgm)}$ can be determined from the line parameters listed in table 7.6 according to
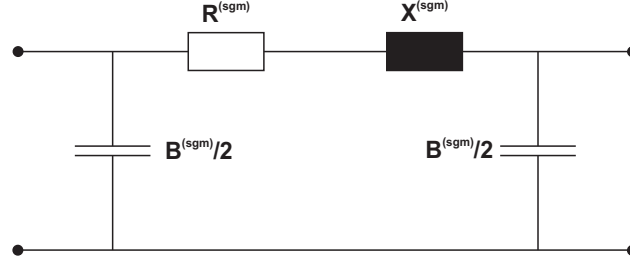

Figure 3.11.: Model of a line

equations (3.3), (3.4) and (3.5).

$$R^{(sgm)} = R' \cdot l \tag{3.3}$$

$$X^{(sgm)} = X'_L \cdot l \tag{3.4}$$

$$B^{(sgm)} = 2\pi f \cdot C' \cdot l \tag{3.5}$$

Where l is the line's length, R' its specific resistance, X'_L its specific reactance, C' its specific capacitance and f the system frequency of $50\,\mathrm{Hz}$.

3.5. Transformer modelling

All transformers are modelled with the equivalent circuit diagram according to figure 3.12. Where $Y^{(tr)} = 0$
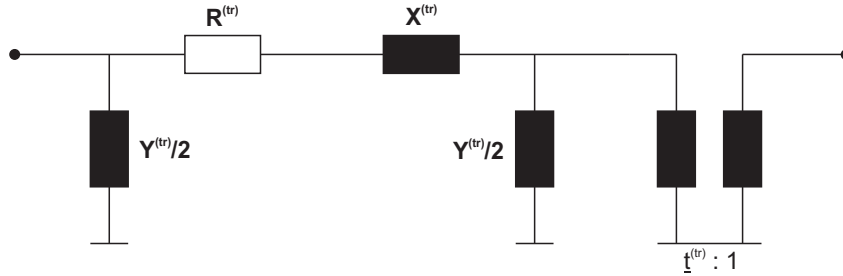
Figure 3.12.: Model of a transformer

since the transformers' core losses are neglected in this thesis. $R^{(tr)}$ and $X^{(tr)}$ can be determined from the transformer parameters listed in table 7.7 according to equations (3.6) and (3.7).

$$R^{(tr)} = u_r \cdot \frac{\left(U^{(r,tr,p)}\right)^2}{S^{(r,tr)}} \tag{3.6}$$

$$X^{(tr)} = \sqrt{u_k^2 - u_r^2} \cdot \frac{\left(U^{(r,tr,p)}\right)^2}{S^{(r,tr)}} \tag{3.7}$$

4. Scenario definition

Several scenarios are defined in this chapter to evaluate the different control strategies. Each of the provided network models includes a base case which correlates with the peak active power measured throughout 2016 at the transformer's secondary side. These base cases are presented in section 4.1. In section 4.2 are set a couple of scenarios to analyse the minimal and maximal load case, while in section 4.3 are included some scenarios which vary the PV-penetration or the distributed electricity production. The combination of different scenarios reveals the most relevant cases of load and production levels. Moreover, the voltage value on the primary side of the distribution transformer affects explicitly the voltages within the LV-networks and thus the loads' and the control devices' behaviour. In section 4.4 is defined a range for the primary voltage of the distribution transformer, while in section 4.5 is presented an overview of all simulated scenarios for the theoretical and the real Link-Grids.

4.1. Base cases

The base case for each of the real Link-Grids is based on the maximum active power flow measured throughout 2016 at secondary side of the distribution transformer (table 3.1). In each base case, each customer is characterised by his individual active power consumption, while his reactive power consumption is calculated based on his P-value and the corresponding power factor (see table 3.4). All customers connected to the Large Urban, the Small Urban and the Rural Link-Grid are residential. All residential customers are modelled to consume the same amount of power. Table 4.1 presents the P- and Q-demand of each customer, the number of customers and the aggregated P- and Q-demand of all customers for the Large Urban, the Small Urban and the Rural Link-Grid. In the Industrial Link-Grid are connected

Link-Grid	$N^{(res)}$	$P_{f,n}^{(load,init)}$ [kW]	$Q_{f,n}^{(load,init)}$ [kvar]	$P_{basecase}^{(load,init)}$ [kW]	$Q_{basecase}^{(load,init)}$ [kvar]
Large urban	175	1.9560	0.6429	342.3000	112.5086
Small urban	91	2.6200	0.8612	238.4200	78.3649
Rural	61	1.3680	0.4496	83.4480	27.4280

Table 4.1.: Base cases of the Large Urban, the Small Urban and the Rural Link-Grid

residential, commercial and industrial customers. In this case, the overall load is portioned according to the customers' billing demands. Table 4.2 presents the individual P- and Q-demand of each customer of the Industrial Link-Grid for the base case. The base case of each network is used in the following sections to define the simulated load/production-scenarios.

Busbar	$P_{f,n}^{(load,init)}$ [kW]	$Q_{f,n}^{(load,init)}$ [kvar]	Customer classification	Busbar	$P_{f,n}^{(load,init)}$ [kW]	$Q_{f,n}^{(load,init)}$ [kvar]	Customer classification
(1,1)	8.9440	2.9398	residential	(1,9)	4.4720	2.1659	commercial
(1,2)	7.8260	3.7903	industrial	(1,10)	5.5900	2.7074	industrial
(1,3)	4.4720	2.1659	industrial	(1,11)	44.7200	21.6589	industrial
(1,4)	4.4720	2.1659	industrial	(2,1)	22.3600	7.3494	residential
(1,5)	41.3660	20.0345	industrial	(2,2)	22.3600	10.8294	commercial
(1,6)	4.4720	2.1659	industrial	(2,3)	27.9500	13.5368	commercial
(1,7)	1.1180	0.5415	industrial	(2,4)	13.4160	6.4977	commercial
(1,8)	11.1800	5.4147	industrial	(3,1)	223.6000	108.2944	industrial

Table 4.2.: Base case of the Industrial Link-Grid

4.2. Consideration of different load values

The above described base cases are used as the maximum (max) load scenarios for each of the real Link-Grids. For the theoretical Link-Grid, the same active and reactive power consumption per customer is assumed as in the Rural Link-Grid. Furthermore, for each Link-Grid one minimum (min) load scenario is derived from its maximum load scenario. To attain a low but still realistic load during periods wherein a high photovoltaic infeed may occur, the load profiles from [16], which are illustrated in figure 4.1, are evaluated at 12 h for each customer class. According to figure 4.1, the minimum consumption of the
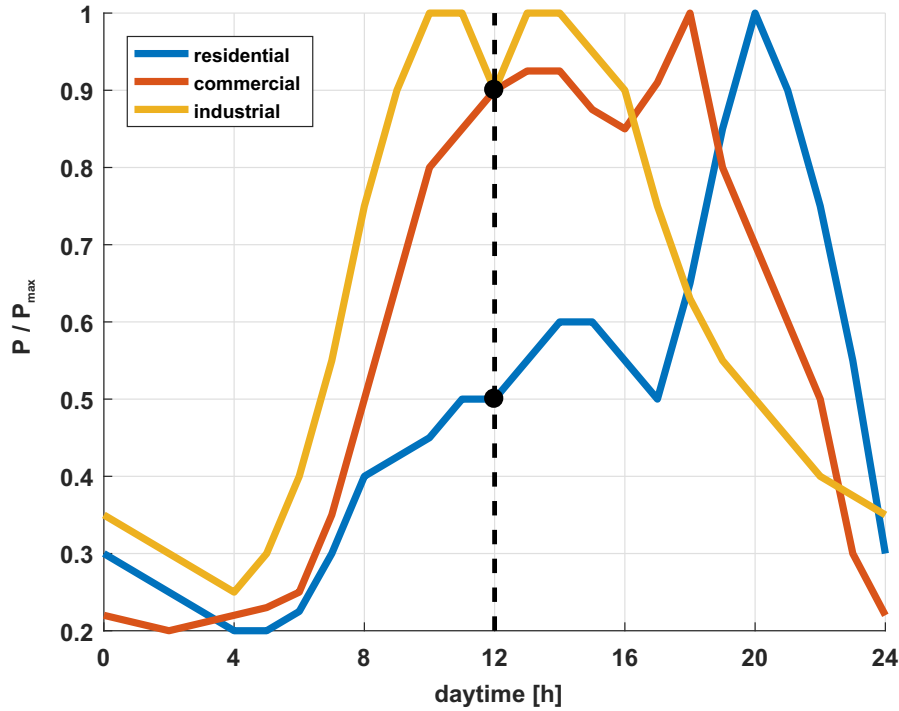

Figure 4.1.: Daily load profiles for different customer classes

residential customers is assumed to be half their maximum consumption. The commercial and industrial customers are assumed to consume 90 % of their maximum consumption during midday. The resulting values are used as the minimum load scenarios. Table 4.3 shows the aggregated P- and Q-consumption of all customers for the maximum and minimum load scenarios of the theoretical and the real Link-Grids. The individual consumption of the Industrial Link-Grid's customers can be found in table 7.1 in the appendix.

Link-Grid	$P_{max}^{(load,init)}$ [kW]	$Q_{max}^{(load,init)}$ [kvar]	$P_{min}^{(load,init)}$ [kW]	$Q_{min}^{(load,init)}$ [kvar]
Theoretical	109.4400	35.9680	54.7200	17.9840
Large urban	342.3000	112.5086	171.1500	56.2543
Small urban	238.4200	78.3649	119.2100	39.1825
Rural	83.4480	27.4280	41.7240	13.7140
Industrial	448.3180	212.2582	390.9646	186.9168

Table 4.3.: Minimum and maximum load scenarios of all Link-Grids

4.3. Consideration of different PV-penetration levels

In the theoretical Link-Grid, exclusively the customers connected to the cable-feeder C2 and the overhead line-feeder L2 own a 5 kWp photovoltaic-system. Two different production scenarios are defined for those PV-systems in section 4.3.1. For the real Link-Grids, three different PV-penetration levels are defined in section 4.3.2.

4.3.1. Theoretical Link-Grid

In the theoretical Link-Grid, an active power production of 5 kW is assumed for each of the photovoltaic-arrays for the maximum (max) production scenario. Furthermore, another scenario is defined where none of the PV-arrays produce any active power. Table 4.4 summarises the production scenarios for the theoretical Link-Grid.

Scenario	$P_{f,n}^{(pv)}$ [kW]	$P^{(pv)}$ [kW]
no production	0	0
max production	5	200

Table 4.4.: Production scenarios for the theoretical Link-Grid

4.3.2. Real Link-Grids

For each of the real Link-Grids, a minimum (min), a medium (mid) and a maximum (max) PV-penetration scenario is considered. For the minimum PV-penetration scenarios, only the already existing PV-systems with their individual ratings according to figures 7.2, 7.3, 7.4 and 7.5 in the appendix are connected to the Link-Grids. For the medium PV-penetration scenarios, half of the customers own the same photovoltaic-system dimensioned according to table 4.5 and these PV-systems are evenly distributed within the Link-Grids. For the maximum PV-penetration scenarios, each of the customers own the same photovoltaic-system dimensioned according to table 4.5. For all three scenarios, the PV-arrays are assumed to produce 100 % of their ratings. Table 4.5 summarises the aggregated active power production of the PV-arrays for each of the real Link-Grids and each PV-penetration scenario.

Link-Grid	PV-penetration	$P_{f,n}^{(pv)}$ [kW]	$P^{(pv)}$ [kW]
Large Urban	min	-	168
	mid	5	440
	max	5	875
Small Urban	min	-	101
	mid	8	368
	max	8	728
Rural	min	-	20
	mid	5	155
	max	5	305
Industrial	min	-	30
	mid	45	360
	max	45	720

Table 4.5.: Production scenarios of the real Link-Grids

4.4. Consideration of the distribution transformer's primary voltage

LV-grids are connected to MV-grids through distribution transformers which usually have fixed tap positions. This means that the voltage of the MV-feeder is directly applied to the LV-feeder with the corresponding transformation factor. The transformer's primary voltage varies depending on its position at the MV-feeder and the MV-feeder's loading, as exemplary illustrated in figure 4.2. The DSO whose re-

Figure 4.2.: Distribution transformers connected at different locations of a MV-feeder

sponsible for the simulated LV-Link-Grids allows voltage variations between -4 % and +6 % in his medium voltage grids, thus all primary voltage values are assumed to lie between 0.96 p.u. and 1.06 p.u..

4.5. Scenario overview

This section provides an overview of all investigated scenarios for the theoretical and the real Link-Grids.

4.5.1. Theoretical Link-Grid

For the theoretical Link-Grid, all four load/production combinations are simulated with individual values for the transformer's primary voltage. Table 4.6 shows an overview of the investigated scenarios for the theoretical Link-Grid.

Name	Short name	$u^{(tr,p)}$ [p.u.]	Load	Production
min load, no production	$\mathbf{L^{(min)} - G^{(min)}}$	0.99	min	no
max load, no production	$\mathbf{L^{(max)} - G^{(min)}}$	0.96	max	no
min load, max production	$\mathbf{L^{(min)} - G^{(max)}}$	1.06	min	max
max load, max production	$\mathbf{L^{(max)} - G^{(max)}}$	1.01	max	max

Table 4.6.: Overview of the investigated scenarios for the theoretical Link-Grid

4.5.2. Real Link-Grids

For each of the real Link-Grids, all six load/production combinations are simulated with a voltage of 1.06 p.u. at the transformer's primary side. Table 4.7 shows an overview of the investigated scenarios for the real Link-Grids.

Link-Grid	Name	Short name	$u^{(tr,p)}$ [p.u.]	Load	Production
Large urban	min load, min production	$\mathbf{L^{(min)} - G^{(min)}}$	1.06	min	min
	max load, min production	$\mathbf{L^{(max)} - G^{(min)}}$	1.06	max	min
	min load, mid production	$\mathbf{L^{(min)} - G^{(mid)}}$	1.06	min	mid
	max load, mid production	$\mathbf{L^{(max)} - G^{(mid)}}$	1.06	max	mid
	min load, max production	$\mathbf{L^{(min)} - G^{(max)}}$	1.06	min	max
	max load, max production	$\mathbf{L^{(max)} - G^{(max)}}$	1.06	max	max
Small urban	min load, min production	$\mathbf{L^{(min)} - G^{(min)}}$	1.06	min	min
	max load, min production	$\mathbf{L^{(max)} - G^{(min)}}$	1.06	max	min
	min load, mid production	$\mathbf{L^{(min)} - G^{(mid)}}$	1.06	min	mid
	max load, mid production	$\mathbf{L^{(max)} - G^{(mid)}}$	1.06	max	mid
	min load, max production	$\mathbf{L^{(min)} - G^{(max)}}$	1.06	min	max
	max load, max production	$\mathbf{L^{(max)} - G^{(max)}}$	1.06	max	max
Rural	min load, min production	$\mathbf{L^{(min)} - G^{(min)}}$	1.06	min	min
	max load, min production	$\mathbf{L^{(max)} - G^{(min)}}$	1.06	max	min
	min load, mid production	$\mathbf{L^{(min)} - G^{(mid)}}$	1.06	min	mid
	max load, mid production	$\mathbf{L^{(max)} - G^{(mid)}}$	1.06	max	mid
	min load, max production	$\mathbf{L^{(min)} - G^{(max)}}$	1.06	min	max
	max load, max production	$\mathbf{L^{(max)} - G^{(max)}}$	1.06	max	max
Industrial	min load, min production	$\mathbf{L^{(min)} - G^{(min)}}$	1.06	min	min
	max load, min production	$\mathbf{L^{(max)} - G^{(min)}}$	1.06	max	min
	min load, mid production	$\mathbf{L^{(min)} - G^{(mid)}}$	1.06	min	mid
	max load, mid production	$\mathbf{L^{(max)} - G^{(mid)}}$	1.06	max	mid
	min load, max production	$\mathbf{L^{(min)} - G^{(max)}}$	1.06	min	max
	max load, max production	$\mathbf{L^{(max)} - G^{(max)}}$	1.06	max	max

Table 4.7.: Overview of the investigated scenarios for the real Link-Grids

5. Evaluation procedure

Section 5.1 describes how the simulation results are summarised to attain a clear overview of the Link-Grids' behaviours. Not all of the quantities defined in section 5.1 are used to evaluate the performance of the grid. Section 5.2 describes the evaluation criteria, i.e. the quantities which are used to evaluate the performances of the grids. Furthermore, it describes how the results of multiple simulations are processed to enable the visualisation of the grid's performance within a single diagram.

5.1. Result evaluation

The simulation results contain all node-voltages ($U_{f,n}$, $u_{f,n}$), the P- and Q-flows through ($P^{(tr,p)}$, $Q^{(tr,p)}$, $P_{f,n}^{(sgm)}$, $Q_{f,n}^{(sgm)}$, $P_{f,n}^{(rct)}$, $Q_{f,n}^{(rct)}$) and the loading of the electrical equipment ($\mathcal{L}_{f,n}^{(sgm)}$, $\mathcal{L}^{(tr)}$) and the active and reactive power consumption ($P_{f,n}^{(load)}$, $Q_{f,n}^{(load)}$) and production ($P_{f,n}^{(inv)}$, $Q_{f,n}^{(inv)}$) of each customer. This large amount of data is summarised according to the following definitions in order to attain an informative overview of the Link-Grids' behaviour for each of the simulated scenarios.

5.1.1. Voltage violation index

The voltage violation index $N^{(viol)}$, called shortly violation index in the following, represents the number of network-nodes which violate the lower or upper voltage limitation of 0.9 p.u. and 1.1 p.u., respectively.

5.1.2. Voltage spreading

The voltage spreading $\Delta U^{(sdg)}$ is the difference between the maximum and minimum node-voltage within the simulated Link-Grid. It is calculated with equation (5.1).

$$\Delta U^{(sdg)} = max\left(U^{(tr,s)}, U_{f,n}\right) - min\left(U^{(tr,s)}, U_{f,n}\right) \tag{5.1}$$

Since the voltage values from the simulation results ($U^{(tr,s)}$ and $U_{f,n}$) represent line to line voltages, also the determined voltage spreading represents a line to line voltage.

5.1.3. Power losses

The active $P^{(loss)}$ and reactive power losses $Q^{(loss)}$ are a direct output of the load flow simulation. They include the active and reactive power losses of the transformer, all line segments and all reactive power devices connected to the simulated Link-Grid.

5.1.4. Maximal line loading

The loading of each line segment $\mathcal{L}_{f,n}^{(sgm)}$ is a direct output of the load flow simulation. The maximal line loading $\mathcal{L}_{max}^{(sgm)}$ is calculated with equation (5.2).

$$\mathcal{L}_{max}^{(sgm)} = max\left(\mathcal{L}_{f,n}^{(sgm)}\right) \tag{5.2}$$

5.1.5. Transformer loading

The transformer loading $\mathcal{L}^{(tr)}$ is a direct output of the load flow simulation and thus it don't has to be calculated.

5.1.6. Power exchange between the LV- and the MV-grid

The active power exchange between the LV- and the MV-grid $P^{(ex)}$ equals to the active power at the transformer's primary side $P^{(tr,p)}$ according to figure 2.3, which is a direct output of the load flow simulation.

$$P^{(ex)} = P^{(tr,p)} \tag{5.3}$$

The reactive power exchange between the LV- and the MV-grid $Q^{(ex)}$ equals to the reactive power at the transformer's primary side $Q^{(tr,p)}$ according to figure 2.3, which is a direct output of the load flow simulation.

$$Q^{(ex)} = Q^{(tr,p)} \tag{5.4}$$

5.1.7. Power exchange between the CP-grids and the LV-grid

The active power exchange between the CP-grids and the LV-grid $P^{(pro)}$ is determined according to equation (5.5).

$$P^{(pro)} = \sum_{i=1}^{F} \sum_{j=1}^{N_i} \left(P_{i,j}^{(inv)} - P_{i,j}^{(load)} \right) \tag{5.5}$$

The reactive power exchange between the CP-grids and the LV-grid $Q^{(pro)}$ is determined according to equation (5.6).

$$Q^{(pro)} = \sum_{i=1}^{F} \sum_{j=1}^{N_i} \left(Q_{i,j}^{(inv)} - Q_{i,j}^{(load)} \right) \tag{5.6}$$

5.1.8. Active power curtailment

The active power curtailment of a photovoltaic-inverter located at node (f, n) is the difference of the inverter's input $P_{f,n}^{(pv)}$ and output active power $P_{f,n}^{(inv)}$. The values of all customers connected to the Link-Grid are added up according to equation (5.7) to attain the overall active power curtailment $P^{(ctl)}$ within the Link-Grid.

$$P^{(ctl)} = \sum_{i=1}^{F} \sum_{j=1}^{N_i} \left(P_{i,j}^{(pv)} - P_{i,j}^{(inv)} \right) \tag{5.7}$$

5.2. Performance evaluation

The performance of the theoretical grid is evaluated for each scenario defined in table 4.6 and control strategy defined in table 6.1 by means of a set of evaluation criteria. These criteria are defined in section 5.2.1. To convey a clear overview of each control strategy's advantages and disadvantages, *one* spider chart is created for each reactive power control strategy. The procedure which is used to determine the data for the spider charts is described in section 5.2.2.

5.2.1. Evaluation criteria

The performance of a LV-Link-Grid for a given scenario and voltage control strategy is evaluated by means of the emerging voltage violation index, active power losses, transformer loading, reactive power exchange between the MV- and the LV-grid and active power curtailment, which are defined in section 5.1, and by means of customer discrimination and the data exchange between customers and the DSO which is required to enable a coordinated Q-control.

5.2.2. Performance visualisation

For each reactive power control strategy, the simulation results[1] for all scenarios defined in table 4.6 are summarised according to the following procedure in order to attain a single value for each evaluation criterion. These values are normalised afterwards to attain values between 0 and 1 for each criterion. Only the simulation results[2] without or with inactive voltage protections are considered for these purposes.

Firstly, for each control strategy C the evaluation criteria of all scenarios S are added up according to equations (5.8) to (5.11).

$$N_C^{(viol)} = \sum_{\forall S} N_{C,S}^{(viol)} \tag{5.8}$$

$$P_C^{(loss)} = \sum_{\forall S} P_{C,S}^{(loss)} \tag{5.9}$$

$$Q_C^{(ex)} = \sum_{\forall S} Q_{C,S}^{(ex)} \tag{5.10}$$

$$\mathcal{L}_C^{(tr)} = \sum_{\forall S} \mathcal{L}_{C,S}^{(tr)} \tag{5.11}$$

Afterwards, a reference value is determined according to equations (5.12) to (5.15) for each evaluation criterion.

$$N_{ref}^{(viol)} = \max_{\forall C} \left(N_C^{(viol)} \right) \tag{5.12}$$

$$P_{ref}^{(loss)} = \max_{\forall C} \left(P_C^{(loss)} \right) \tag{5.13}$$

$$Q_{ref}^{(ex)} = \max_{\forall C} \left(Q_C^{(ex)} \right) \tag{5.14}$$

$$\mathcal{L}_{ref}^{(tr)} = \max_{\forall C} \left(\mathcal{L}_C^{(tr)} \right) \tag{5.15}$$

The evaluation criteria yielded from equations (5.8) to (5.11) are finally normalised according to equa-

---

[1] $N^{(viol)}$, $P^{(loss)}$, $Q^{(ex)}$ and $\mathcal{L}^{(tr)}$.

[2] These results are listed in tables 6.13, 6.14, 6.15 and 6.16.

tions (5.16) to (5.19).

$$n_C^{(viol)} = \frac{N_C^{(viol)}}{N_{ref}^{(viol)}} \qquad (5.16)$$

$$p_C^{(loss)} = \frac{P_C^{(loss)}}{P_{ref}^{(loss)}} \qquad (5.17)$$

$$q_C^{(ex)} = \frac{Q_C^{(ex)}}{Q_{ref}^{(ex)}} \qquad (5.18)$$

$$l_C^{(tr)} = \frac{\mathcal{L}_C^{(tr)}}{\mathcal{L}_{ref}^{(tr)}} \qquad (5.19)$$

These normalised values are used for the spider charts. For the evaluation of the customer discrimination only the values 1 and 0 are used, since the customers are either discriminated ($P(U)$-, $Q(U)$- and $cos\varphi(P)$-control) or not ($L(U)$-control with and without Q-autarkic customers). For the evaluation of the data exchange only the values 1 and 0 are used, since either there is a data exchange required to enable a coordinated Q-control ($P(U)$-, $Q(U)$- and $cos\varphi(P)$-control) or not ($L(U)$-control with and without Q-autarkic customers). Figure 5.1 shows the spider chart which is used to visualise the performances of the theoretical Link-Grid for the different control strategies. Since low values of the evaluation criteria correspond to a good performance, an empty chart represents the optimal performance. The more area is covered by the diagram the worse is the performance.
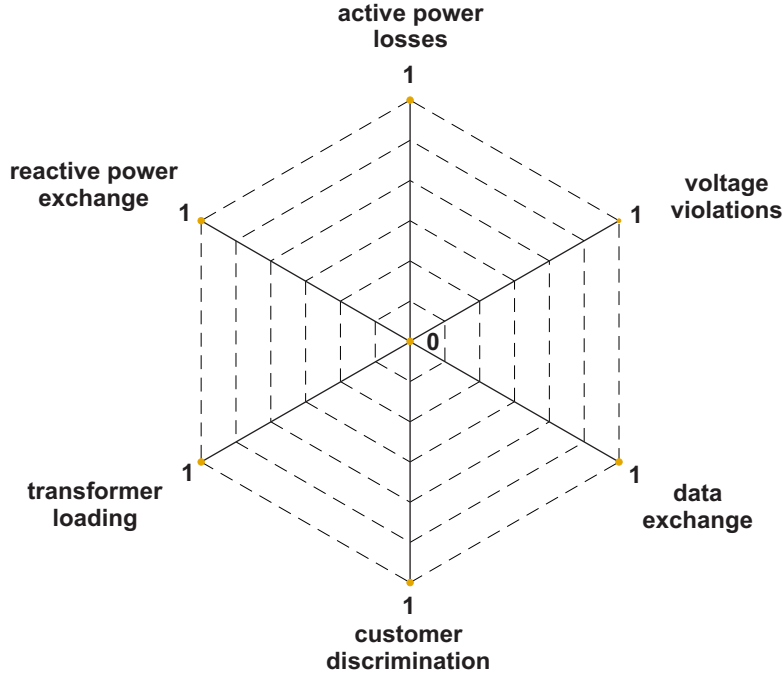
Figure 5.1.: Spider chart for an optimal performance

6. Impact of CP-Grid-Links on the behaviour of LV-Grid-Links

The investigated control concepts can be categorised according to the control responsibility. While the $L(U)$-control is performed by the DSO and the corresponding control devices are located within the LV-Grid-Link, the $P(U)$-, $Q(U)$- and $cos\varphi(P)$-control as well as the customers' Q-autarky is performed by the customers and the corresponding control devices are located within the CP-Producer-Links. Figure 6.1 illustrates this categorisation. According to the Link-Solution, the CP-Grid-Links behave like black boxes from the DSO's point of view. For that reason, the CP-Grid-Links and the connected CP-Producer-Links are illustrated with a dark background in figure 6.1. In this thesis the CP-Producer-Links are assumed to be photovoltaic-systems according to the producer in figure 2.4. Table 6.1 shows the combinations of
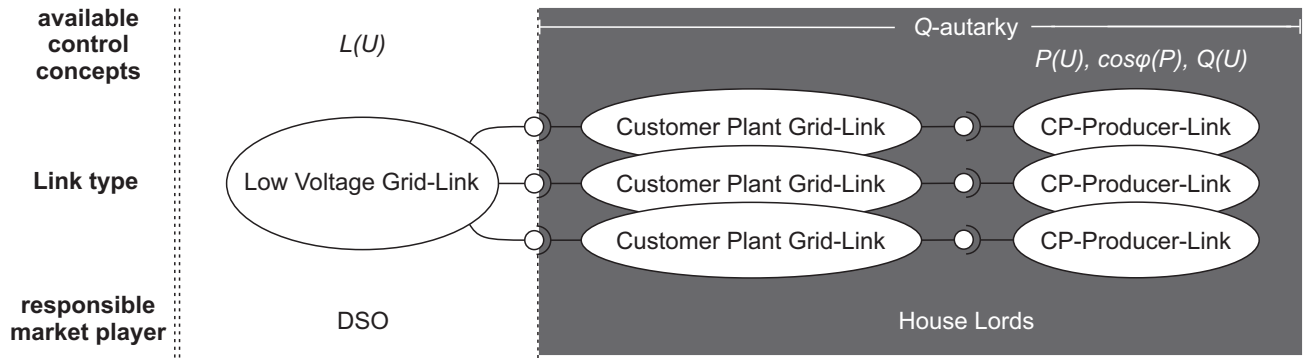
Figure 6.1.: Responsibilities for voltage control for the investigated control concepts

these control concepts which are simulated in this thesis. For the theoretical Link-Grid, the combinations according to table 6.1 are simulated for all scenarios listed in table 4.6. The results of these simulations are used to compare the different control concepts with each other. For the real Link-Grids, the combinations

Test network	Control concept	Responsibility	
		DSO	House Lords
Theoretical Link-Grid	No control	×	×
	$P(U)$	×	$P(U)$-control
	$Q(U)$	×	$Q(U)$-control
	$cos\varphi(\mathbf{P})$	×	$cos\varphi(P)$-control
	$L(U)$	$L(U)$-control	×
	$L(U)$ & Q-autarky	$L(U)$-control	Q-autarky
Real Link-Grids	No control	×	×
	$L(U)$	$L(U)$-control	×
	$L(U)$ & Q-autarky	$L(U)$-control	Q-autarky

Table 6.1.: Investigated control concepts for the theoretical and the real Link-Grids

according to table 6.1 are simulated for all scenarios listed in table 4.7. The results of these simulations are used to verify the functionality of the $L(U)$-control under realistic network conditions with and without Q-autarkic CP-Grid-Links.

6.1. No control

This section presents and discusses the simulation results of the LV-Grid-Link operation without any control on the LV-Grid-, CP-Grid-, CP-Producer-Link chain. Both types of grids, the theoretical and the real grids are analysed. Figure 6.2 shows an overview of the LV-Grid-, CP-Grid-, CP-Producer-Link chain without any control.
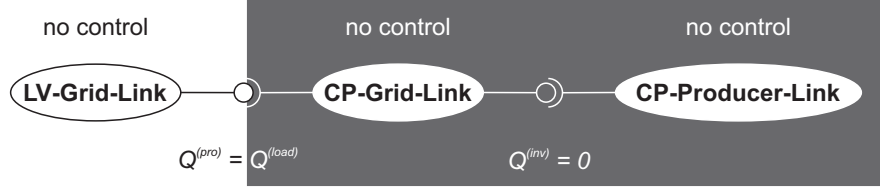
Figure 6.2.: Overview of the LV-Grid-, CP-Grid-, CP-Producer-Link chain without any control

6.1.1. Behaviour of the theoretical Link-Grid

Figure 6.3 shows an overview of the theoretical Link-Grid. Within this grid, the overhead line-feeders L1 and L2 have higher specific resistances and much higher specific reactances than the cable-feeders C1 and C2. Hence, according to equation (2.8), the voltage profiles of the overhead line-feeders are more sensitive to active and especially to reactive power flows than those of the cable-feeders. Due to the low voltages within the LV-grid, the cable-feeders capacitance only produce a very small amount of reactive power and thus it doesn't impact the simulation results significantly.
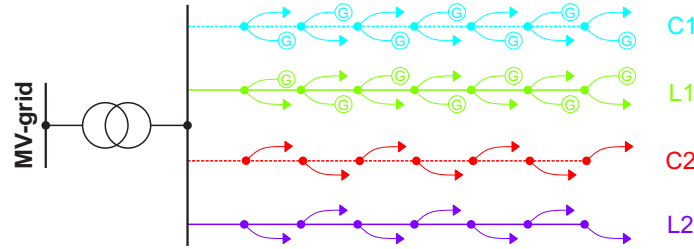
Figure 6.3.: Overview of the theoretical Link-Grid

A. Without distributed electricity production

Figure 6.4 shows the voltage profiles of the theoretical Link-Grid without any control on the LV-Grid-, CP-Grid-, CP-Producer-Link chain for a $P^{(inv)} = 0kW$ in two loading cases. Both overhead line-feeders, L1 and L2, and both cable-feeders, C1 and C2, show the same voltage profile since the DGs don't inject or absorb any active and reactive power and thus exactly the same power flows through these feeders. As a consequence, their voltage profiles overlay and thus only two profiles can be seen. The voltage profiles of the cable- and the overhead line-feeders differ from each other due to their different impedances. In both scenarios, the active and reactive power flows unidirectionally from the transformer's primary side through the transformer and the LV-grid to the customers. These downstream power flows lead to a voltage drop along the transformer and monotonically decreasing node-voltages along all four feeders. Since the upper voltage limitation isn't violated by any network-node in both scenarios, no overvoltage protection trips and thus no active power is curtailed.

Regarding the "min load, no production"-scenario, neither the upper nor the lower voltage limitation is violated by any node-voltage. The decreasing node-voltages along the overhead line-feeders cause a voltage spreading of 15.18 V, determined according to equation (5.1). The relatively low node-voltages reduce the consumers' active and reactive power demand in total according to the characteristics shown
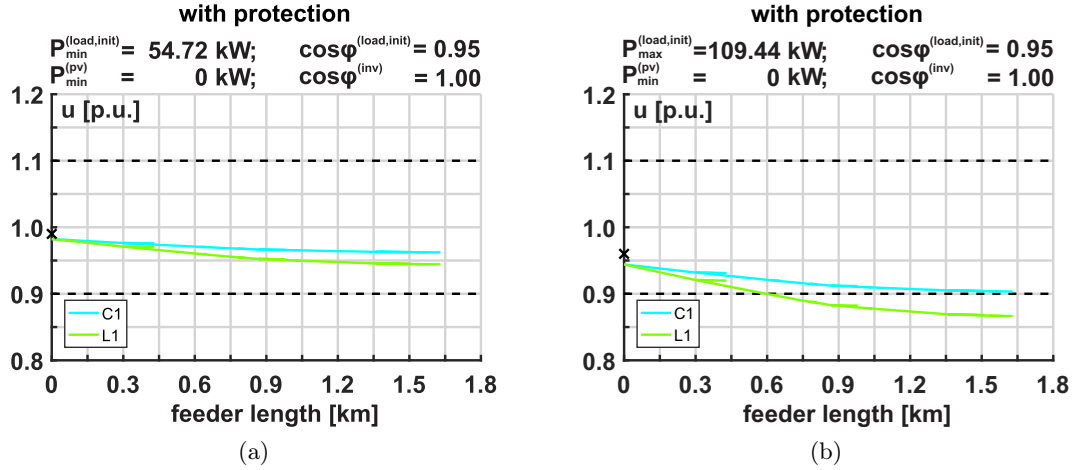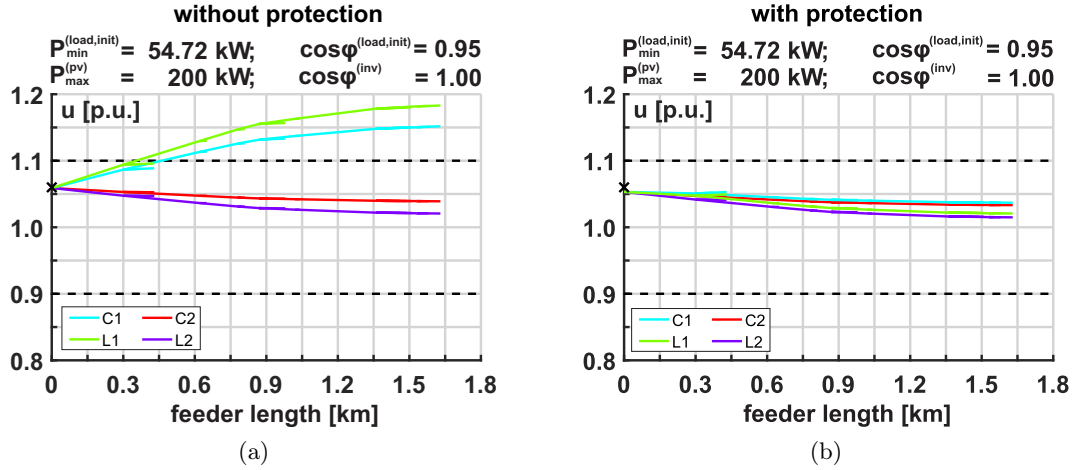
Figure 6.4.: Voltage profiles of the theoretical Link-Grid without any control on the LV-Grid-, CP-Grid-, CP-Producer-Link chain for a $P^{(inv)} = 0kW$ in two loading cases: (a) minimal load, (b) maximal load

in figure 2.16. Since their inverters don't inject or absorb any active and reactive power, this reduced demand results in a reduced active (-53.14 kW) and reactive power exchange (-16.42 kvar) between the CP-grids and the LV-grid, determined according to equations (5.5) and (5.6). These power exchanges lead to active and reactive power flows within the LV-grid and thus to active (1.32 kW) and reactive power losses (1.50 kvar), to an active (54.46 kW) and reactive power exchange (17.92 kvar) between the LV- and the MV-grid, to a transformer loading of 36.19% and to a maximal line loading of 7.58%.

Regarding the "max load, no production"-scenario, 48 node-voltages deceed the lower voltage limitation. The decreasing node-voltages along the overhead line-feeders cause a voltage spreading of 31.03 V, determined according to equation (5.1). The relatively low node-voltages reduce the consumers' active and reactive power demand in total according to the characteristics shown in figure 2.16. Since their inverters don't inject or absorb any active and reactive power, this reduced demand results in a reduced active (-102.13 kW) and reactive power exchange (-29.55 kvar) between the CP-grids and the LV-grid, determined according to equations (5.5) and (5.6). These power exchanges lead to active and reactive power flows within the LV-grid and thus to active (5.43 kW) and reactive power losses (6.89 kvar), to an active (107.57 kW) and reactive power exchange (36.44 kvar) between the LV- and the MV-grid, to a transformer loading of 73.94% and to a maximal line loading of 15.43%. Figure 6.4b shows that the lower voltage limitation is violated in the "max load, no generation"-scenario by both overhead line feeders, L1 and L2. All in all, 48 node-voltages of the theoretical Link-Grid violate the lower voltage limitation in this scenario.

B. With distributed electricity production

Figure 6.5 shows the voltage profiles of the theoretical Link-Grid without any control on the LV-Grid-, CP-Grid-, CP-Producer-Link chain for a $P^{(inv)} = 200kW$ and a $P^{(load,init)} = 54.72kW$ without and with overvoltage protections. Without overvoltage protections, 48 node-voltages exceed the upper voltage limitation. The active power production of the photovoltaic systems leads to active power injecting and reactive power absorbing customers at the feeders C1 and L1. Despite their reactive power consumption, their active power injection increases the corresponding node-voltages far above the upper limit. The customers located at feeders C2 and L2 still consume active and reactive power and thus they decrease the node-voltages of the corresponding feeders. This leads to a voltage spreading of 64.92 V, determined according to equation (5.1). The relatively high node-voltages increase the consumers' active and reactive power demand in total according to the characteristics shown in figure 2.16. The active power injection of the inverters overcompensates the consumers' P-demand in total, resulting in an active power exchange

Figure 6.5.: Voltage profiles of the theoretical Link-Grid without any control on the LV-Grid-, CP-Grid-, CP-Producer-Link chain for a $P^{(inv)} = 200kW$ and a $P^{(load,init)} = 54.72kW$: (a) without overvoltage protections, (b) with overvoltage protections

between the CP-grids and the LV-grid of 140.98 kW, determined according to equation (5.5). The reactive power exchange between the CP-grids and the LV-grid of -23.17 kvar, determined according to equation (5.6), corresponds to the consumers' Q-demand, since their inverters don't inject or absorb any reactive power. These power exchanges lead to active and reactive power flows within the LV-grid and thus to active (15.79 kW) and reactive power losses (15.42 kvar), to an active (-125.19 kW) and reactive power exchange (38.59 kvar) between the LV- and the MV-grid, to a transformer loading of 77.24 % and to a maximal line loading of 39.38 %. Due to the low R/X-ratio of the supplying transformer of about 0.25, the upstream active power flow through the transformer is not sufficient to fully compensate the voltage drop caused by the downstream reactive power flow through the transformer. All in all, 48 node-voltages of the theoretical Link-Grid violate the upper voltage limitation in this scenario.

With overvoltage protections, neither the upper nor the lower voltage limitation is violated by any node-voltage. Most of the photovoltaic-systems are disconnected from the grid and thus they don't inject or absorb any active and reactive power. 180 kW of the photovoltaic arrays' active power output is curtailed in this scenario, but in return, no voltage violations occur. The active power injection of those PV-systems which aren't disconnected from the grid by their overvoltage protections increases the node-voltages of the corresponding feeders, C1 and L1, but in total, the consumers' P- and Q-demand decreases the node-voltages of these feeders. The customers located at feeders C2 and L2 only consume active and reactive power and thus they decrease the node-voltages of the corresponding feeders. This leads to an voltage spreading of 15.29 V, determined according to equation (5.1). The relatively high node-voltages increase the consumers' active and reactive power demand in total according to the characteristics shown in figure 2.16. The active power injection of the inverters is not sufficient to compensate the consumers' P-demand in total, resulting in an active power exchange between the CP-grids and the LV-grid of -36.11 kW, determined according to equation (5.5). The reactive power exchange between the CP-grids and the LV-grid of -19.52 kvar, determined according to equation (5.6), corresponds to the consumers' Q-demand, since their inverters don't inject or absorb any reactive power. These power exchanges lead to active and reactive power flows within the LV-grid and thus to active (1.05 kW) and reactive power losses (0.89 kvar), to an active (37.16 kW) and reactive power exchange (20.42 kvar) between the LV- and the MV-grid, to a transformer loading of 25.00 % and to a maximal line loading of 7.53 %.

Figure 6.6 shows the voltage profiles of the theoretical Link-Grid without any control on the LV-Grid-, CP-Grid-, CP-Producer-Link chain for a $P^{(inv)} = 200kW$ and a $P^{(load,init)} = 109.44kW$ without and with overvoltage protections. Without overvoltage protections, 6 node-voltages exceed the upper voltage limitation. The active power production of the photovoltaic systems leads to active power injecting and reactive power absorbing customers at the feeders C1 and L1. Despite their reactive power consumption,
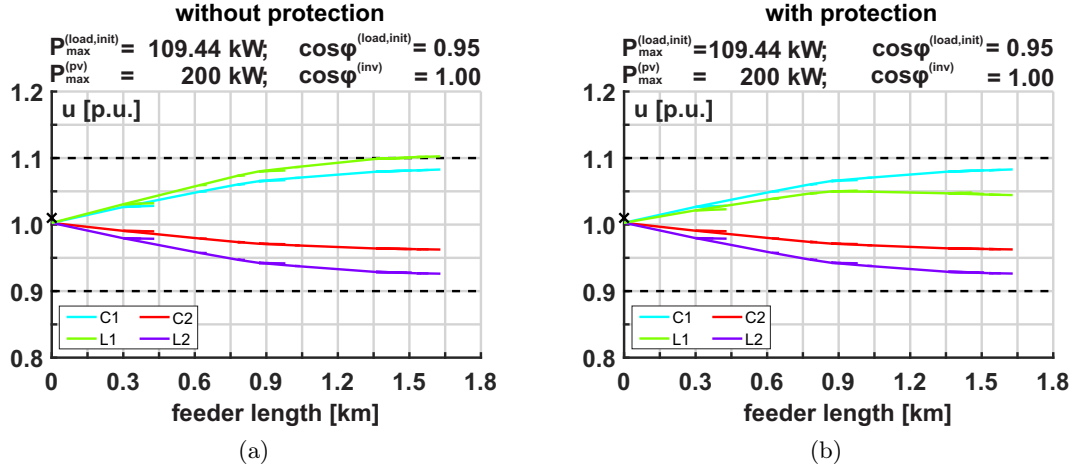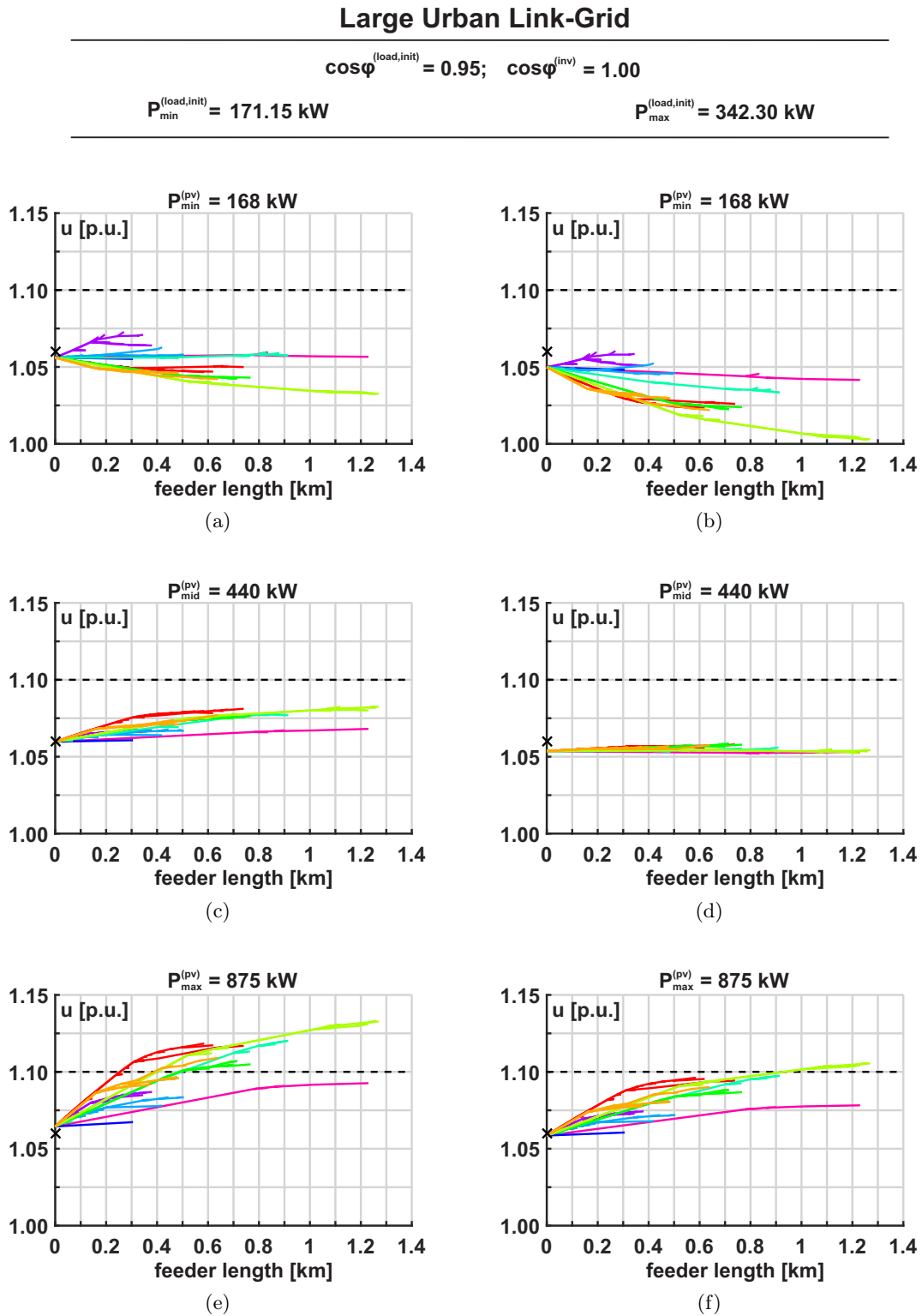
Figure 6.6.: Voltage profiles of the theoretical Link-Grid without any control on the LV-Grid-, CP-Grid-, CP-Producer-Link chain for a $P^{(inv)} = 200kW$ and a $P^{(load,init)} = 109.44kW$: (a) without overvoltage protections, (b) with overvoltage protections

their active power injection increases the corresponding node-voltages slightly above the upper limit. The customers located at feeders C2 and L2 still consume active and reactive power and thus they decrease the node-voltages of the corresponding feeders. This leads to a voltage spreading of 70.56 V, determined according to equation (5.1). The relatively high node-voltages increase the consumers' active and reactive power demand in total according to the characteristics shown in figure 2.16. The active power injection of the inverters overcompensates the consumers' P-demand in total, resulting in an active power exchange between the CP-grids and the LV-grid of 88.93 kW, determined according to equation (5.5). The reactive power exchange between the CP-grids and the LV-grid of -38.14 kvar, determined according to equation (5.6), corresponds to the consumers' Q-demand, since their inverters don't inject or absorb any reactive power. These power exchanges lead to active and reactive power flows within the LV-grid and thus to active (14.23 kW) and reactive power losses (12.74 kvar), to an active (-74.69 kW) and reactive power exchange (50.89 kvar) between the LV- and the MV-grid, to a transformer loading of 55.93 % and to a maximal line loading of 35.44 %. Due to the low R/X-ratio of the supplying transformer of about 0.25, the upstream active power flow through the transformer is not sufficient to fully compensate the voltage drop caused by the downstream reactive power flow through the transformer. All in all, 6 node-voltages of the theoretical Link-Grid violate the upper voltage limitation in this scenario.

With overvoltage protections, neither the upper nor the lower voltage limitation is violated by any node-voltage. Some of the photovoltaic-systems are disconnected from the grid and thus they don't inject or absorb any active and reactive power. 25 kW of the photovoltaic arrays' active power output is curtailed in this scenario, but in return, no voltage violations occur. The active power injection of those PV-systems which aren't disconnected from the grid by their overvoltage protections increases the node-voltages of the corresponding feeders, C1 and L1. The customers located at feeders C2 and L2 still consume active and reactive power and thus they decrease the node-voltages of the corresponding feeders. This leads to a voltage spreading of 62.62 V, determined according to equation (5.1). The relatively high node-voltages increase the consumers' active and reactive power demand in total according to the characteristics shown in figure 2.16. The active power injection of the inverters overcompensates the consumers' P-demand in total, resulting in an active power exchange between the CP-grids and the LV-grid of 64.78 kW, determined according to equation (5.5). The reactive power exchange between the CP-grids and the LV-grid of -37.12 kvar, determined according to equation (5.6), corresponds to the consumers' Q-demand, since their inverters don't inject or absorb any reactive power. These power exchanges lead to active and reactive power flows within the LV-grid and thus to active (9.93 kW) and reactive power losses (7.55 kvar), to an active (-54.84 kW) and reactive power exchange (44.67 kvar) between the LV- and the MV-grid, to a transformer loading of 43.77 % and to a maximal line loading of 35.43 %.

C. Summary

Table 6.2 summarises the simulation results of the theoretical Link-Grid without any control on the LV-Grid-, CP-Grid-, CP-Producer-Link chain. The most critical scenarios concerning the voltage violation

Scenario	volt. prot.	viol. index	$\Delta U^{(sdg)}$ [V]	$P^{(loss)}$ [kW]	$Q^{(loss)}$ [kvar]	$P^{(pro)}$ [kW]	$Q^{(pro)}$ [kvar]	$P^{(ex)}$ [kW]	$Q^{(ex)}$ [kvar]	$\mathcal{L}^{(tr)}$ [%]	$\mathcal{L}^{(sgm)}_{max}$ [%]	$P^{(ctl)}$ [kW]
$\mathbf{L^{(min)}} - \mathbf{G^{(min)}}$	$(\checkmark)$	0	15.18	1.32	1.50	-53.14	-16.42	54.46	17.92	36.19	7.58	0
$\mathbf{L^{(max)}} - \mathbf{G^{(min)}}$	$(\checkmark)$	48	31.03	5.43	6.89	-102.13	-29.55	107.57	36.44	73.94	15.43	0
$\mathbf{L^{(min)}} - \mathbf{G^{(max)}}$	$\times$	48	64.92	15.79	15.42	140.98	-23.17	-125.19	38.59	77.24	39.38	0
$\mathbf{L^{(min)}} - \mathbf{G^{(max)}}$	$\checkmark$	0	15.29	1.05	0.89	-36.11	-19.52	37.16	20.42	25.00	7.53	180
$\mathbf{L^{(max)}} - \mathbf{G^{(max)}}$	$\times$	6	70.56	14.23	12.74	88.93	-38.14	-74.69	50.89	55.93	35.44	0
$\mathbf{L^{(max)}} - \mathbf{G^{(max)}}$	$\checkmark$	0	62.62	9.93	7.55	64.78	-37.12	-54.84	44.67	43.77	35.43	25

Table 6.2.: Summarised simulation results of the theoretical Link-Grid without any control on the LV-Grid-, CP-Grid-, CP-Producer-Link chain

index, the voltage spreading, the active power losses, the reactive power exchange between the LV- and the MV-grid, the transformer loading, the maximal line loading and the active power curtailment are presented in the following. The maximum voltage violation index occurs in the $L^{(max)} - G^{(min)}$ scenario with overvoltage protections and in the $L^{(min)} - G^{(max)}$ scenario without overvoltage protections. The maximum voltage spreading occurs in the $L^{(max)} - G^{(max)}$ scenario without overvoltage protections. The maximum active power losses occur in the $L^{(min)} - G^{(max)}$ scenario without overvoltage protections. The maximum reactive power exchange between the LV- and the MV-grid occurs in the $L^{(max)} - G^{(max)}$ scenario without overvoltage protections. The maximum transformer loading occurs in the $L^{(min)} - G^{(max)}$ scenario without overvoltage protections. The maximum maximal line loading occurs in the $L^{(min)} - G^{(max)}$ scenario without overvoltage protections. The maximum active power curtailment occurs in the $L^{(min)} - G^{(max)}$ scenario with overvoltage protections.

Regarding the compliance with the legally stipulated voltage range and the lost active power ($P^{(loss)} + P^{(ctl)}$) as the crucial performance indicators, the $L^{(max)} - G^{(min)}$ scenario with and without overvoltage protections and the $L^{(min)} - G^{(max)}$ scenario with overvoltage protections are the most critical scenarios for the theoretical Link-Grid's operation without any control on the LV-Grid-, CP-Grid-, CP-Producer-Link chain.

6.1.2. Behaviour of the real Link-Grids

This section presents the simulation results of the real Link-Grids described in section 3.1.2 for the scenarios defined in table 4.7 without any control on the LV-Grid, CP-Grid, CP-Producer-Link chain and without overvoltage protections.

A. Large Urban Link-Grid

Large Urban Link-Grid

$\cos\varphi^{(load,init)} = 0.95;$ $\cos\varphi^{(inv)} = 1.00$

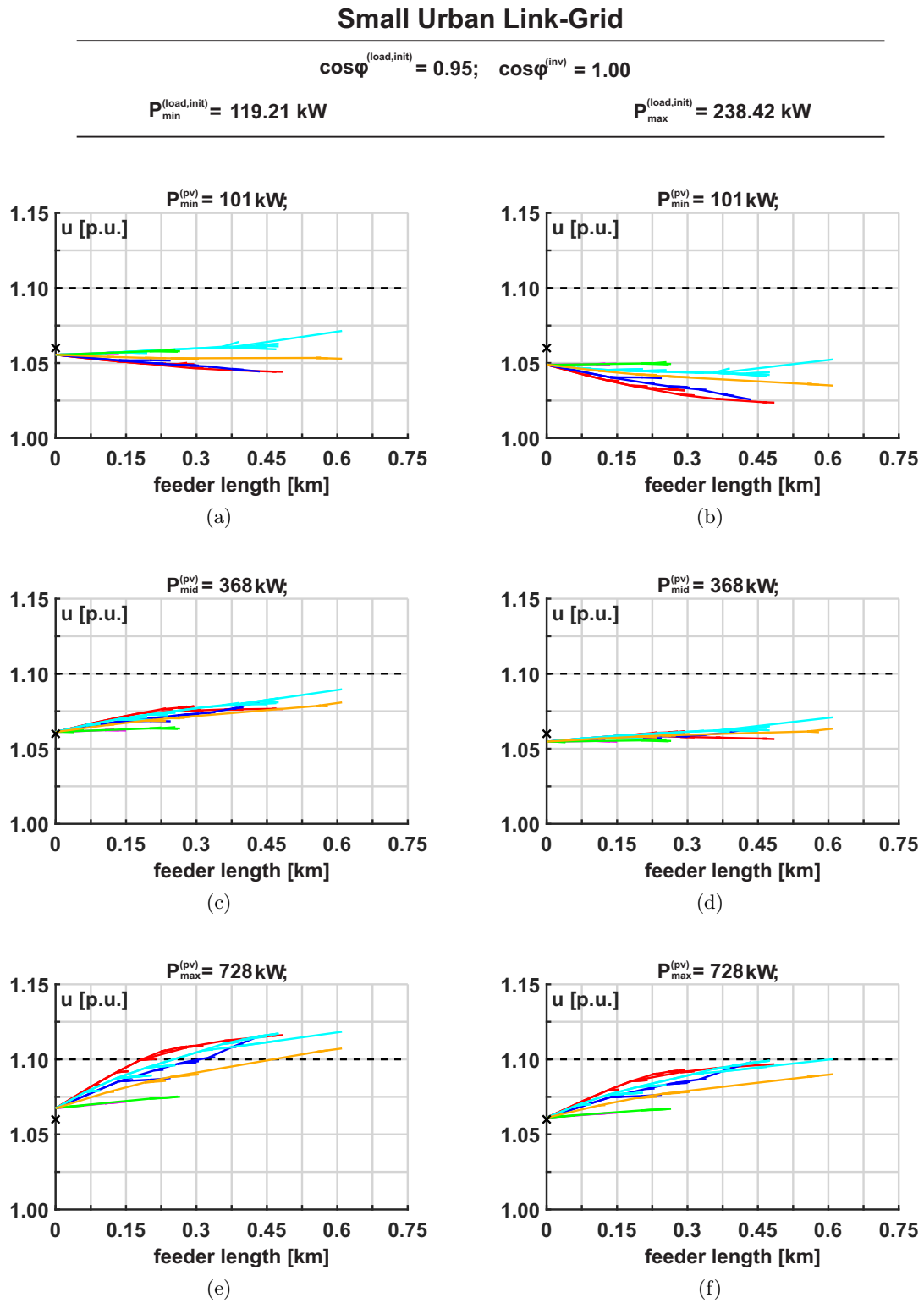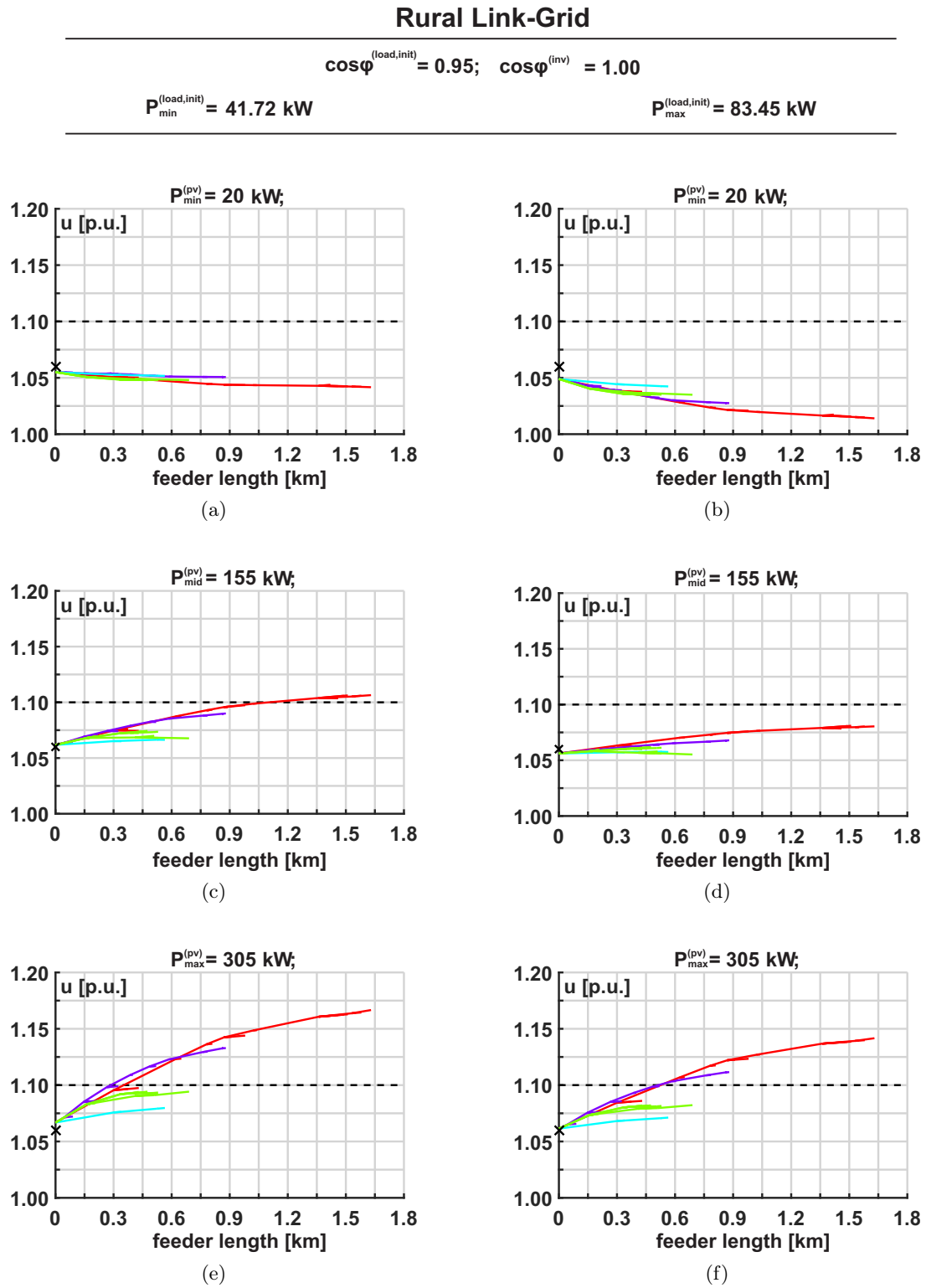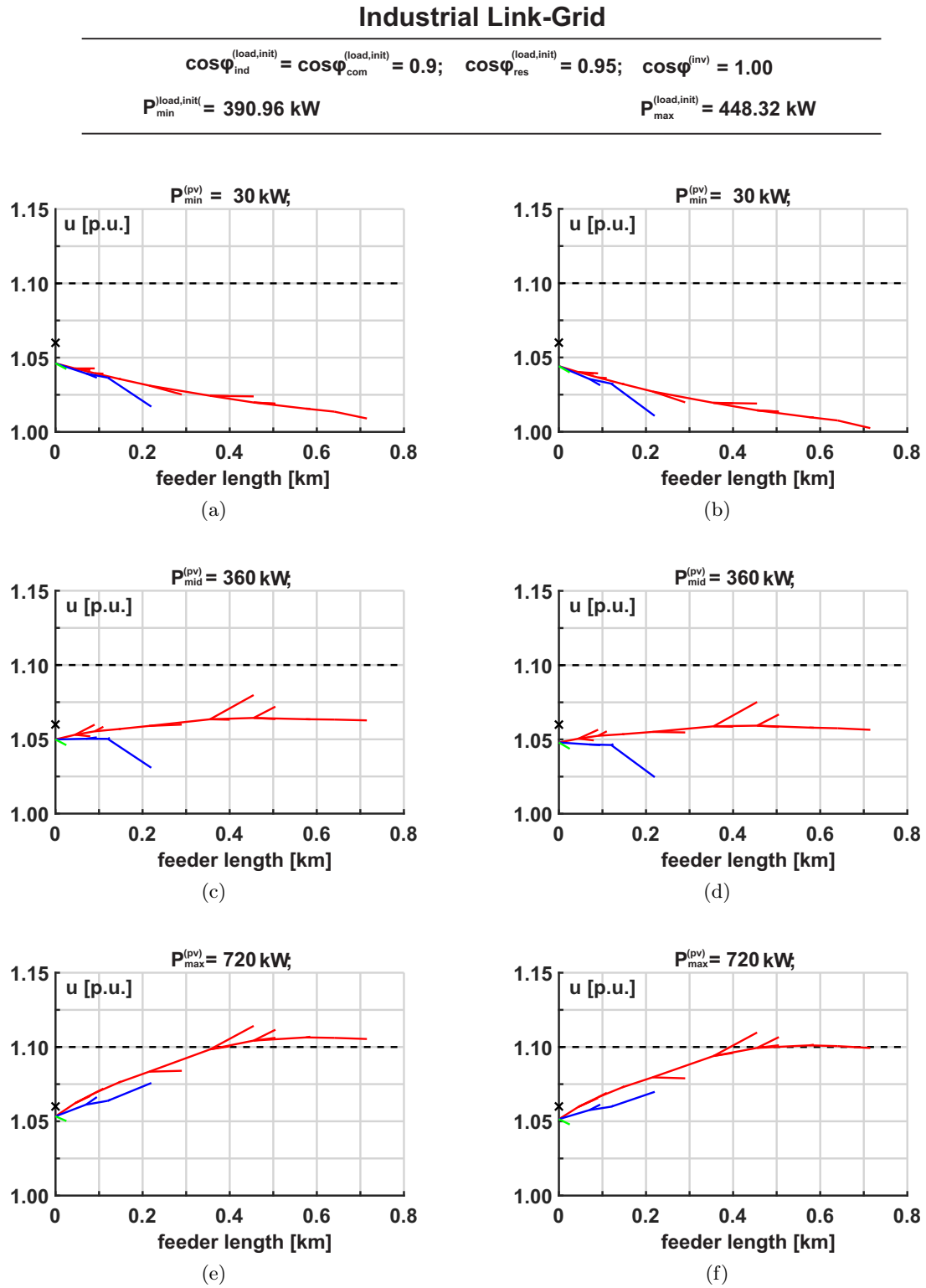$P_{min}^{(load,init)} = 171.15$ kW $P_{max}^{(load,init)} = 342.30$ kW

Figure 6.7.: Voltage profiles of the Large Urban Link-Grid without any control on the LV-Grid-, CP-Grid-, CP-Producer-Link chain for different load/production scenarios: (a) min load, min production, (b) max load, min production, (c) min load, mid production, (d) max load, mid production, (e) min load, max production, (f) max load, max production

B. Small Urban Link-Grid

Small Urban Link-Grid

$\cos\varphi^{(load,init)} = 0.95$; $\cos\varphi^{(inv)} = 1.00$

$P_{min}^{(load,init)} = 119.21$ kW $P_{max}^{(load,init)} = 238.42$ kW

Figure 6.8.: Voltage profiles of the Small Urban Link-Grid without any control on the LV-Grid-, CP-Grid-, CP-Producer-Link chain for different load/production scenarios: (a) min load, min production, (b) max load, min production, (c) min load, mid production, (d) max load, mid production, (e) min load, max production, (f) max load, max production

Rural Link-Grid

$\cos\varphi^{(load,init)} = 0.95; \quad \cos\varphi^{(inv)} = 1.00$

$P_{min}^{(load,init)} = 41.72$ kW $\qquad\qquad P_{max}^{(load,init)} = 83.45$ kW

Figure 6.9.: Voltage profiles of the Rural Link-Grid without any control on the LV-Grid-, CP-Grid-, CP-Producer-Link chain for different load/production scenarios: (a) min load, min production, (b) max load, min production, (c) min load, mid production, (d) max load, mid production, (e) min load, max production, (f) max load, max production

D. Industrial Link-Grid

Industrial Link-Grid

$\cos\varphi_{ind}^{(load,init)} = \cos\varphi_{com}^{(load,init)} = 0.9; \quad \cos\varphi_{res}^{(load,init)} = 0.95; \quad \cos\varphi^{(inv)} = 1.00$

$P_{min}^{)load,init(} = 390.96 \text{ kW}$ $\qquad\qquad\qquad P_{max}^{(load,init)} = 448.32 \text{ kW}$

Figure 6.10.: Voltage profiles of the Industrial Link-Grid without any control on the LV-Grid-, CP-Grid-, CP-Producer-Link chain for different load/production scenarios: (a) min load, min production, (b) max load, min production, (c) min load, mid production, (d) max load, mid production, (e) min load, max production, (f) max load, max production

E. Summary

Table 6.3 summarises the simulation results of the real Link-Grids without any control on the LV-Grid-, CP-Grid-, CP-Producer-Link chain and without overvoltage protections. The most critical scenario re-

Link-Grid	Scenario	Viol. idx.	$\Delta U^{(sdg)}$ [V]	$P^{(loss)}$ [kW]	$Q^{(loss)}$ [kvar]	$P^{(pro)}$ [kW]	$Q^{(pro)}$ [kvar]	$P^{(ex)}$ [kW]	$Q^{(ex)}$ [kvar]	$\mathcal{L}^{(tr)}$ [%]	$\mathcal{L}^{(sgm)}_{max}$ [%]	$P^{(ctl)}$ [kW]
Large Urban	$L^{(min)} - G^{(min)}$	0	16.11	2.32	0.45	-10.18	-64.14	12.49	64.59	9.84	32.26	0
	$L^{(max)} - G^{(min)}$	0	23.01	6.49	4.47	-183.38	-122.57	189.88	127.03	34.18	33.45	0
	$L^{(min)} - G^{(mid)}$	0	9.19	4.69	4.63	258.74	-67.85	-254.04	72.48	39.53	26.98	0
	$L^{(max)} - G^{(mid)}$	0	2.65	1.72	1.20	82.56	-129.57	-80.83	130.76	23.00	15.81	0
	$L^{(min)} - G^{(max)}$	112	27.41	29.38	32.91	689.42	-73.27	-660.05	106.19	100.04	65.59	0
	$L^{(max)} - G^{(max)}$	17	18.81	17.60	19.44	509.13	-139.85	-491.53	159.29	77.32	50.79	0
Small Urban	$L^{(min)} - G^{(min)}$	0	10.91	0.75	0.27	-23.03	-46.16	23.78	46.43	12.35	18.50	0
	$L^{(max)} - G^{(min)}$	0	11.51	2.82	3.06	-144.29	-88.19	147.11	91.24	40.99	31.94	0
	$L^{(min)} - G^{(mid)}$	0	11.38	4.69	5.84	241.93	-49.30	-237.24	55.14	57.68	33.85	0
	$L^{(max)} - G^{(mid)}$	0	6.62	1.97	2.18	118.71	-94.18	-116.75	96.36	35.85	20.98	0
	$L^{(min)} - G^{(max)}$	58	20.39	24.70	33.76	599.30	-53.47	-574.59	87.23	137.63	81.55	0
	$L^{(max)} - G^{(max)}$	1	15.60	16.45	22.39	473.59	-102.15	-457.15	124.54	112.20	66.58	0
Rural	$L^{(min)} - G^{(min)}$	0	5.34	0.23	0.11	-23.34	-15.53	23.58	15.64	16.75	5.59	0
	$L^{(max)} - G^{(min)}$	0	13.95	1.35	1.66	-65.48	-29.67	66.83	31.32	43.70	13.42	0
	$L^{(min)} - G^{(mid)}$	9	17.87	3.21	4.06	110.41	-17.04	-107.20	21.10	64.68	19.15	0
	$L^{(max)} - G^{(mid)}$	0	10.31	1.52	1.76	67.06	-32.54	-65.55	34.30	43.80	13.17	0
	$L^{(min)} - G^{(max)}$	42	39.93	15.35	21.08	259.09	-18.74	-243.74	39.82	146.22	44.34	0
	$L^{(max)} - G^{(max)}$	36	32.09	11.09	15.16	214.49	-35.78	-203.40	50.94	124.14	37.68	0
Indus-trial	$L^{(min)} - G^{(min)}$	0	14.85	6.99	9.54	-371.68	-197.95	378.67	207.49	50.90	58.75	0
	$L^{(max)} - G^{(min)}$	0	16.68	9.20	12.69	-429.19	-223.55	438.38	236.24	58.71	65.26	0
	$L^{(min)} - G^{(mid)}$	0	19.57	5.78	3.33	-47.06	-203.96	52.84	207.29	25.22	58.78	0
	$L^{(max)} - G^{(mid)}$	0	20.22	6.12	4.27	-105.31	-230.39	111.43	234.67	30.63	65.29	0
	$L^{(min)} - G^{(max)}$	9	25.61	18.63	11.67	307.29	-211.14	-288.66	222.81	42.99	89.07	0
	$L^{(max)} - G^{(max)}$	6	24.76	17.28	10.51	248.31	-238.51	-231.03	249.01	40.05	85.52	0

Table 6.3.: Summarised simulation results of the real Link-Grids without any control on the LV-Grid-, CP-Grid-, CP-Producer-Link chain and without overvoltage protections

garding the voltage violation index, the voltage spreading, the active power losses and the equipment loading is the "min load, max generation"-scenario. Only for the Industrial Link-Grid the maximum transformer loading occurs in the "max load, min generation"-scenario due to the customers' large active and reactive power consumption and the PV-inverters' small active power injection. Regarding the reactive power exchange between the MV- and the LV-grid, the most critical scenario is the "max load, max generation"-scenario, since due to the high voltages within the Link-Grids the customers consume the largest amount of reactive power.

Due to the upper voltage violations in both "max production"-scenarios, the Large Urban Link-Grid without any control on the LV-Grid-, CP-Grid, CP-Producer-Link chain is not able to host 5 kWp of installed photovoltaic rating per customer, even though potentially much more distributed generation could be hosted since the lines aren't fully loaded at all.

Due to the upper voltage violations in both "max production"-scenarios, the Small Urban Link-Grid without any control on the LV-Grid-, CP-Grid, CP-Producer-Link chain is not able to host 8 kWp of installed photovoltaic rating per customer, even though potentially slightly more distributed generation could be hosted since the lines aren't fully loaded at all.

Due to the upper voltage violations in the "min load, mid production"-scenario, the Rural Link-Grid without any control on the LV-Grid-, CP-Grid, CP-Producer-Link chain is not able to host 2.5 kWp of installed photovoltaic rating per customer, even though potentially much more distributed generation could be hosted since the lines aren't fully loaded at all.

Due to the upper voltage violations in both "max production"-scenarios, the Industrial Link-Grid without any control on the LV-Grid-, CP-Grid, CP-Producer-Link chain is not able to host 45 kWp of installed photovoltaic rating per customer, even though potentially slightly more distributed generation could be hosted since the lines aren't fully loaded at all.

6.2. *P(U)*-controlled inverters

This section presents and discusses the simulation results of the LV-Grid-Link operation with *P(U)*-controlled CP-Producer-Links on the LV-Grid-, CP-Grid-, CP-Producer-Link chain. Only the theoretical grid is analysed. Figure 6.11 shows an overview of the LV-Grid-, CP-Grid-, CP-Producer-Link chain with *P(U)*-controlled CP-Producer-Links.
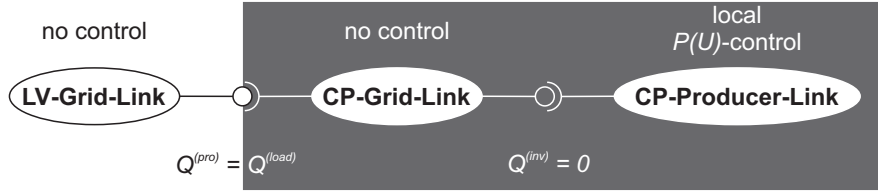

Figure 6.11.: Overview of the LV-Grid-, CP-Grid-, CP-Producer-Link chain with *P(U)*-controlled CP-Producer-Links

6.2.1. Behaviour of the theoretical Link-Grid

Figure 6.12 shows an overview of the theoretical Link-Grid.
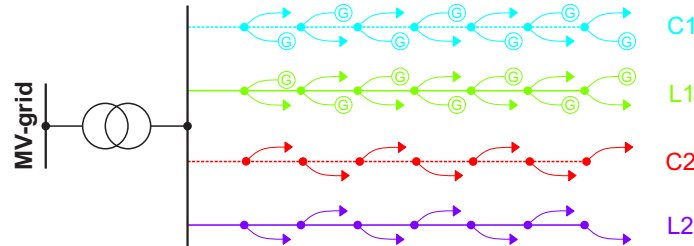
Figure 6.12.: Overview of the theoretical Link-Grid

A. Without distributed electricity production

With the settings assumed in section 3.3.2, a *P(U)*-controlled inverter only curtails active power if the local voltage exceeds 1.074 p.u.. Hence, simulating the "min load, no generation"- and the "max load, no generation"-scenarios with *P(U)*-controlled CP-Producer-Links yields the same results as with uncontrolled CP-Producer-Links. Therefore, only the simulation results of the "min load, max generation"- and the "max load, max generation"-scenarios are presented in the following.

B. With distributed electricity production

Figure 6.13 shows the voltage profiles of the theoretical Link-Grid with *P(U)*-controlled CP-Producer-Links and without any control on the LV-Grid-, CP-Grid-, CP-Producer-Link chain for a $P^{(inv)} = 200kW$ and a $P^{(load,init)} = 54.72kW$. With *P(U)*-control, the node-voltages of the feeders C1 and L1 stay close below the upper voltage limit and prevent the photovoltaic systems from being disconnected from the grid by their overvoltage protections. Neither the upper nor the lower voltage limitation is violated by any node-voltage. However, still 106.37 kW of the photovoltaic-arrays output active power is curtailed by the *P(U)*-controlled inverters, whereby the major part is curtailed at the overhead line-feeder L1 due to its large resistance. Compared to simple overvoltage protections (figure 6.5b), the *P(U)*-controls save 73.63 kW of active power in this scenario. Regarding the case with *P(U)*-controlled CP-Producer-Links, the increasing node-voltages along the feeder C1 and the decreasing node-voltages along the feeder L2 cause a voltage spreading of 27.99 V, determined according to equation (5.1). The relatively high node-voltages increase the consumers' active and reactive power demand in total according to the characteristics shown

$P_{min}^{(load,init)}$ = 54.72 kW; $\cos\varphi^{(load,init)}$ = 0.95
$P_{max}^{(pv)}$ = 200 kW; $\cos\varphi^{(inv)}$ = 1.00

(a)

$P_{min}^{(load,init)}$ = 54.72 kW; $\cos\varphi^{(load,init)}$ = 0.95
$P_{max}^{(pv)}$ = 200 kW; $\cos\varphi^{(inv)}$ = 1.00

(b)
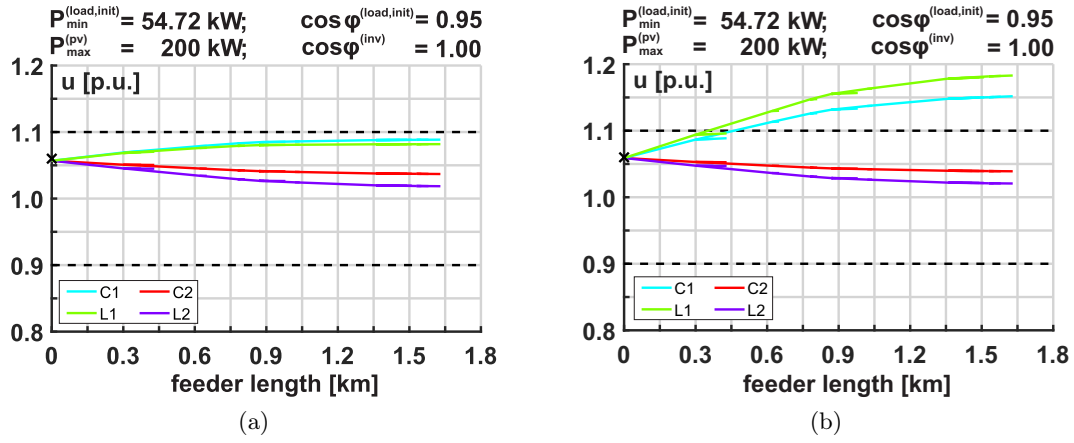
Figure 6.13.: Voltage profiles of the theoretical Link-Grid with different control strategies for a $P^{(inv)} = 200kW$ and a $P^{(load,init)} = 54.72kW$: (a) with $P(U)$-controlled CP-Producer-Links and without any control on the LV-,CP-Grid-Link chain, (b) without any control on the LV-Grid-, CP-Grid-, CP-Producer-Link chain

in figure 2.16. The active power injection of the inverters is not sufficient to compensate the consumers' P-demand in total, resulting in an active power exchange between the CP-grids and the LV-grid of 36.34 kW, determined according to equation (5.5). The reactive power exchange between the CP-grids and the LV-grid of −20.93 kvar, determined according to equation (5.6), corresponds to the consumers' Q-demand, since their inverters don't inject or absorb any reactive power. These power exchanges lead to active and reactive power flows within the LV-grid and thus to active (2.27 kW) and reactive power losses (1.66 kvar), to an active (−34.06 kW) and reactive power exchange (22.59 kvar) between the LV- and the MV-grid, to a transformer loading of 24.10 % and to a maximal line loading of 18.20 %.

Figure 6.13 shows the voltage profiles of the theoretical Link-Grid with $P(U)$-controlled CP-Producer-Links and without any control on the LV-Grid-, CP-Grid-, CP-Producer-Link chain for a $P^{(inv)} = 200kW$ and a $P^{(load,init)} = 109.44kW$. With $P(U)$-control, the node-voltages of the feeders C1 and L1 stay close

$P_{max}^{(load,init)}$ = 109.44 kW; $\cos\varphi^{(load,init)}$ = 0.95
$P_{max}^{(pv)}$ = 200 kW; $\cos\varphi^{(inv)}$ = 1.00

(a)

$P_{max}^{(load,init)}$ = 109.44 kW; $\cos\varphi^{(load,init)}$ = 0.95
$P_{max}^{(pv)}$ = 200 kW; $\cos\varphi^{(inv)}$ = 1.00

(b)
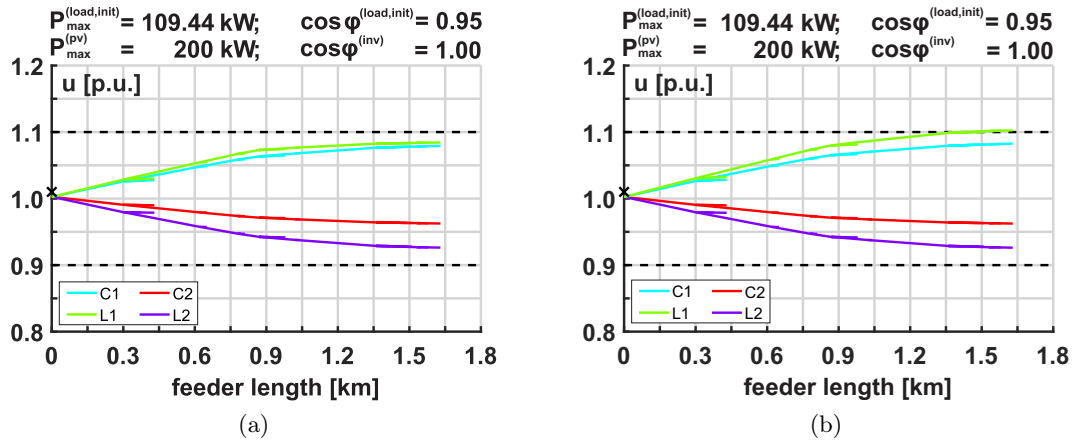
Figure 6.14.: Voltage profiles of the theoretical Link-Grid with different control strategies for a $P^{(inv)} = 200kW$ and a $P^{(load,init)} = 109.44kW$: (a) with $P(U)$-controlled CP-Producer-Links and without any control on the LV-,CP-Grid-Link chain, (b) without any control on the LV-Grid-, CP-Grid-, CP-Producer-Link chain

below the upper voltage limit and prevent the photovoltaic systems from being disconnected from the grid by their overvoltage protections. Neither the upper nor the lower voltage limitation is violated by

any node-voltage. However, still 8.88 kW of the photovoltaic-arrays output active power is curtailed by the $P(U)$-controlled inverters, whereby the major part is curtailed at the overhead line-feeder L1 due to its large resistance. Compared to simple overvoltage protections (figure 6.14b), the $P(U)$-controls save 16.12 kW of active power in this scenario. Regarding the case with $P(U)$-controlled CP-Producer-Links, the increasing node-voltages along the feeder L1 an the decreasing node-voltages along the feeder L2 cause a voltage spreading of 63.21 V, determined according to equation (5.1). The relatively high node-voltages increase the consumers' active and reactive power demand in total according to the characteristics shown in figure 2.16. The active power injection of the inverters is not sufficient to compensate the consumers' P-demand in total, resulting in an active power exchange between the CP-grids and the LV-grid of 80.33 kW, determined according to equation (5.5). The reactive power exchange between the CP-grids and the LV-grid of -37.79 kvar, determined according to equation (5.6), corresponds to the consumers' Q-demand, since their inverters don't inject or absorb any reactive power. These power exchanges lead to active and reactive power flows within the LV-grid and thus to active (12.43 kW) and reactive power losses (10.81 kvar), to an active (-67.90 kW) and reactive power exchange (48.59 kvar) between the LV- and the MV-grid, to a transformer loading of 51.67 % and to a maximal line loading of 34.51 %.

C. Summary

Table 6.4 summarises the simulation results of the theoretical Link-Grid with $P(U)$-controlled CP-Producer-Links on the LV-Grid-, CP-Grid-, CP-Producer-Link chain. The most critical scenarios concerning the

Scenario	Volt. prot.	Viol. index	$\Delta U^{(sdg)}$ [V]	$P^{(loss)}$ [kW]	$Q^{(loss)}$ [kvar]	$P^{(pro)}$ [kW]	$Q^{(pro)}$ [kvar]	$P^{(ex)}$ [kW]	$Q^{(ex)}$ [kvar]	$\mathcal{L}^{(tr)}$ [%]	$\mathcal{L}_{max}^{(sgm)}$ [%]	$P^{(ctl)}$ [kW]
$\mathbf{L^{(min)}} - \mathbf{G^{(min)}}$	$(\checkmark)$	0	15.18	1.32	1.50	-53.14	-16.42	54.46	17.92	36.19	7.58	0
$\mathbf{L^{(max)}} - \mathbf{G^{(min)}}$	$(\checkmark)$	48	31.03	5.43	6.89	-102.13	-29.55	107.57	36.44	73.94	15.43	0
$\mathbf{L^{(min)}} - \mathbf{G^{(max)}}$	$(\checkmark)$	0	27.99	2.27	1.66	36.34	-20.93	-34.06	22.59	24.10	18.20	106.37
$\mathbf{L^{(max)}} - \mathbf{G^{(max)}}$	$(\checkmark)$	0	63.21	12.43	10.81	80.33	-37.79	-67.90	48.59	51.67	34.51	8.88

Table 6.4.: Summarised simulation results of the theoretical Link-Grid with $P(U)$-controlled CP-Producer-Links and without any control on the LV-, CP-Grid-Link chain

voltage violation index, the voltage spreading, the active power losses, the reactive power exchange between the LV- and the MV-grid, the transformer loading, the maximal line loading and the active power curtailment are presented in the following. The maximum voltage violation index occurs in the $L^{(max)} - G^{(min)}$ scenario with overvoltage protections. The maximum voltage spreading occurs in the $L^{(max)} - G^{(max)}$ scenario with overvoltage protections. The maximum active power losses occur in the $L^{(max)} - G^{(max)}$ scenario with overvoltage protections. The maximum reactive power exchange between the LV- and the MV-grid occurs in the $L^{(max)} - G^{(max)}$ scenario with overvoltage protections. The maximum transformer loading occurs in the $L^{(max)} - G^{(min)}$ scenario with overvoltage protections. The maximum maximal line loading occurs in the $L^{(max)} - G^{(max)}$ scenario with overvoltage protections. The maximum active power curtailment occurs in the $L^{(min)} - G^{(max)}$ scenario with overvoltage protections.

Regarding the compliance with the legally stipulated voltage range and the lost active power ($P^{(loss)} + P^{(ctl)}$) as the crucial performance indicators, the $L^{(max)} - G^{(min)}$ scenario with overvoltage protections and the $L^{(min)} - G^{(max)}$ scenario with overvoltage protections are the most critical scenarios for the theoretical Link-Grid's operation with $P(U)$-controlled CP-Producer-Links and without any control on the LV-, CP-Grid-Link chain.

6.3. *Q(U)*-controlled inverters

This section presents and discusses the simulation results of the LV-Grid-Link operation with *Q(U)*-controlled CP-Producer-Links on the LV-Grid-, CP-Grid-, CP-Producer-Link chain. Only the theoretical grid is analysed. Figure 6.15 shows an overview of the LV-Grid-, CP-Grid-, CP-Producer-Link chain with *Q(U)*-controlled CP-Producer-Links.
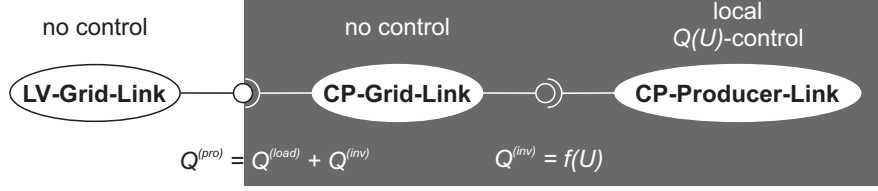
Figure 6.15.: Overview of the LV-Grid-, CP-Grid-, CP-Producer-Link chain with *Q(U)*-controlled CP-Producer-Links

6.3.1. Behaviour of the theoretical Link-Grid

Figure 6.16 shows an overview of the theoretical Link-Grid.
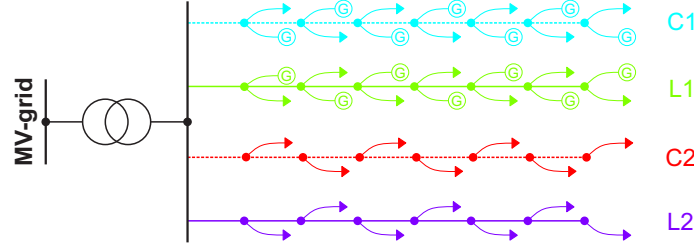
Figure 6.16.: Overview of the theoretical Link-Grid

A. Without distributed electricity production

Figure 6.17 shows the voltage profiles of the theoretical Link-Grid with *Q(U)*-controlled CP-Producer-Links and without any control on the LV-Grid-, CP-Grid-, CP-Producer-Link chain for a $P^{(inv)} = 0kW$ and a $P^{(load,init)} = 54.72kW$. With *Q(U)*-control, neither the upper nor the lower voltage limitation is violated by any node-voltage. The inverters increase their local voltages by injecting reactive power, even though the lower voltage limitation wouldn't by violated without an inverter control. Regarding the case with *Q(U)*-controlled CP-Producer-Links, the increasing node-voltages along the feeder L1 and the decreasing node-voltages along the feeder L2 cause a voltage spreading of 15.18 V, determined according to equation (5.1). The relatively low node-voltages reduce the consumers' active and reactive power demand in total according to the characteristics shown in figure 2.16. Since the inverters don't inject any active power, this results in a reduced active power exchange between the CP-grids and the LV-grid of −53.48 kW, determined according to equation (5.5). The inverters *Q*-injection overcompensates the consumers' *Q*-demand in total, resulting in a reactive power exchange between the CP-grids and the LV-grid of 6.31 kvar, determined according to equation (5.6). These power exchanges lead to active and reactive power flows within the LV-grid and thus to active (1.23 kW) and reactive power losses (1.40 kvar), to an active (54.72 kW) and reactive power exchange (−4.91 kvar) between the LV- and the MV-grid, to a transformer loading of 34.68 % and to a maximal line loading of 8.35 %. The upstream reactive power flow through the transformer overcompensates the active power caused voltage drop along the transformer. This also increases the node-voltages of the feeders without distributed generation, C2 and L2.

Figure 6.18 shows the voltage profiles of the theoretical Link-Grid with *Q(U)*-controlled CP-Producer-Links and without any control on the LV-Grid-, CP-Grid-, CP-Producer-Link chain for a $P^{(inv)} = 0kW$
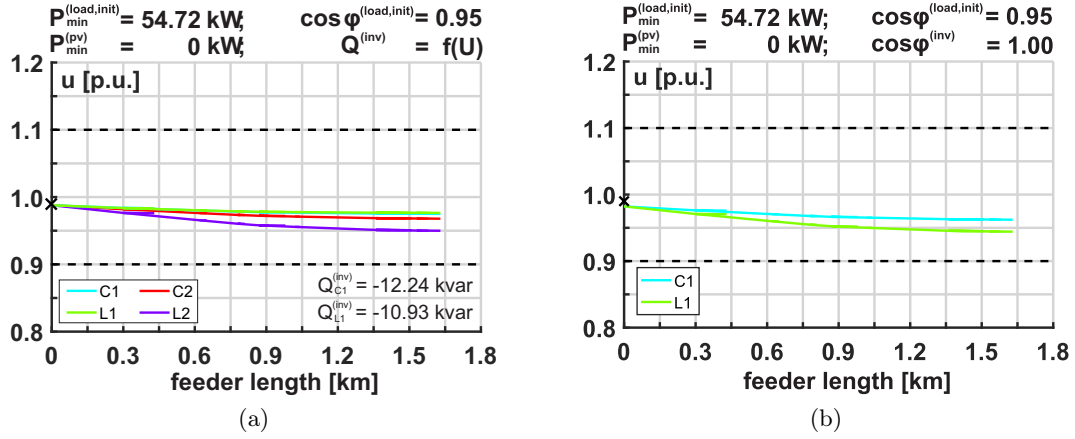
Figure 6.17.: Voltage profiles of the theoretical Link-Grid with different control strategies for a $P^{(inv)} = 0kW$ and a $P^{(load,init)} = 54.72kW$: (a) with $Q(U)$-controlled CP-Producer-Links and without any control on the LV-,CP-Grid-Link chain, (b) without any control on the LV-Grid-, CP-Grid-, CP-Producer-Link chain

and a $P^{(load,init)} = 109.44kW$. With $Q(U)$-control, 11 node-voltages deceed the lower voltage limita-
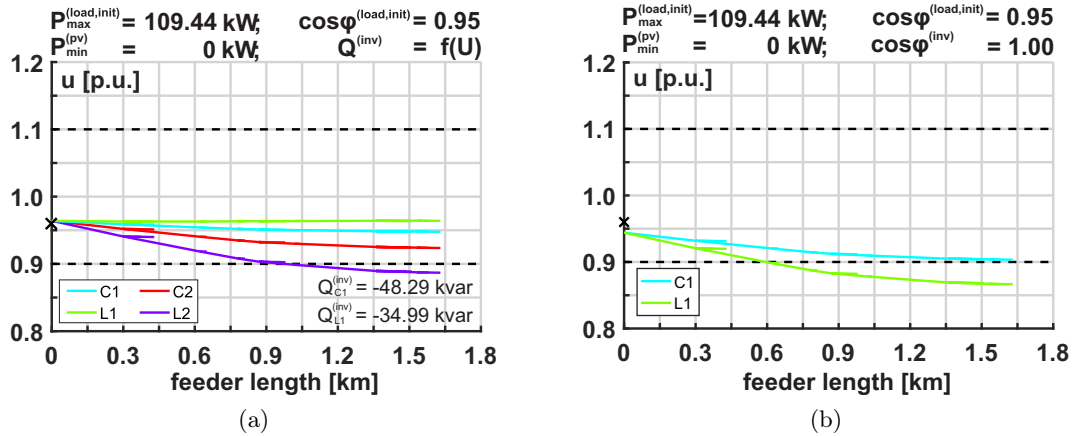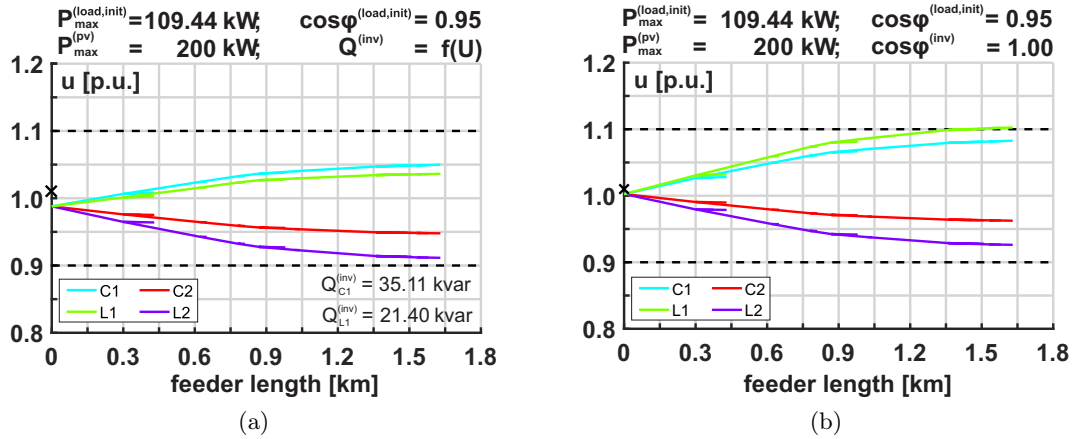

Figure 6.18.: Voltage profiles of the theoretical Link-Grid with different control strategies for a $P^{(inv)} = 0kW$ and a $P^{(load,init)} = 109.44kW$: (a) with $Q(U)$-controlled CP-Producer-Links and without any control on the LV-,CP-Grid-Link chain, (b) without any control on the LV-Grid-, CP-Grid-, CP-Producer-Link chain

tion. The inverters increase their local voltages by injecting reactive power. Regarding the case with $Q(U)$-controlled CP-Producer-Links, the increasing node-voltages along the feeder L1 and the decreasing node-voltages along the feeder L2 cause a voltage spreading of 30.92 V, determined according to equation (5.1). The relatively low node-voltages reduce the consumers' active and reactive power demand in total according to the characteristics shown in figure 2.16. Since the inverters don't inject any active power, this reduced demand results in a reduced active power exchange between the CP-grids and the LV-grid of -104.56 kW, determined according to equation (5.5). The inverters Q-injection overcompensates the consumers' Q-demand in total, resulting in a reactive power exchange between the CP-grids and the LV-grid of 51.71 kvar, determined according to equation (5.6). These power exchanges lead to active and reactive power flows within the LV-grid and thus to active (8.29 kW) and reactive power losses (9.09 kvar), to an active (112.85 kW) and reactive power exchange (-42.62 kvar) between the LV- and the MV-grid, to a transformer loading of 78.54 % and to a maximal line loading of 26.58 %. The upstream

reactive power flow through the transformer overcompensates the active power caused voltage drop along the transformer. This also increases the node-voltages of the feeders without distributed generation, C2 and L2. Compared to the case without $Q(U)$-control (figure 6.18b), the number of node-voltages which violate the lower voltage limitation is reduced from 48 to 11 by the $Q(U)$-control in this scenario.

B. With distributed electricity production

Figure 6.19 shows the voltage profiles of the theoretical Link-Grid with $Q(U)$-controlled CP-Producer-Links on the LV-Grid-, CP-Grid-, CP-Producer-Link chain for a $P^{(inv)} = 200kW$ and a $P^{(load,init)} = 54.72kW$ without and with overvoltage protections. Without overvoltage protections, 9 node-voltages exceed the
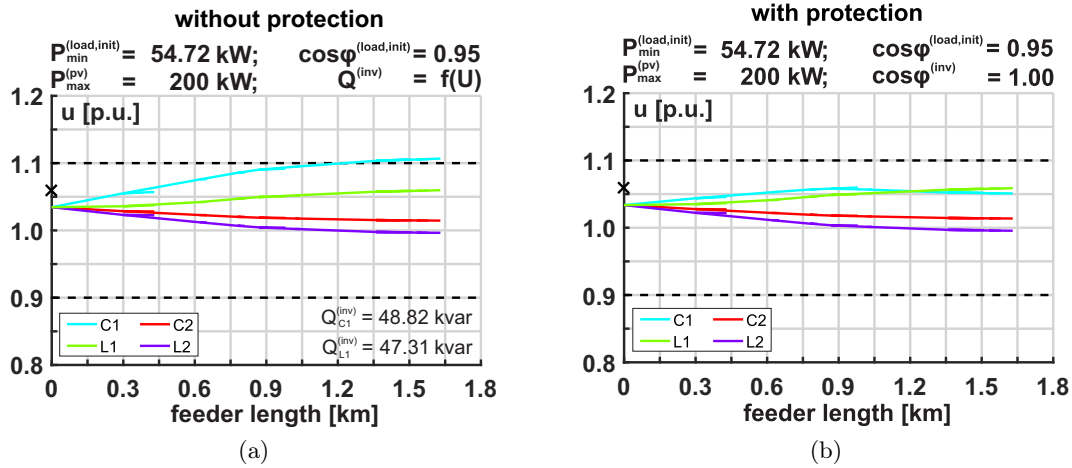
Figure 6.19.: Voltage profiles of the theoretical Link-Grid with $Q(U)$-controlled CP-Producer-Links on the LV-Grid-, CP-Grid-, CP-Producer-Link chain for a $P^{(inv)} = 200kW$ and a $P^{(load,init)} = 54.72kW$: (a) without overvoltage protections, (b) with overvoltage protections

upper voltage limitation. The inverters decrease their local voltages by absorbing reactive power. In this scenario almost all inverters absorb reactive power with a $cos\varphi = 0.9$. Only three of the 40 inverters absorb reactive power with a $cos\varphi > 0.9$. The increasing node-voltages along the feeder C1 and the decreasing node-voltages along the feeder L2 cause a voltage spreading of 44.13 V, determined according to equation (5.1). The relatively high node-voltages increase the consumers' active and reactive power demand in total according to the characteristics shown in figure 2.16. Since the inverters inject active power, this increased demand results in a decreased active power exchange between the CP-grids and the LV-grid of 143.43 kW, determined according to equation (5.5). The inverters Q-absorption together with the consumers' Q-demand results in a reactive power exchange between the CP-grids and the LV-grid of -116.22 kvar, determined according to equation (5.6). These power exchanges lead to active and reactive power flows within the LV-grid and thus to active (25.98 kW) and reactive power losses (27.07 kvar), to an active (-117.46 kW) and reactive power exchange (143.30 kvar) between the LV- and the MV-grid, to a transformer loading of 109.25 % and to a maximal line loading of 48.65 %. The additional reactive power flow through the transformer which is provoked by the $Q(U)$-controlled inverters decreases the transformer's secondary voltage and thus also the node-voltages of the feeders without distributed generation, C2 and L2. Compared to the case without $Q(U)$-control (figure 6.5a), the number of node-voltages which violate the upper voltage limitation is reduced from 48 to 9 by the $Q(U)$-control in this scenario.

With overvoltage protections, neither the upper nor the lower voltage limitation is violated by any node-voltage. Only 35 kW of active power are curtailed instead of 180 kW with uncontrolled inverters (figure 6.5b). The increasing node-voltages along the feeder C1 and the decreasing node-voltages along the feeder L2 cause a voltage spreading of 25.68 V, determined according to equation (5.1). The relatively high node-voltages increase the consumers' active and reactive power demand in total according to the

characteristics shown in figure 2.16. Since the inverters inject active power, this increased demand results in a decreased active power exchange between the CP-grids and the LV-grid of 108.93 kW, determined according to equation (5.5). The inverters Q-absorption together with the consumers' Q-demand results in a reactive power exchange between the CP-grids and the LV-grid of -115.41 kvar, determined according to equation (5.6). These power exchanges lead to active and reactive power flows within the LV-grid and thus to active (19.96 kW) and reactive power losses (23.25 kvar), to an active (-88.98 kW) and reactive power exchange (138.66 kvar) between the LV- and the MV-grid, to a transformer loading of 97.14 % and to a maximal line loading of 42.99 %. The additional reactive power flow through the transformer which is provoked by the $Q(U)$-controlled inverters decreases the transformer's secondary voltage and thus also the node-voltages of the feeders without distributed generation, C2 and L2.

Figure 6.20 shows the voltage profiles of the theoretical Link-Grid with $Q(U)$-controlled CP-Producer-Links and without any control on the LV-Grid-, CP-Grid-, CP-Producer-Link chain for a $P^{(inv)} = 200kW$ and a $P^{(load,init)} = 109.44kW$. With $Q(U)$-control, neither the upper nor the lower voltage limitation

Figure 6.20.: Voltage profiles of the theoretical Link-Grid with different control strategies for a $P^{(inv)} = 200kW$ and a $P^{(load,init)} = 109.44kW$: (a) with $Q(U)$-controlled CP-Producer-Links and without any control on the LV-,CP-Grid-Link chain, (b) without any control on the LV-Grid-, CP-Grid-, CP-Producer-Link chain

is violated by any node-voltage. The inverters decrease their local voltages by absorbing reactive power. The increasing node-voltages along the feeder C1 and the decreasing node-voltages along the feeder L2 cause a voltage spreading of 55.36 V, determined according to equation (5.1). The relatively low node-voltages reduce the consumers' active and reactive power demand in total according to the characteris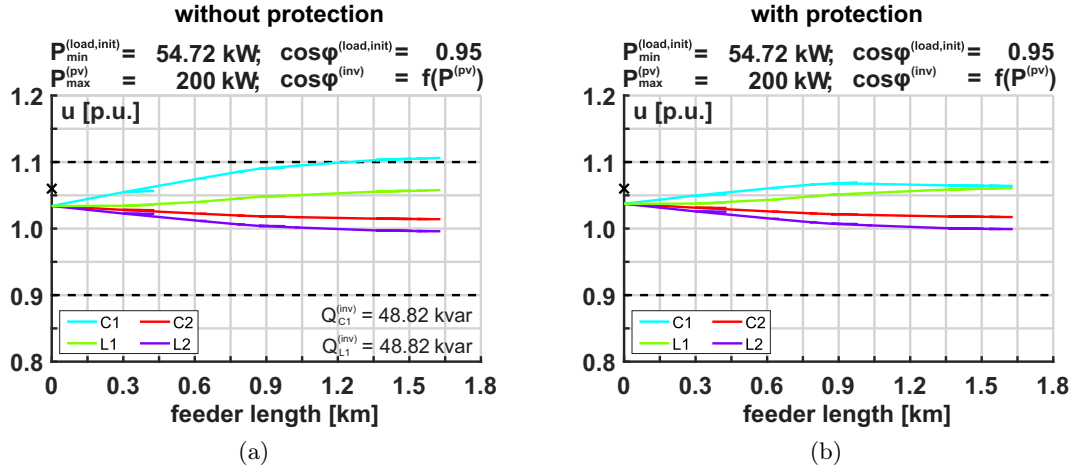tics shown in figure 2.16. Since the inverters inject active power, this reduced demand results in an increased active power exchange between the CP-grids and the LV-grid of 91.40 kW, determined according to equation (5.5). The inverters Q-absorption together with the consumers' Q-demand results in a reactive power exchange between the CP-grids and the LV-grid of -91.86 kvar, determined according to equation (5.6). These power exchanges lead to active and reactive power flows within the LV-grid and thus to active (19.86 kW) and reactive power losses (18.67 kvar), to an active (-71.54 kW) and reactive power exchange (110.53 kvar) between the LV- and the MV-grid, to a transformer loading of 81.48 % and to a maximal line loading of 42.69 %. The additional reactive power flow through the transformer which is provoked by the $Q(U)$-controlled inverters decreases the transformer's secondary voltage and thus also the node-voltages of the feeders without distributed generation, C2 and L2. Compared to the case without $Q(U)$-control (figure 6.20b), the number of node-voltages which violate the upper voltage limitation is reduced from 6 to 0 by the $Q(U)$-control in this scenario. Hence, none of the overvoltage protections trips and thus no active power is curtailed.

C. Summary

Table 6.5 summarises the simulation results of the theoretical Link-Grid with $Q(U)$-controlled CP-Producer-Links on the LV-Grid-, CP-Grid-, CP-Producer-Link chain. The most critical scenarios concerning the

Scenario	Volt. prot.	Viol. index	$\Delta U^{(sdg)}$ [V]	$P^{(loss)}$ [kW]	$Q^{(loss)}$ [kvar]	$P^{(pro)}$ [kW]	$Q^{(pro)}$ [kvar]	$P^{(ex)}$ [kW]	$Q^{(ex)}$ [kvar]	$\mathcal{L}^{(tr)}$ [%]	$\mathcal{L}_{max}^{(sgm)}$ [%]	$P^{(ctl)}$ [kW]
$L^{(min)} - G^{(min)}$	$(\checkmark)$	0	15.18	1.23	1.40	-53.48	6.31	54.72	-4.91	34.68	8.35	0
$L^{(max)} - G^{(min)}$	$(\checkmark)$	11	30.92	8.29	9.09	-104.56	51.71	112.85	-42.62	78.54	26.58	0
$L^{(min)} - G^{(max)}$	$\times$	9	44.13	25.98	27.07	143.43	-116.22	-117.46	143.30	109.25	48.65	0
$L^{(min)} - G^{(max)}$	$\checkmark$	0	25.68	19.96	23.25	108.93	-115.41	-88.98	138.66	97.14	42.99	35
$L^{(max)} - G^{(max)}$	$(\checkmark)$	0	55.36	19.86	18.67	91.40	-91.86	-71.54	110.53	81.48	42.69	0

Table 6.5.: Summarised simulation results of the theoretical Link-Grid with $Q(U)$-controlled CP-Producer-Links and without any control on the LV-, CP-Grid-Link chain

voltage violation index, the voltage spreading, the active power losses, the reactive power exchange between the LV- and the MV-grid, the transformer loading, the maximal line loading and the active power curtailment are presented in the following. The maximum voltage violation index occurs in the $L^{(max)} - G^{(min)}$ scenario with overvoltage protections and in the $L^{(min)} - G^{(max)}$ scenario without overvoltage protections. The maximum voltage spreading occurs in the $L^{(max)} - G^{(max)}$ scenario with overvoltage protections. The maximum active power losses occur in the $L^{(min)} - G^{(max)}$ scenario without overvoltage protections. The maximum reactive power exchange between the LV- and the MV-grid occurs in the $L^{(min)} - G^{(max)}$ scenario without overvoltage protections. The maximum transformer loading occurs in the $L^{(min)} - G^{(max)}$ scenario without overvoltage protections. The maximum maximal line loading occurs in the $L^{(min)} - G^{(max)}$ scenario without overvoltage protections. The maximum active power curtailment occurs in the $L^{(min)} - G^{(max)}$ scenario with overvoltage protections.

Regarding the compliance with the legally stipulated voltage range and the lost active power ($P^{(loss)} + P^{(ctl)}$) as the crucial performance indicators, the $L^{(max)} - G^{(min)}$ scenario with overvoltage protections, the $L^{(min)} - G^{(max)}$ scenario without overvoltage protections and the $L^{(min)} - G^{(max)}$ scenario with overvoltage protections are the most critical scenarios for the theoretical Link-Grid's operation with $Q(U)$-controlled CP-Producer-Links and without any control on the LV-, CP-Grid-Link chain.

6.4. cosφ(P)-controlled inverters

This section presents and discusses the simulation results of the LV-Grid-Link operation with $cos\varphi(P)$-controlled CP-Producer-Links on the LV-Grid-, CP-Grid-, CP-Producer-Link chain. Only the theoretical grid is analysed. Figure 6.21 shows an overview of the LV-Grid-, CP-Grid-, CP-Producer-Link chain with $cos\varphi(P)$-controlled CP-Producer-Links.
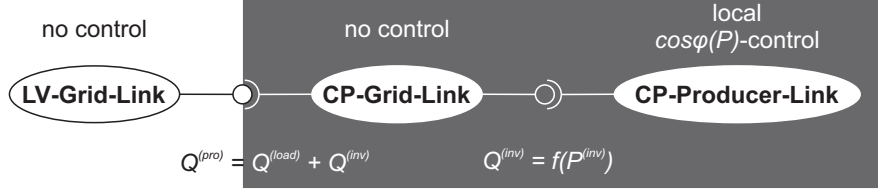
Figure 6.21.: Overview of the LV-Grid-, CP-Grid-, CP-Producer-Link chain with $cos\varphi(P)$-controlled CP-Producer-Links

6.4.1. Behaviour of the theoretical Link-Grid

Figure 6.22 shows an overview of the theoretical Link-Grid.
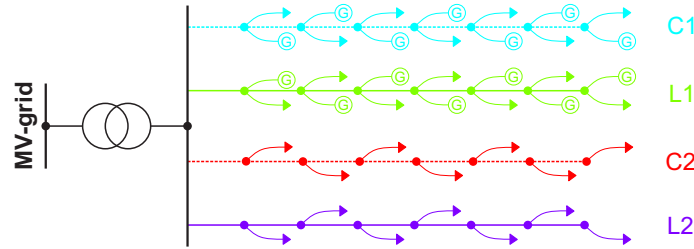
Figure 6.22.: Overview of the theoretical Link-Grid

A. Without distributed electricity production

With the settings assumed in section 3.3.4, a $cos\varphi(P)$-controlled inverter only absorbs reactive power if its injecting active power. Hence, simulating the "min load, no generation"- and the "max load, no generation"-scenarios with $cos\varphi(P)$-controlled CP-Producer-Links yields the same results as with uncontrolled CP-Producer-Links. Therefore only the simulation results of the "min load, max generation"- and the "max load, max generation"-scenarios are presented in the following.

B. With distributed electricity production

According to the setting assumed in section 3.3.4, all inverters inject active power with a power factor of 0.90 during peak generation periods.

Figure 6.23 shows the voltage profiles of the theoretical Link-Grid with $cos\varphi(P)$-controlled CP-Producer-Links on the LV-Grid-, CP-Grid-, CP-Producer-Link chain for a $P^{(inv)} = 200kW$ and a $P^{(load,init)} = 54.72kW$ without and with overvoltage protections. In both cases, the $cos\varphi(P)$-control behaves quiet similar to the $Q(U)$-control (figure 6.19), since also with $Q(U)$-control almost all inverters absorb reactive power with a $cos\varphi = 0.9$ in this scenario.

Without overvoltage protections, 9 node-voltages exceed the upper voltage limitation. The inverters decrease their local voltages by absorbing reactive power. The increasing node-voltages along the feeder C1 and the decreasing node-voltages along the feeder L2 cause a voltage spreading of 44.14 V, determined according to equation (5.1). The relatively high node-voltages increase the consumers' active and reactive power demand in total according to the characteristics shown in figure 2.16. Since the inverters inject active
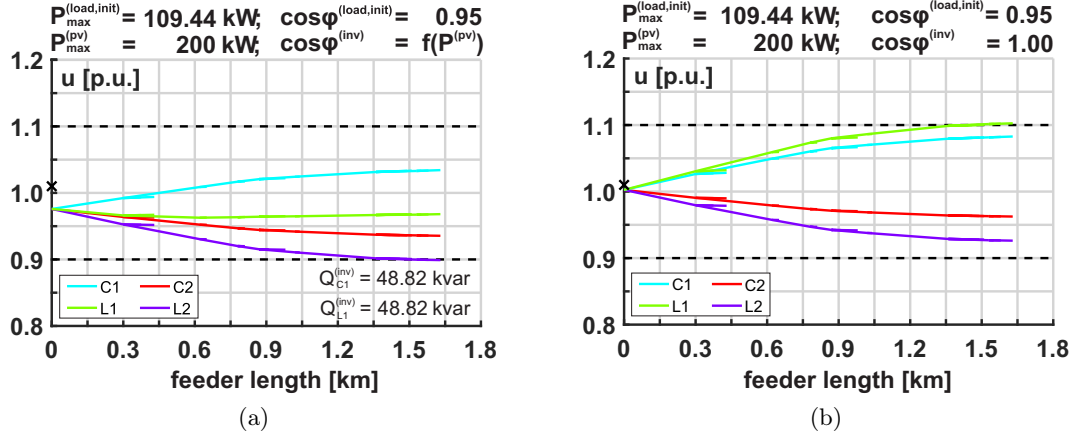
Figure 6.23.: Voltage profiles of the theoretical Link-Grid with $cos\varphi(P)$-controlled CP-Producer-Links on the LV-Grid-, CP-Grid-, CP-Producer-Link chain for a $P^{(inv)} = 200kW$ and a $P^{(load,init)} = 54.72kW$: (a) without overvoltage protections, (b) with overvoltage protections

power, this increased demand results in a decreased active power exchange between the CP-grids and the LV-grid of 143.47 kW, determined according to equation (5.5). The inverters Q-absorption together with the consumers' Q-demand results in a reactive power exchange between the CP-grids and the LV-grid of -117.70 kvar, determined according to equation (5.6). These power exchanges lead to active and reactive power flows within the LV-grid and thus to active (26.27 kW) and reactive power losses (27.46 kvar), to an active (-117.20 kW) and reactive power exchange (145.16 kvar) between the LV- and the MV-grid, to a transformer loading of 110.00 % and to a maximal line loading of 48.67 %. The additional reactive power flow through the transformer which is provoked by the $cos\varphi(P)$-controlled inverters decreases the transformer's secondary voltage and thus also the node-voltages of the feeders without distributed generation, C2 and L2. Compared to the case without $cos\varphi(P)$-control (figure 6.5a), the number of node-voltages which violate the upper voltage limitation is reduced from 48 to 9 by the $cos\varphi(P)$-control in this scenario.

With overvoltage protections, neither the upper nor the lower voltage limitation is violated by any node-voltage. Only 35 kW of active power are curtailed instead of 180 kW with uncontrolled inverters (figure 6.5b). The increasing node-voltages along the feeder C1 and the decreasing node-voltages along the feeder L2 cause a voltage spreading of 28.08 V, determined according to equation (5.1). The relatively high node-voltages increase the consumers' active and reactive power demand in total according to the characteristics shown in figure 2.16. Since the inverters inject active power, this increased demand results in a decreased active power exchange between the CP-grids and the LV-grid of 108.69 kW, determined according to equation (5.5). The inverters Q-absorption together with the consumers' Q-demand results in a reactive power exchange between the CP-grids and the LV-grid of -100.33 kvar, determined according to equation (5.6). These power exchanges lead to active and reactive power flows within the LV-grid and thus to active (19.67 kW) and reactive power losses (22.54 kvar), to an active (-89.02 kW) and reactive power exchange (122.87 kvar) between the LV- and the MV-grid, to a transformer loading of 89.46 % and to a maximal line loading of 43.36 %. The additional reactive power flow through the transformer which is provoked by the $cos\varphi(P)$-controlled inverters decreases the transformer's secondary voltage and thus also the node-voltages of the feeders without distributed generation, C2 and L2.

Figure 6.24 shows the voltage profiles of the theoretical Link-Grid with $cos\varphi(P)$-controlled CP-Producer-Links and without any control on the LV-Grid-, CP-Grid-, CP-Producer-Link chain for a $P^{(inv)} = 200kW$ and a $P^{(load,init)} = 109.44kW$. With $cos\varphi(P)$-control, 4 node-voltages deceed the lower voltage limitation. The inverters decrease their local voltages by absorbing reactive power. The increasing node-voltages along the feeder C1 and the decreasing node-voltages along the feeder L2 cause a voltage spreading of 54.10 V, determined according to equation (5.1). The relatively low node-voltages reduce the consumers' active and reactive power demand in total according to the characteristics shown in figure 2.16. Since the
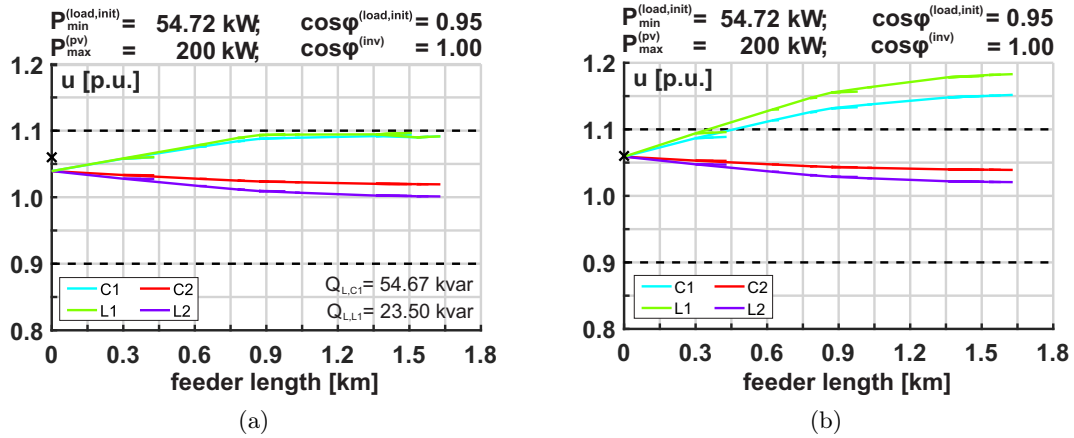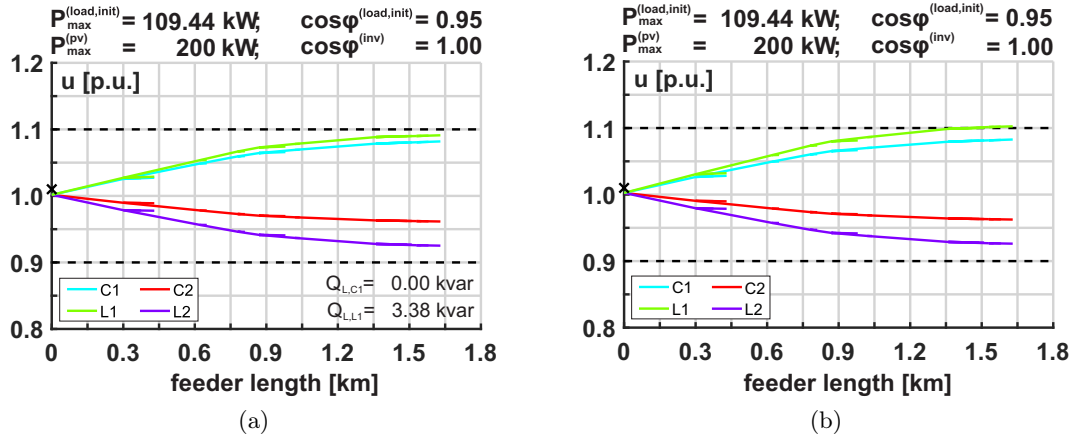
Figure 6.24.: Voltage profiles of the theoretical Link-Grid with different control strategies for a $P^{(inv)} = 200kW$ and a $P^{(load,init)} = 109.44kW$: (a) with $cos\varphi(P)$-controlled CP-Producer-Links and without any control on the LV-,CP-Grid-Link chain, (b) without any control on the LV-Grid-, CP-Grid-, CP-Producer-Link chain

inverters inject active power, this reduced demand results in an increased active power exchange between the CP-grids and the LV-grid of 93.40 kW, determined according to equation (5.5). The inverters Q-absorption together with the consumers' Q-demand results in a reactive power exchange between the CP-grids and the LV-grid of -131.00 kvar, determined according to equation (5.6). These power exchanges lead to active and reactive power flows within the LV-grid and thus to active (27.46 kW) and reactive power losses (28.25 kvar), to an active (-65.93 kW) and reactive power exchange (159.25 kvar) between the LV- and the MV-grid, to a transformer loading of 106.66 % and to a maximal line loading of 47.63 %. The additional reactive power flow through the transformer which is provoked by the $cos\varphi(P)$-controlled inverters decreases the transformer's secondary voltage and thus also the node-voltages of the feeders without distributed generation, C2 and L2. Compared to the case without $cos\varphi(P)$-control (figure 6.24b), the number of node-voltages which violate the upper voltage limitation is reduced from 6 to 0, but on the other hand, the number of node-voltages which violate the lower voltage limitation is increased from 0 to 4 by the $cos\varphi(P)$-control in this scenario. Hence, none of the overvoltage protections trips and thus no active power is curtailed.

C. Summary

Table 6.6 summarises the simulation results of the theoretical Link-Grid with $cos\varphi(P)$-controlled CP-Producer-Links on the LV-Grid-, CP-Grid-, CP-Producer-Link chain. The most critical scenarios con-

Scenario	Volt. prot.	Viol. index	$\Delta U^{(sdg)}$ [V]	$P^{(loss)}$ [kW]	$Q^{(loss)}$ [kvar]	$P^{(pro)}$ [kW]	$Q^{(pro)}$ [kvar]	$P^{(ex)}$ [kW]	$Q^{(ex)}$ [kvar]	$\mathcal{L}^{(tr)}$ [%]	$\mathcal{L}_{max}^{(sgm)}$ [%]	$P^{(ctl)}$ [kW]
$L^{(min)} - G^{(min)}$	$(\checkmark)$	0	15.18	1.32	1.50	-53.14	-16.42	54.46	17.92	36.19	7.58	0
$L^{(max)} - G^{(min)}$	$(\checkmark)$	48	31.03	5.43	6.89	-102.13	-29.55	107.57	36.44	73.94	15.43	0
$L^{(min)} - G^{(max)}$	$\times$	9	44.14	26.27	27.46	143.47	-117.70	-117.20	145.16	110.00	48.67	0
$L^{(min)} - G^{(max)}$	$\checkmark$	0	28.08	19.67	22.54	108.69	-100.33	-89.02	122.87	89.46	43.36	35
$L^{(max)} - G^{(max)}$	$(\checkmark)$	4	54.10	27.46	28.25	93.40	-131.00	-65.93	159.25	106.66	47.63	0

Table 6.6.: Summarised simulation results of the theoretical Link-Grid with $cos\varphi(P)$-controlled CP-Producer-Links and without any control on the LV-, CP-Grid-Link chain

cerning the voltage violation index, the voltage spreading, the active power losses, the reactive power exchange between the LV- and the MV-grid, the transformer loading, the maximal line loading and the active power curtailment are presented in the following. The maximum voltage violation index occurs in the $L^{(max)} - G^{(min)}$ scenario with overvoltage protections. The maximum voltage spreading occurs

in the $L^{(max)} - G^{(max)}$ scenario with overvoltage protections. The maximum active power losses occur in the $L^{(max)} - G^{(max)}$ scenario with overvoltage protections. The maximum reactive power exchange between the LV- and the MV-grid occurs in the $L^{(max)} - G^{(max)}$ scenario with overvoltage protections. The maximum transformer loading occurs in the $L^{(min)} - G^{(max)}$ scenario without overvoltage protections. The maximum maximal line loading occurs in the $L^{(min)} - G^{(max)}$ scenario without overvoltage protections. The maximum active power curtailment occurs in the $L^{(min)} - G^{(max)}$ scenario with overvoltage protections.

Regarding the compliance with the legally stipulated voltage range and the lost active power ($P^{(loss)} + P^{(ctl)}$) as the crucial performance indicators, the $L^{(max)} - G^{(min)}$ scenario with overvoltage protections and the $L^{(min)} - G^{(max)}$ scenario with overvoltage protections are the most critical scenarios for the theoretical Link-Grid's operation with $cos\varphi(P)$-controlled CP-Producer-Links and without any control on the LV-, CP-Grid-Link chain.

6.5. *L(U)*-controlled LV-Grid-Link

This section presents and discusses the simulation results of the LV-Grid-Link operation with *L(U)*-controlled LV-Grid-Links on the LV-Grid-, CP-Grid-, CP-Producer-Link chain. Both types of grids, the theoretical and the real grids are analysed. Figure 6.25 shows an overview of the LV-Grid-, CP-Grid-, CP-Producer-Link chain with *L(U)*-controlled LV-Grid-Links.
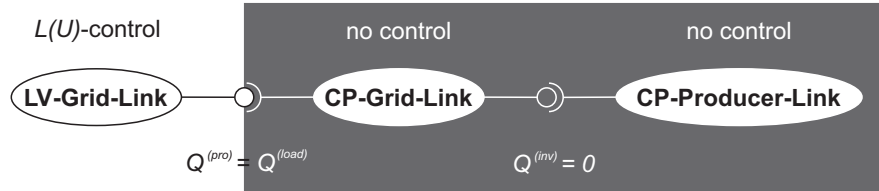
Figure 6.25.: Overview of the LV-Grid-, CP-Grid-, CP-Producer-Link chain with *L(U)*-controlled LV-Grid-Links

6.5.1. Behaviour of the theoretical Link-Grid

Figure 6.26 shows an overview of the theoretical Link-Grid with control coils at the end of the feeders C1 and L1.
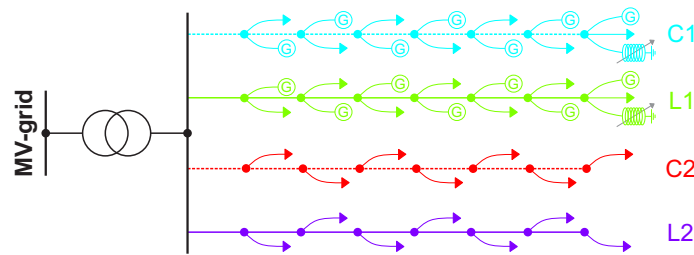
Figure 6.26.: Overview of the theoretical Link-Grid with control coils

A. Without distributed electricity production

With the settings assumed in section 3.3.5, the control coils only absorb reactive power if their local voltages exceed 1.09 p.u.. Hence, simulating the "min load, no generation"- and the "max load, no generation"-scenarios with *L(U)*-controlled LV-Grid-Links yields the same results as with uncontrolled LV-Grid-Links. Therefore only the simulation results of the "min load, max generation"- and the "max load, max generation"-scenarios are presented in the following.

B. With distributed electricity production

Figure 6.27 shows the voltage profiles of the theoretical Link-Grid with $L(U)$-controlled LV-Grid-Links and without any control on the LV-Grid-, CP-Grid-, CP-Producer-Link chain for a $P^{(inv)} = 200kW$ and a $P^{(load,init)} = 54.72kW$. With $L(U)$-control, neither the upper nor the lower voltage limitation is violated

Figure 6.27.: Voltage profiles of the theoretical Link-Grid with different control strategies for a $P^{(inv)} = 200kW$ and a $P^{(load,init)} = 54.72kW$: (a) with $L(U)$-controlled LV-Grid-Links and without any control on the CP-Grid-, CP-Producer-Link chain, (b) without any control on the LV-Grid-, CP-Grid-, CP-Producer-Link chain

by any node-voltage. The control coils decrease their local voltages by absorbing reactive power. The control coil located at feeder C1 absorbs 54.67 kvar while the control coil located at feeder L1 absorbs 23.50 kvar. The increasing node-voltages along the feeder L1 and the decreasing node-voltages along the feeder L2 cause a voltage spreading of 38.18 V, determined according to equation (5.1). The relatively high node-voltages increase the consumers' active and reactive power demand in total according to the characteristics shown in figure 2.16. Since the inverters inject active power, this increased demand results in an decreased active power exchange between the CP-grids and the LV-grid of 142.94 kW, determined according to equation (5.5). The reactive power exchange between the CP-grids and the LV-grid of -20.68 kvar, determined according to equation (5.6), corresponds to the consumers' Q-demand, since their inverters don't inject or absorb any reactive power. To keep their local voltages at 1.09 p.u., the control coil located at feeder C1 absorbs 54.67 kvar and that located at feeder L1 absorbs 23.50 kvar of reactive power. The power exchanges between the CP-grids and the LV-grid together with the control coils Q-absorption lead to active and reactive power flows within the LV-grid and thus to active (25.36 kW) and reactive power losses (101.70 kvar), to an active (-117.58 kW) and reactive power exchange (122.38 kvar) between the LV- and the MV-grid, to a transformer loading of 100.07 % and to a maximal line loading of 49.52 %. Since the reactive power losses represent the Q-consumption of the LV-grid's electrical equipment they also contain the control coils Q-absorption. The additional reactive power flow through the transformer which is provoked by the $L(U)$-controlled coils decreases the transformer's secondary voltage and thus also the node-voltages of the feeders without distributed generation, C2 and L2. Compared to the case without $L(U)$-control (figure 6.27b), the number of node-voltages which violate the upper voltage limitation is reduced from 48 to 0 by the $L(U)$-control in this scenario. Hence, none of the overvoltage protections trips and thus no active power is curtailed.
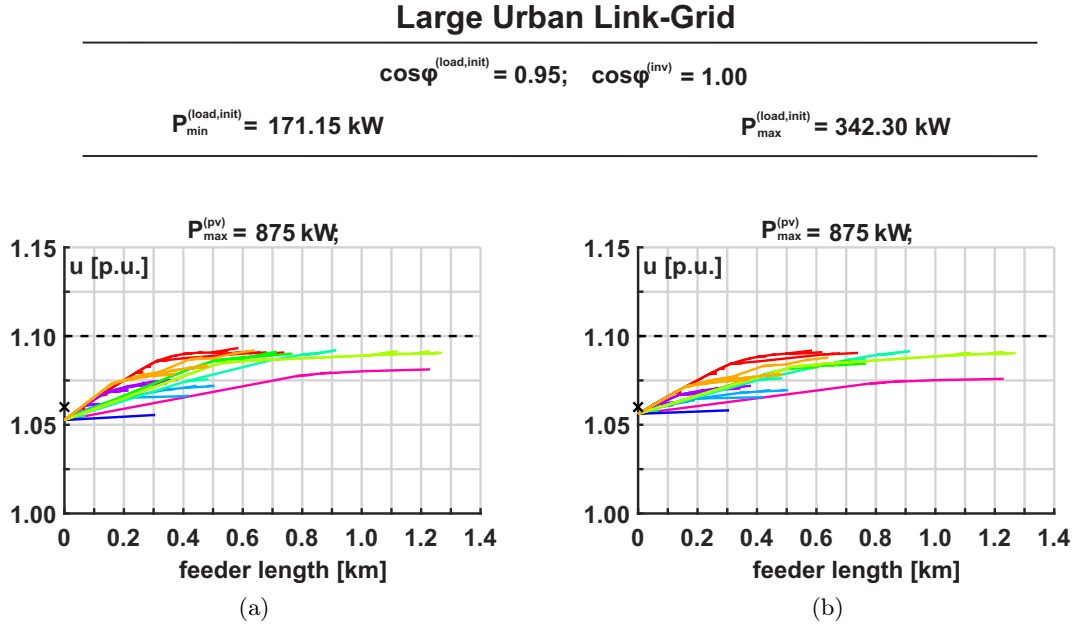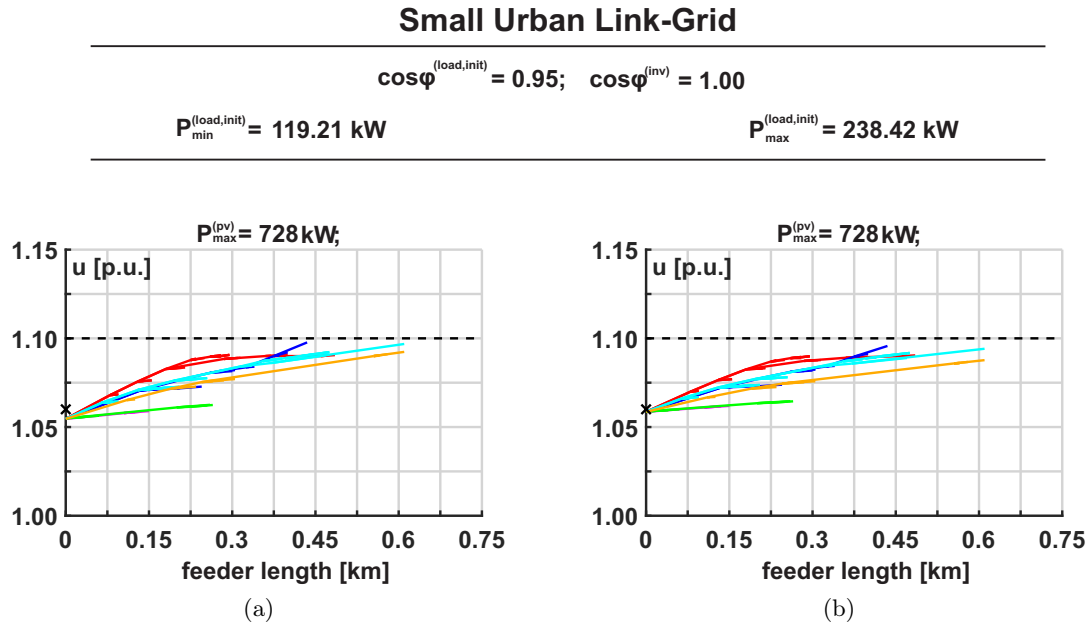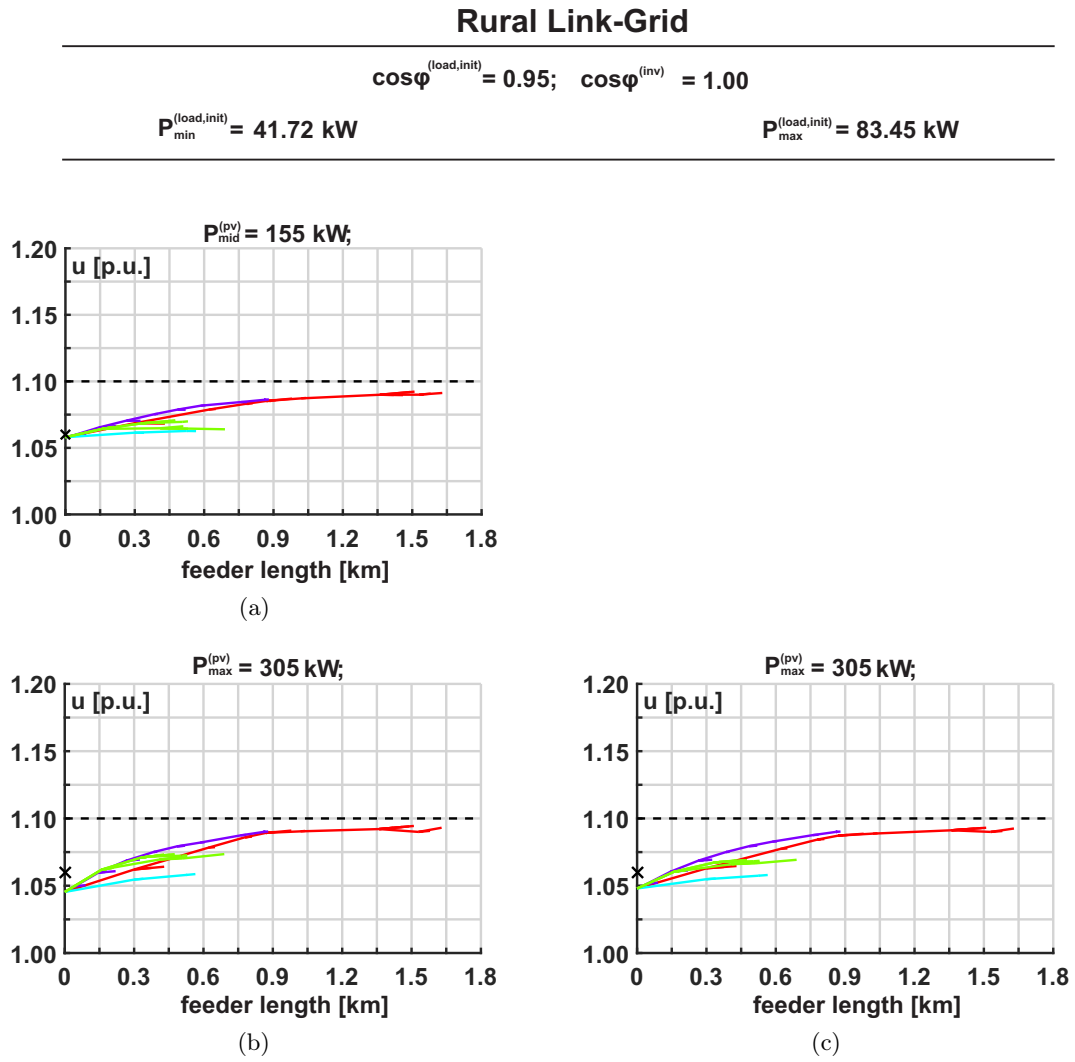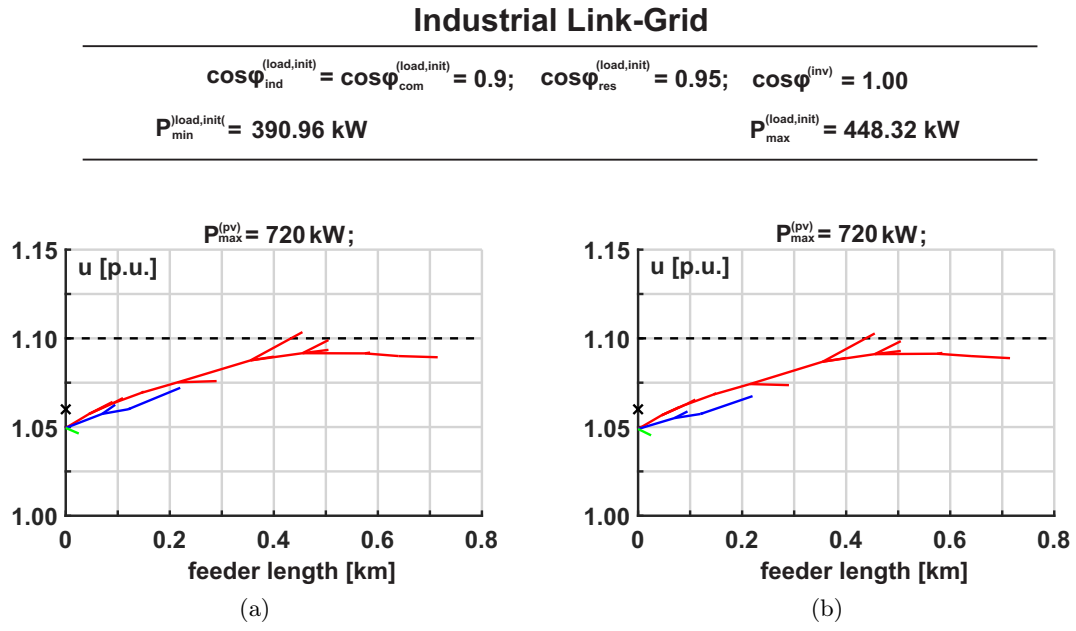
Figure 6.28 shows the voltage profiles of the theoretical Link-Grid with $L(U)$-controlled LV-Grid-Links and without any control on the LV-Grid-, CP-Grid-, CP-Producer-Link chain for a $P^{(inv)} = 200kW$ and a $P^{(load,init)} = 109.44kW$. With $L(U)$-control, neither the upper nor the lower voltage limitation is violated by any node-voltage. The control coils decrease their local voltages by absorbing reactive power. The control coil located at feeder C1 doesn't absorb any reactive power while the control coil located at feeder L1 absorbs 3.38 kvar. The increasing node-voltages along the feeder L1 and the decreasing node-

Figure 6.28.: Voltage profiles of the theoretical Link-Grid with different control strategies for a $P^{(inv)} = 200kW$ and a $P^{(load,init)} = 109.44kW$: (a) with $L(U)$-controlled LV-Grid-Links and without any control on the CP-Grid-, CP-Producer-Link chain, (b) without any control on the LV-Grid-, CP-Grid-, CP-Producer-Link chain

voltages along the feeder L2 cause a voltage spreading of 66.36 V, determined according to equation (5.1). The relatively high node-voltages increase the consumers' active and reactive power demand in total according to the characteristics shown in figure 2.16. Since the inverters inject active power, this increased demand results in an decreased active power exchange between the CP-grids and the LV-grid of 89.16 kW, determined according to equation (5.5). The reactive power exchange between the CP-grids and the LV-grid of -37.87 kvar, determined according to equation (5.6), corresponds to the consumers' Q-demand, since their inverters don't inject or absorb any reactive power. To keep its local voltage at 1.09 p.u., the control coil located at feeder L1 absorbs 3.38 kvar of reactive power. The control coil located at feeder C1 doesn't absorb any reactive power since its local voltage is below 1.09 p.u.. The power exchanges between the CP-grids and the LV-grid together with the control coils Q-absorption lead to active and reactive power flows within the LV-grid and thus to active (14.71 kW) and reactive power losses (16.74 kvar), to an active (-74.45 kW) and reactive power exchange (54.61 kvar) between the LV- and the MV-grid, to a transformer loading of 57.14 % and to a maximal line loading of 35.46 %. Since the reactive power losses represent the Q-consumption of the LV-grid's electrical equipment they also contain the control coils Q-absorption. The additional reactive power flow through the transformer which is provoked by the $L(U)$-controlled coils decreases the transformer's secondary voltage and thus also the node-voltages of the feeders without distributed generation, C2 and L2. Compared to the case without $L(U)$-control (figure 6.27b), the number of node-voltages which violate the upper voltage limitation is reduced from 6 to 0 by the $L(U)$-control in this scenario. Hence, none of the overvoltage protections trips and thus no active power is curtailed.

C. Summary

Table 6.7 summarises the simulation results of the theoretical Link-Grid with $L(U)$-controlled LV-Grid-Links on the LV-Grid-, CP-Grid-, CP-Producer-Link chain. The most critical scenarios concerning the

Scenario	Volt. prot.	Viol. index	$\Delta U^{(sdg)}$ [V]	$P^{(loss)}$ [kW]	$Q^{(loss)}$ [kvar]	$P^{(pro)}$ [kW]	$Q^{(pro)}$ [kvar]	$P^{(ex)}$ [kW]	$Q^{(ex)}$ [kvar]	$\mathcal{L}^{(tr)}$ [%]	$\mathcal{L}^{(sgm)}_{max}$ [%]	$P^{(ctl)}$ [kW]
$L^{(min)} - G^{(min)}$	($\checkmark$)	0	15.18	1.32	1.50	-53.14	-16.42	54.46	17.92	36.19	7.58	0
$L^{(max)} - G^{(min)}$	($\checkmark$)	48	31.03	5.43	6.89	-102.13	-29.55	107.57	36.44	73.94	15.43	0
$L^{(min)} - G^{(max)}$	($\checkmark$)	0	38.18	25.36	101.70	142.94	-20.68	-117.58	122.38	100.07	49.52	0
$L^{(max)} - G^{(max)}$	($\checkmark$)	0	66.36	14.71	16.74	89.16	-37.87	-74.45	54.61	57.14	35.46	0

Table 6.7.: Summarised simulation results of the theoretical Link-Grid with $L(U)$-controlled LV-Grid-Links and without any control on the CP-Grid-, CP-Producer-Link chain

voltage violation index, the voltage spreading, the active power losses, the reactive power exchange between the LV- and the MV-grid, the transformer loading, the maximal line loading and the active power curtailment are presented in the following. The maximum voltage violation index occurs in the $L^{(max)} - G^{(min)}$ scenario with overvoltage protections. The maximum voltage spreading occurs in the $L^{(max)} - G^{(max)}$ scenario with overvoltage protections. The maximum active power losses occur in the $L^{(min)} - G^{(max)}$ scenario with overvoltage protections. The maximum reactive power exchange between the LV- and the MV-grid occurs in the $L^{(min)} - G^{(max)}$ scenario with overvoltage protections. The maximum transformer loading occurs in the $L^{(min)} - G^{(max)}$ scenario with overvoltage protections. The maximum maximal line loading occurs in the $L^{(min)} - G^{(max)}$ scenario with overvoltage protections. No active power curtailment occurs in any of the simulated scenarios. Regarding the compliance with the legally stipulated voltage range and the lost active power $(P^{(loss)} + P^{(ctl)})$ as the crucial performance indicators, the $L^{(max)} - G^{(min)}$ scenario with overvoltage protections and the $L^{(min)} - G^{(max)}$ scenario with overvoltage protections are the most critical scenarios for the theoretical Link-Grid's operation with $L(U)$-controlled LV-Grid-Links and without any control on the CP-Grid-, CP-Producer-Link chain.

6.5.2. Behaviour of the real Link-Grids

A. Large Urban Link-Grid

Figure 6.29.: Voltage profiles of the Large Urban Link-Grid with $L(U)$-controlled LV-Grid-Links and without any control on the CP-Grid-, CP-Producer-Link chain for different load/production scenarios: (a) min load, max production, (b) max load, max production

B. Small Urban Link-Grid

Small Urban Link-Grid

$\cos\varphi^{(load,init)} = 0.95;\quad \cos\varphi^{(inv)} = 1.00$

$P_{min}^{(load,init)} = 119.21\ \text{kW}$ $P_{max}^{(load,init)} = 238.42\ \text{kW}$

(a)   (b)

Figure 6.30.: Voltage profiles of the Small Urban Link-Grid with $L(U)$-controlled LV-Grid-Links and without any control on the CP-Grid-, CP-Producer-Link chain for different load/production scenarios: (a) min load, max production, (b) max load, max production

C. Rural Link-Grid

Rural Link-Grid

$\cos\varphi^{(load,init)} = 0.95;$ $\cos\varphi^{(inv)} = 1.00$

$P_{min}^{(load,init)} = 41.72$ kW

$P_{max}^{(load,init)} = 83.45$ kW

(a)

(b)

(c)

Figure 6.31.: Voltage profiles of the Rural Link-Grid with *L(U)*-controlled LV-Grid-Links and without any control on the CP-Grid-, CP-Producer-Link chain for different load/production scenarios: (a) min load, mid production, (b) min load, max production, (c) max load, max production

D. Industrial Link-Grid

Industrial Link-Grid

$\cos\varphi_{ind}^{(load,init)} = \cos\varphi_{com}^{(load,init)} = 0.9; \quad \cos\varphi_{res}^{(load,init)} = 0.95; \quad \cos\varphi^{(inv)} = 1.00$

$P_{min}^{)load,init(} = 390.96\ kW$ $\qquad\qquad\qquad\qquad P_{max}^{(load,init)} = 448.32\ kW$

(a) (b)

Figure 6.32.: Voltage profiles of the Industrial Link-Grid with $L(U)$-controlled LV-Grid-Links and without any control on the CP-Grid-, CP-Producer-Link chain for different load/production scenarios: (a) min load, max production, (b) max load, max production

E. Summary

Table 6.8 summarises the simulation results of the real Link-Grids with $L(U)$-controlled LV-Grid-Links and without any control on the CP-Grid-, CP-Producer-Link chain and without overvoltage protections. In those scenarios where the control coils' local voltages don't exceed 1.09 p.u. they don't absorb any

Link-Grid	Scenario	Viol. idx.	$\Delta U^{(sdg)}$ [V]	$P^{(loss)}$ [kW]	$Q^{(loss)}$ [kvar]	$P^{(pro)}$ [kW]	$Q^{(pro)}$ [kvar]	$P^{(ex)}$ [kW]	$Q^{(ex)}$ [kvar]	$\mathcal{L}^{(tr)}$ [%]	$\mathcal{L}_{max}^{(sgm)}$ [%]	$P^{(ctl)}$ [kW]
Large Urban	$\mathbf{L}^{(min)} - \mathbf{G}^{(min)}$	0	16.11	2.32	0.45	-10.18	-64.14	12.49	64.59	9.84	32.26	0
	$\mathbf{L}^{(max)} - \mathbf{G}^{(min)}$	0	23.01	6.49	4.47	-183.38	-122.57	189.88	127.03	34.18	33.45	0
	$\mathbf{L}^{(min)} - \mathbf{G}^{(mid)}$	0	9.19	4.69	4.63	258.74	-67.85	-254.04	72.48	39.53	26.98	0
	$\mathbf{L}^{(max)} - \mathbf{G}^{(mid)}$	0	2.65	1.72	1.20	82.56	-129.57	-80.83	130.76	23.00	15.81	0
	$\mathbf{L}^{(min)} - \mathbf{G}^{(max)}$	0	16.24	41.13	239.71	692.41	-69.50	-651.28	309.20	107.88	76.12	0
	$\mathbf{L}^{(max)} - \mathbf{G}^{(max)}$	0	14.29	19.70	62.74	510.41	-138.26	-490.70	201.00	79.35	52.37	0
Small Urban	$\mathbf{L}^{(min)} - \mathbf{G}^{(min)}$	0	10.91	0.75	0.27	-23.03	-46.16	23.78	46.43	12.35	18.50	0
	$\mathbf{L}^{(max)} - \mathbf{G}^{(min)}$	0	11.51	2.82	3.06	-144.29	-88.19	147.11	91.24	40.99	31.94	0
	$\mathbf{L}^{(min)} - \mathbf{G}^{(mid)}$	0	11.38	4.69	5.84	241.93	-49.30	-237.24	55.14	57.68	33.85	0
	$\mathbf{L}^{(max)} - \mathbf{G}^{(mid)}$	0	6.62	1.97	2.18	118.71	-94.18	-116.75	96.36	35.85	20.98	0
	$\mathbf{L}^{(min)} - \mathbf{G}^{(max)}$	0	17.25	31.09	190.14	601.18	-50.48	-570.09	240.62	146.54	88.79	0
	$\mathbf{L}^{(max)} - \mathbf{G}^{(max)}$	0	14.85	17.59	54.14	474.35	-100.94	-456.77	155.08	114.23	67.52	0
Rural	$\mathbf{L}^{(min)} - \mathbf{G}^{(min)}$	0	5.34	0.23	0.11	-23.34	-15.53	23.58	15.64	16.75	5.59	0
	$\mathbf{L}^{(max)} - \mathbf{G}^{(min)}$	0	13.95	1.35	1.66	-65.48	-29.67	66.83	31.32	43.70	13.42	0
	$\mathbf{L}^{(min)} - \mathbf{G}^{(mid)}$	0	13.70	3.93	20.63	110.65	-16.74	-106.72	37.38	66.94	21.76	0
	$\mathbf{L}^{(max)} - \mathbf{G}^{(mid)}$	0	10.31	1.52	1.76	67.06	-32.54	-65.55	34.30	43.80	13.17	0
	$\mathbf{L}^{(min)} - \mathbf{G}^{(max)}$	0	19.63	25.96	114.54	260.62	-16.78	-234.66	131.32	159.20	54.85	0
	$\mathbf{L}^{(max)} - \mathbf{G}^{(max)}$	0	18.05	17.31	75.21	216.32	-33.46	-199.01	108.67	134.24	45.48	0
Indus-trial	$\mathbf{L}^{(min)} - \mathbf{G}^{(min)}$	0	14.85	6.99	9.54	-371.68	-197.95	378.67	207.49	50.90	58.75	0
	$\mathbf{L}^{(max)} - \mathbf{G}^{(min)}$	0	16.68	9.20	12.69	-429.19	-223.55	438.38	236.24	58.71	65.26	0
	$\mathbf{L}^{(min)} - \mathbf{G}^{(mid)}$	0	19.57	5.78	3.33	-47.06	-203.96	52.84	207.29	25.22	58.78	0
	$\mathbf{L}^{(max)} - \mathbf{G}^{(mid)}$	0	20.22	6.12	4.27	-105.31	-230.39	111.43	234.67	30.63	65.29	0
	$\mathbf{L}^{(min)} - \mathbf{G}^{(max)}$	1	22.87	24.01	97.86	309.46	-208.60	-285.45	306.46	49.37	95.01	0
	$\mathbf{L}^{(max)} - \mathbf{G}^{(max)}$	1	22.97	20.51	67.53	249.91	-236.62	-229.40	304.15	44.91	89.52	0

Table 6.8.: Summarised simulation results of the real Link-Grids with $L(U)$-controlled LV-Grid-Links and without any control on the CP-Grid-, CP-Producer-Link chain and without overvoltage protections

reactive power and thus they don't impair the grids' performances. In the other scenarios the control coils maintain their local voltages by absorbing reactive power while reducing the number of upper voltage violations as well as the voltage spreading and while increasing the active power losses, the reactive power exchange between the MV- and the LV-grid and the equipment loading.

Regarding the Large Urban Link-Grid, the $L(U)$-control manages to maintain all node-voltages within the admissible voltage range. With a maximum maximal line loading of 76.12 % in the "min load, max production"-scenario, the Large Urban Link-Grid with $L(U)$-control is able to host more than 5 kWp of installed photovoltaic rating per customer if the distribution transformer is exchanged.

Regarding the Small Urban Link-Grid, the $L(U)$-control manages to maintain all node-voltages within the admissible voltage range. With a maximum maximal line loading of 88.79 % in the "min load, max production"-scenario, the Small Urban Link-Grid with $L(U)$-control is able to host more than 8 kWp of installed photovoltaic rating per customer if the distribution transformer is exchanged.

Regarding the Rural Link-Grid, the $L(U)$-control manages to maintain all node-voltages within the admissible voltage range. With a maximum maximal line loading of 54.85 % in the "min load, max production"-scenario, the Rural Link-Grid with $L(U)$-control is able to host more than 5 kWp of installed photovoltaic rating per customer if the distribution transformer is exchanged.

Regarding the Industrial Link-Grid, the $L(U)$-control doesn't manage to maintain all node-voltages within the admissible voltage range. In both "max production"-scenarios, one node-voltage still exceeds the upper voltage limitation. This may be avoided by different settings of the $L(U)$-control (voltage set point or location in the grid). With a maximum maximal line loading of 95.01 % in the "min load, max production"-scenario, the Industrial Link-Grid with $L(U)$-control is not able to host significantly more than 45 kWp of installed photovoltaic rating per customer.

Table 7.9 in the appendix lists the individual control coils' reactive power consumption for the simulations summarised in table 6.8.

6.6. *L(U)*-controlled LV-Grid-Link with *Q*-autarkic customers

This section presents and discusses the simulation results of the LV-Grid-Link operation with *L(U)*-controlled LV-Grid-Links and *Q*-autarkic customers. Both types of grids, the theoretical and the real grids are analysed. Figure 6.33 shows an overview of the LV-Grid-, CP-Grid-, CP-Producer-Link chain with *L(U)*-controlled LV-Grid-Links and *Q*-autarkic customers.
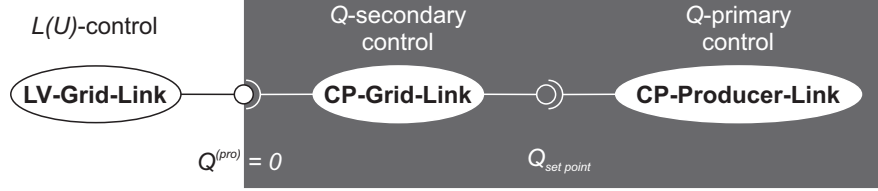
Figure 6.33.: Overview of the LV-Grid-, CP-Grid-, CP-Producer-Link chain with *L(U)*-controlled LV-Grid-Links and *Q*-autarkic customers

6.6.1. Behaviour of the theoretical Link-Grid

Figure 6.34 shows an overview of the theoretical Link-Grid with control coils at the end of the feeders C1 and L1.
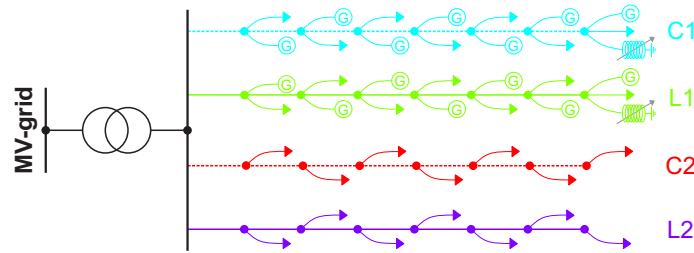
Figure 6.34.: Overview of the theoretical Link-Grid with control coils

A. Without distributed electricity production

Figure 6.35 shows the voltage profiles of the theoretical Link-Grid with *L(U)*-controlled LV-Grid-Links and *Q*-autarkic customers and without any control on the LV-Grid-, CP-Grid-, CP-Producer-Link chain for a $P^{(inv)} = 0kW$ and a $P^{(load,init)} = 54.72kW$. Regarding the case with *Q*-autarkic customers, both overhead line-feeders, L1 and L2, and both cable-feeders, C1 and C2, show the same voltage profile since the DGs and the control coils don't inject or absorb any active and reactive power and thus exactly the same power flows through these feeders. As a consequence, their voltage profiles overlay and thus only two profiles can be seen. The voltage profiles of the cable- and the overhead line-feeders differ from each other due to their different impedances. Neither the upper nor the lower voltage limitation is violated by any node-voltage. Both control coils don't absorb any reactive power since their local voltages are below 1.09 p.u.. The decreasing node-voltages along the overhead line-feeders cause a voltage spreading of 11.44 V, determined according to equation (5.1). The relatively low node-voltages reduce the consumers' active power demand in total according to the characteristics shown in figure 2.16. Since their inverters don't inject any active power, this reduced demand results in a reduced active power exchange between the CP-grids and the LV-grid of -53.26 kW, determined according to equation (5.5). Due to the customers' *Q*-autarky no reactive power is exchanged between the CP-grids and the LV-grid. These active power exchanges lead to active flows within the LV-grid and thus to active (1.19 kW) and reactive power losses (1.33 kvar), to an active (54.45 kW) and reactive power exchange (1.33 kvar) between the LV- and the MV-grid, to a transformer loading of 34.39 % and to a maximal line loading of 7.24 %. Since the upper
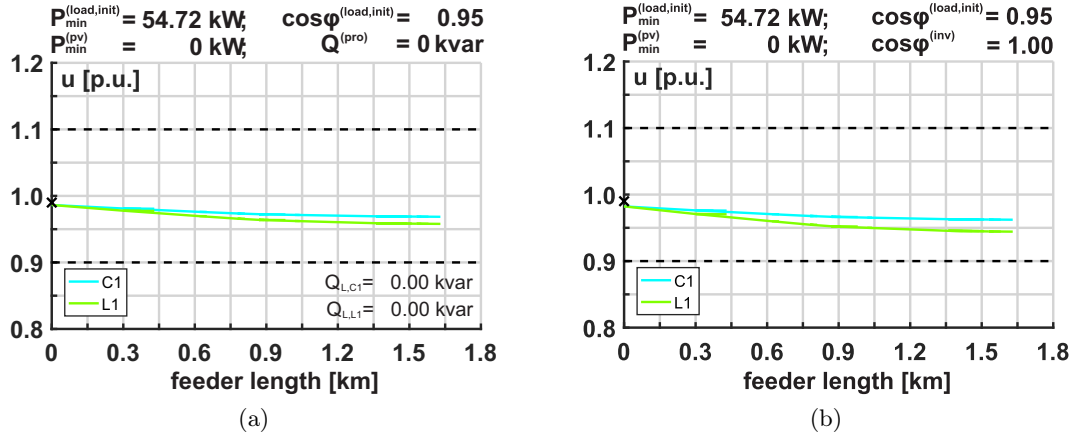
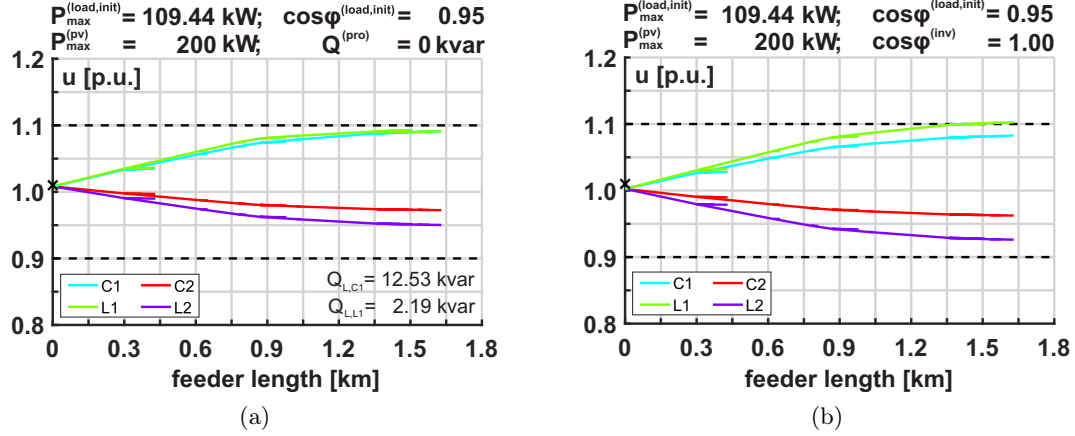Figure 6.35.: Voltage profiles of the theoretical Link-Grid with different control strategies for a $P^{(inv)} = 0kW$ and a $P^{(load,init)} = 54.72kW$: (a) with $L(U)$-controlled LV-Grid-Links and Q-autarkic customers, (b) without any control on the LV-Grid-, CP-Grid-, CP-Producer-Link chain

voltage limitation isn't violated by any network-node in this scenario, no overvoltage protection trips and thus no active power is curtailed.

Figure 6.36 shows the voltage profiles of the theoretical Link-Grid with $L(U)$-controlled LV-Grid-Links and Q-autarkic customers and without any control on the LV-Grid-, CP-Grid-, CP-Producer-Link chain for a $P^{(inv)} = 0kW$ and a $P^{(load,init)} = 109.44kW$. Regarding the case with Q-autarkic customers, both
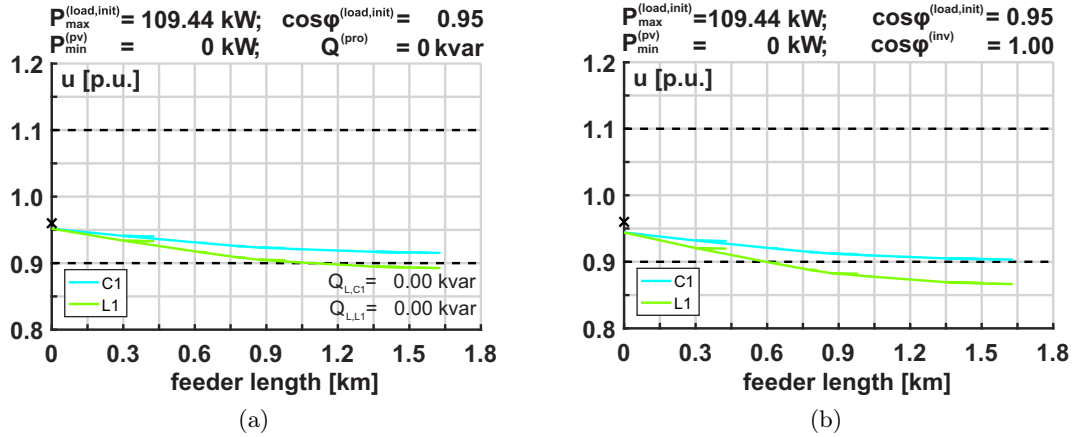
Figure 6.36.: Voltage profiles of the theoretical Link-Grid with different control strategies for a $P^{(inv)} = 0kW$ and a $P^{(load,init)} = 109.44kW$: (a) with $L(U)$-controlled LV-Grid-Links and Q-autarkic customers, (b) without any control on the LV-Grid-, CP-Grid-, CP-Producer-Link chain

overhead line-feeders, L1 and L2, and both cable-feeders, C1 and C2, show the same voltage profile since the DGs and the control coils don't inject or absorb any active and reactive power and thus exactly the same power flows through these feeders. As a consequence, their voltage profiles overlay and thus only two profiles can be seen. The voltage profiles of the cable- and the overhead line-feeders differ from each other due to their different impedances. 18 node-voltages deceed the lower voltage limitation. Both control coils don't absorb any reactive power since their local voltages are below 1.09 p.u.. The decreasing node-voltages along the overhead line-feeders cause a voltage spreading of 23.77 V, determined according to equation (5.1). The relatively low node-voltages reduce the consumers' active power demand in total according to the characteristics shown in figure 2.16. Since their inverters don't inject any active power, this reduced demand results in a reduced active power exchange between the CP-grids and the LV-grid

84

of $-102.96\,\text{kW}$, determined according to equation (5.5). Due to the customers' Q-autarky no reactive power is exchanged between the CP-grids and the LV-grid. These active power exchanges lead to active flows within the LV-grid and thus to active $(4.93\,\text{kW})$ and reactive power losses $(6.22\,\text{kvar})$, to an active $(107.88\,\text{kW})$ and reactive power exchange $(6.22\,\text{kvar})$ between the LV- and the MV-grid, to a transformer loading of $70.35\,\%$ and to a maximal line loading of $14.75\,\%$. Since the upper voltage limitation isn't violated by any network-node in this scenario, no overvoltage protection trips and thus no active power is curtailed. Compared to the case without $Q(U)$-autarkic CP-Grid-Links (figure 6.36b), the number of node-voltages which violate the lower voltage limitation is reduced from 48 to 18 by the customers' $Q(U)$-autarky in this scenario.

B. With distributed electricity production

Figure 6.37 shows the voltage profiles of the theoretical Link-Grid with $L(U)$-controlled LV-Grid-Links and Q-autarkic customers and without any control on the LV-Grid-, CP-Grid-, CP-Producer-Link chain for a $P^{(inv)} = 200kW$ and a $P^{(load,init)} = 54.72kW$. With $L(U)$-control, neither the upper nor the
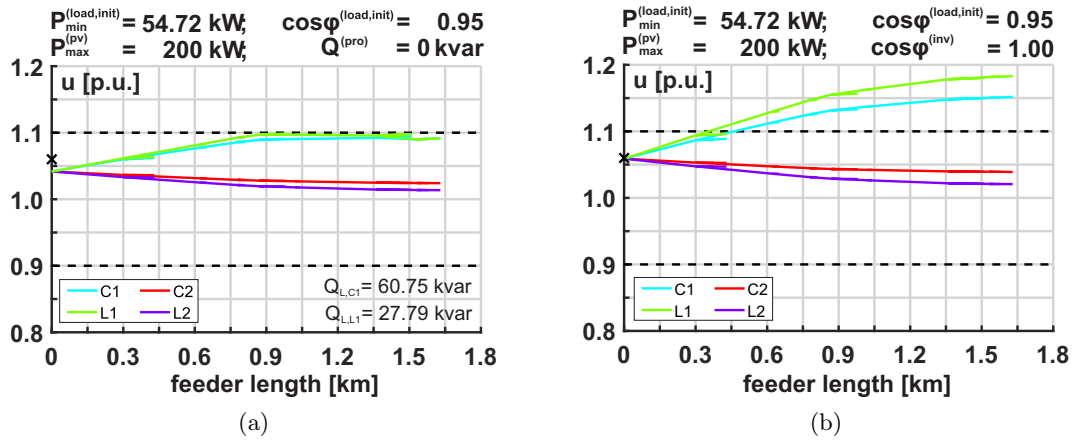
Figure 6.37.: Voltage profiles of the theoretical Link-Grid with different control strategies for a $P^{(inv)} = 200kW$ and a $P^{(load,init)} = 54.72kW$: (a) with $L(U)$-controlled LV-Grid-Links and Q-autarkic customers, (b) without any control on the LV-Grid-, CP-Grid-, CP-Producer-Link chain

lower voltage limitation is violated by any node-voltage. The control coils decrease their local voltages by absorbing reactive power. The control coil located at feeder C1 absorbs $60.75\,\text{kvar}$ while the control coil located at feeder L1 absorbs $27.79\,\text{kvar}$. The increasing node-voltages along the feeder L1 and the decreasing node-voltages along the feeder L2 cause a voltage spreading of $33.98\,\text{V}$, determined according to equation (5.1). The relatively high node-voltages increase the consumers' active and reactive power demand in total according to the characteristics shown in figure 2.16. Since the inverters inject active power, this increased demand results in an decreased active power exchange between the CP-grids and the LV-grid of $142.74\,\text{kW}$, determined according to equation (5.5). Due to the customers' Q-autarky no reactive power is exchanged between the CP-grids and the LV-grid. To keep their local voltages at $1.09\,\text{p.u.}$, the control coil located at feeder C1 absorbs $60.75\,\text{kvar}$ and that located at feeder L1 absorbs $27.79\,\text{kvar}$ of reactive power. The active power exchanges between the CP-grids and the LV-grid together with the control coils Q-absorption lead to active and reactive power flows within the LV-grid and thus to active $(25.53\,\text{kW})$ and reactive power losses $(111.57\,\text{kvar})$, to an active $(-117.21\,\text{kW})$ and reactive power exchange $(111.57\,\text{kvar})$ between the LV- and the MV-grid, to a transformer loading of $95.41\,\%$ and to a maximal line loading of $49.44\,\%$. Since the reactive power losses represent the Q-consumption of the LV-grid's electrical equipment they also contain the control coils Q-absorption. The additional reactive power flow through the transformer which is provoked by the $L(U)$-controlled coils decreases the transformer's secondary voltage and thus also the node-voltages of the feeders without distributed generation, C2 and L2. Compared to the case without $L(U)$-control and Q-autarkic customers (figure 6.37b), the number of

node-voltages which violate the upper voltage limitation is reduced from 48 to 0 by the $L(U)$-control in this scenario. Hence, none of the overvoltage protections trips and thus no active power is curtailed.

Figure 6.38 shows the voltage profiles of the theoretical Link-Grid with $L(U)$-controlled LV-Grid-Links and Q-autarkic customers and without any control on the LV-Grid-, CP-Grid-, CP-Producer-Link chain for a $P^{(inv)} = 200kW$ and a $P^{(load,init)} = 109.44kW$. With $L(U)$-control, neither the upper nor the

Figure 6.38.: Voltage profiles of the theoretical Link-Grid with different control strategies for a $P^{(inv)} = 200kW$ and a $P^{(load,init)} = 109.44kW$: (a) with $L(U)$-controlled LV-Grid-Links and Q-autarkic customers, (b) without any control on the LV-Grid-, CP-Grid-, CP-Producer-Link chain

lower voltage limitation is violated by any node-voltage. The control coils decrease their local voltages by absorbing reactive power. The control coil located at feeder C1 absorbs 12.53 kvar while the control coil located at feeder L1 absorbs 2.19 kvar. The increasing node-voltages along the feeder L1 and the decreasing node-voltages along the feeder L2 cause a voltage spreading of 57.01 V, determined according to equation (5.1). The relatively high node-voltages increase the consumers' active and reactive power demand in total according to the characteristics shown in figure 2.16. Since the inverters inject active power, this increased demand results in an decreased active power exchange between the CP-grids and the LV-grid of 88.24 kW, determined according to equation (5.5). Due to the customers' Q-autarky no reactive power is exchanged between the CP-grids and the LV-grid. To keep their local voltages at 1.09 p.u., the control coil located at feeder C1 absorbs 12.35 kvar and that located at feeder L1 absorbs 2.19 kvar of reactive power. The active power exchanges between the CP-grids and the LV-grid together with the control coils Q-absorption lead to active and reactive power flows within the LV-grid and thus to active (14.08 kW) and reactive power losses (27.01 kvar), to an active (−74.16 kW) and reactive power exchange (27.01 kvar) between the LV- and the MV-grid, to a transformer loading of 48.84 % and to a maximal line loading of 34.69 %. Since the reactive power losses represent the Q-consumption of the LV-grid's electrical equipment they also contain the control coils Q-absorption. The additional reactive power flow through the transformer which is provoked by the $L(U)$-controlled coils decreases the transformer's secondary voltage and thus also the node-voltages of the feeders without distributed generation, C2 and L2. Compared to the case without $L(U)$-control and Q-autarkic customers (figure 6.38b), the number of node-voltages which violate the upper voltage limitation is reduced from 6 to 0 by the $L(U)$-control in this scenario. Hence, none of the overvoltage protections trips and thus no active power is curtailed.

C. Summary

Table 6.9 summarises the simulation results of the theoretical Link-Grid with $L(U)$-controlled LV-Grid-Links and Q-autarkic customers. The most critical scenarios concerning the voltage violation index, the

Scenario	Volt. prot.	Viol. index	$\Delta U^{(sdg)}$ [V]	$P^{(loss)}$ [kW]	$Q^{(loss)}$ [kvar]	$P^{(pro)}$ [kW]	$Q^{(pro)}$ [kvar]	$P^{(ex)}$ [kW]	$Q^{(ex)}$ [kvar]	$\mathcal{L}^{(tr)}$ [%]	$\mathcal{L}^{(sgm)}_{max}$ [%]	$P^{(ctl)}$ [kW]
$\mathbf{L^{(min)}-G^{(min)}}$	($\checkmark$)	0	11.44	1.19	1.33	-53.26	0	54.45	1.33	34.39	7.24	0
$\mathbf{L^{(max)}-G^{(min)}}$	($\checkmark$)	18	23.77	4.93	6.22	-102.96	0	107.88	6.22	70.35	14.75	0
$\mathbf{L^{(min)}-G^{(max)}}$	($\checkmark$)	0	33.98	25.53	111.57	142.74	0	-117.21	111.57	95.41	49.44	0
$\mathbf{L^{(max)}-G^{(max)}}$	($\checkmark$)	0	57.01	14.08	27.01	88.24	0	-74.16	27.01	48.84	34.69	0

Table 6.9.: Summarised simulation results of the theoretical Link-Grid with $L(U)$-controlled LV-Grid-Links and Q-autarkic customers

voltage spreading, the active power losses, the reactive power exchange between the LV- and the MV-grid, the transformer loading, the maximal line loading and the active power curtailment are presented in the following. The maximum voltage violation index occurs in the $L^{(max)}-G^{(min)}$ scenario with overvoltage protections. The maximum voltage spreading occurs in the $L^{(max)}-G^{(max)}$ scenario with overvoltage protections. The maximum active power losses occur in the $L^{(min)}-G^{(max)}$ scenario with overvoltage protections. The maximum reactive power exchange between the LV- and the MV-grid occurs in the $L^{(min)}-G^{(max)}$ scenario with overvoltage protections. The maximum transformer loading occurs in the $L^{(min)}-G^{(max)}$ scenario with overvoltage protections. The maximum maximal line loading occurs in the $L^{(min)}-G^{(max)}$ scenario with overvoltage protections. No active power curtailment occurs in any of the simulated scenarios.

Regarding the compliance with the legally stipulated voltage range and the lost active power ($P^{(loss)} + P^{(ctl)}$) as the crucial performance indicators, the $L^{(max)}-G^{(min)}$ scenario with overvoltage protections and the $L^{(min)}-G^{(max)}$ scenario with overvoltage protections are the most critical scenarios for the theoretical Link-Grid's operation with $L(U)$-controlled LV-Grid-Links and Q-autarkic customers.

6.6.2. Behaviour of the real Link-Grids

A. Large Urban Link-Grid
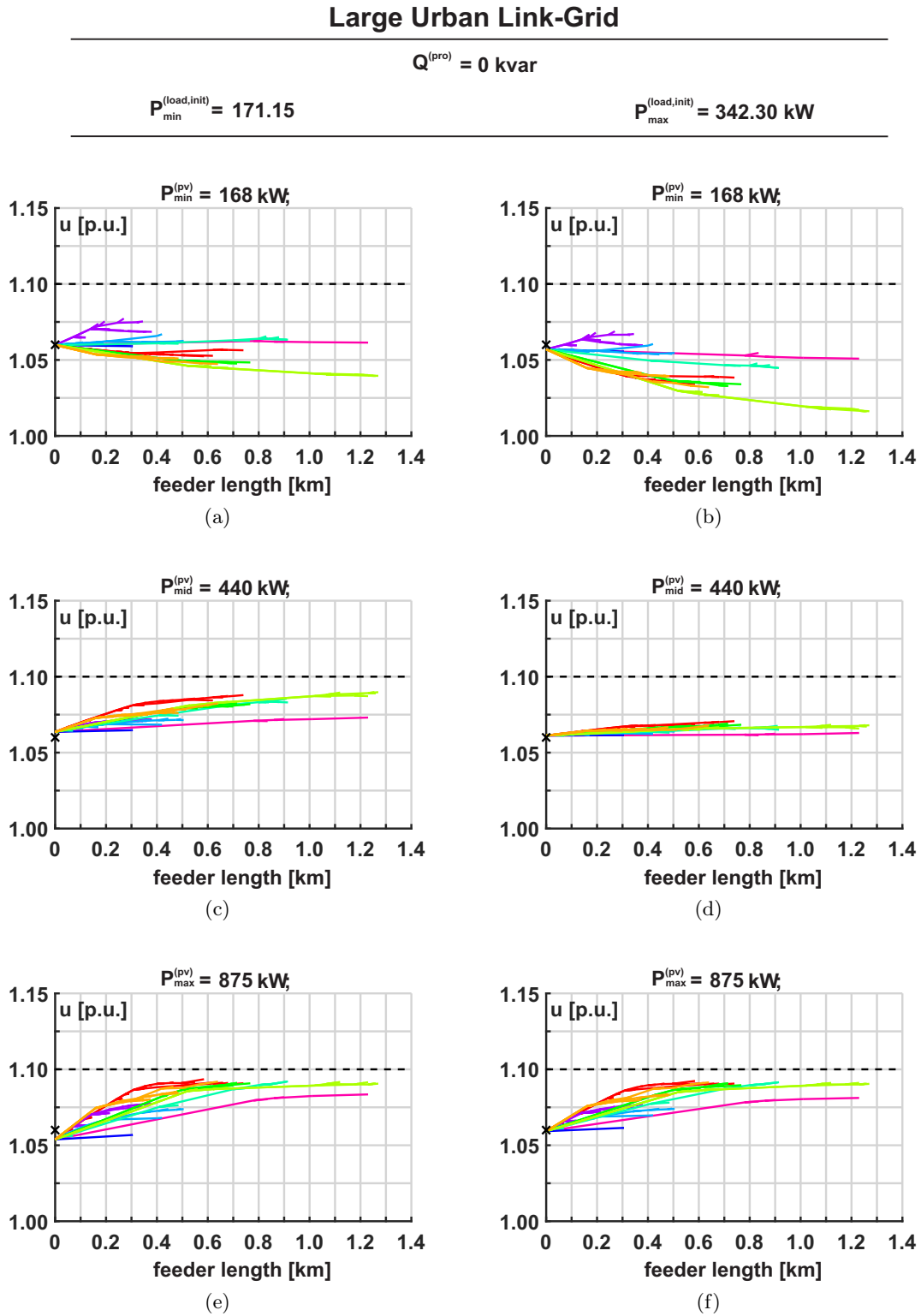
Figure 6.39.: Voltage profiles of the Large Urban Link-Grid with *L(U)*-controlled LV-Grid-Links and *Q*-autarkic CP-Grid-Links for different load/production scenarios: (a) min load, min production, (b) max load, min production, (c) min load, mid production, (d) max load, mid production, (e) min load, max production, (f) max load, max production

B. Small Urban Link-Grid

Small Urban Link-Grid

$Q^{(pro)} = 0$ kvar

$P_{min}^{(load,init)} = 119.21$ kW $P_{max}^{(load,init)} = 238.42$ kW

(a)

(b)

(c)

(d)

(e)

(f)
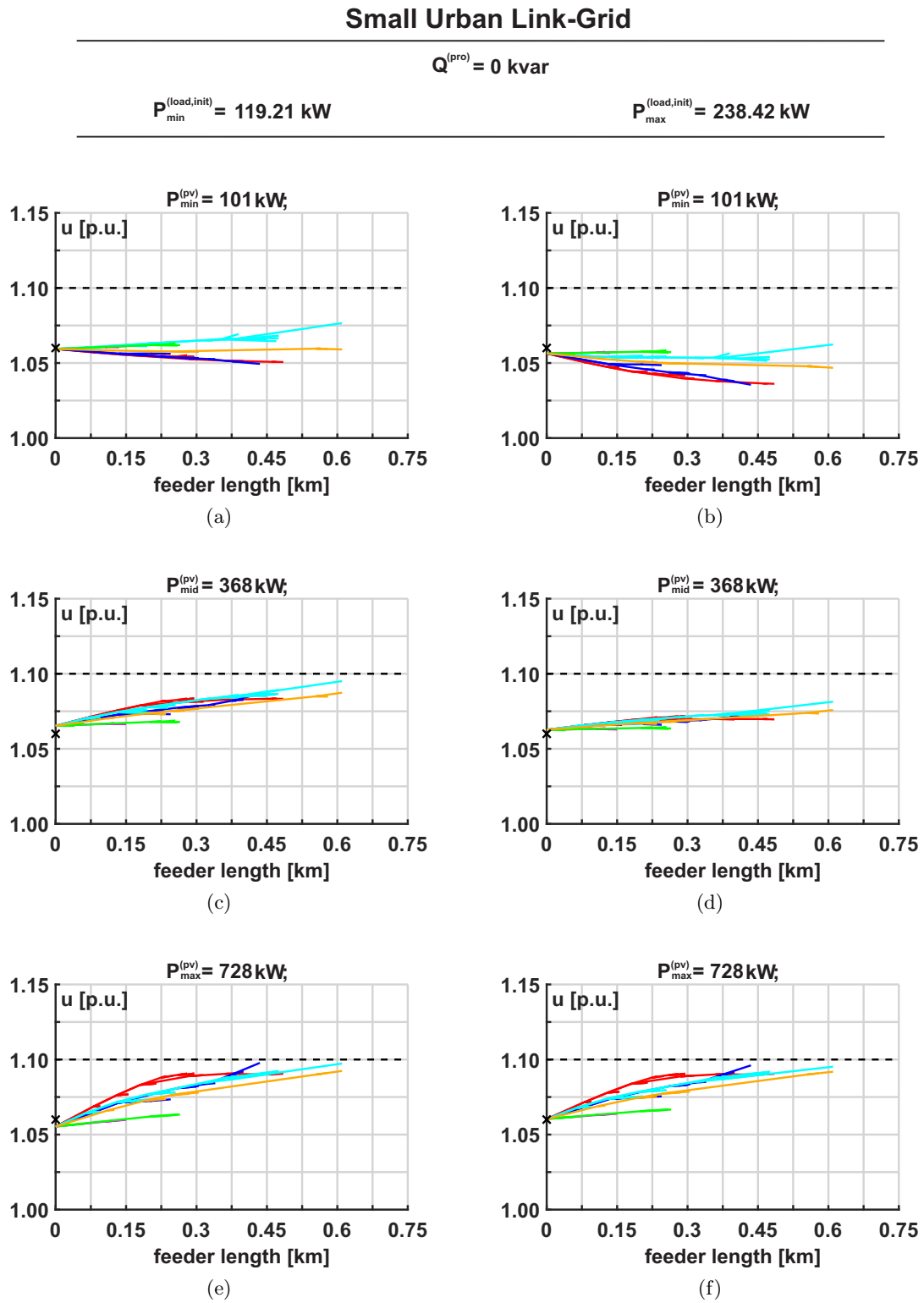
Figure 6.40.: Voltage profiles of the Small Urban Link-Grid with $L(U)$-controlled LV-Grid-Links and Q-autarkic CP-Grid-Links for different load/production scenarios: (a) min load, min production, (b) max load, min production, (c) min load, mid production, (d) max load, mid production, (e) min load, max production, (f) max load, max production

Figure 6.41.: Voltage profiles of the Rural Link-Grid with $L(U)$-controlled LV-Grid-Links and Q-autarkic CP-Grid-Links for different load/production scenarios: (a) min load, min production, (b) max load, min production, (c) min load, mid production, (d) max load, mid production, (e) min load, max production, (f) max load, max production

D. Industrial Link-Grid

Industrial Link-Grid

$Q^{(pro)} = 0$ kvar

$P^{(load,init)}_{min} = 390.96$ kW

$P^{(load,init)}_{max} = 448.32$ kW

$P^{(pv)}_{min} = 30$ kW;

$P^{(pv)}_{min} = 30$ kW;

(a)

(b)

$P^{(pv)}_{mid} = 360$ kW;

$P^{(pv)}_{mid} = 360$ kW;

(c)

(d)

$P^{(pv)}_{max} = 720$ kW;

$P^{(pv)}_{max} = 720$ kW;

(e)

(f)

Figure 6.42.: Voltage profiles of the Industrial Link-Grid with $L(U)$-controlled LV-Grid-Links and Q-autarkic CP-Grid-Links for different load/production scenarios: (a) min load, min production, (b) max load, min production, (c) min load, mid production, (d) max load, mid production, (e) min load, max production, (f) max load, max production

E. Summary

Table 6.10 summarises the simulation results of the real Link-Grids with $L(U)$-controlled LV-Grid-Links and Q-autarkic customers without overvoltage protections. In those scenarios with few distributed elec-

Link-Grid	Scenario	Viol. idx.	$\Delta U^{(sdg)}$ [V]	$P^{(loss)}$ [kW]	$Q^{(loss)}$ [kvar]	$P^{(pro)}$ [kW]	$Q^{(pro)}$ [kvar]	$P^{(ex)}$ [kW]	$Q^{(ex)}$ [kvar]	$\mathcal{L}^{(tr)}$ [%]	$\mathcal{L}_{max}^{(sgm)}$ [%]	$P^{(ctl)}$ [kW]
Large Urban	$\mathbf{L}^{(min)} - \mathbf{G}^{(min)}$	0	15.12	1.98	0.06	-10.92	0.00	12.90	0.06	1.93	31.79	0
	$\mathbf{L}^{(max)} - \mathbf{G}^{(min)}$	0	21.10	5.13	2.99	-186.17	0.00	191.30	2.99	28.63	31.47	0
	$\mathbf{L}^{(min)} - \mathbf{G}^{(mid)}$	0	10.49	4.31	4.22	257.91	0.00	-253.60	4.22	37.95	25.92	0
	$\mathbf{L}^{(max)} - \mathbf{G}^{(mid)}$	0	3.84	0.55	-0.14	79.52	0.00	-78.96	-0.14	11.82	8.73	0
	$\mathbf{L}^{(min)} - \mathbf{G}^{(max)}$	0	15.86	41.91	288.61	692.26	0.00	-650.35	288.61	106.47	76.02	0
	$\mathbf{L}^{(max)} - \mathbf{G}^{(max)}$	0	13.23	20.08	146.51	509.47	0.00	-489.39	146.51	76.44	52.88	0
Small Urban	$\mathbf{L}^{(min)} - \mathbf{G}^{(min)}$	0	10.86	0.58	0.04	-23.51	0.00	24.09	0.04	5.71	18.38	0
	$\mathbf{L}^{(max)} - \mathbf{G}^{(min)}$	0	10.74	2.19	2.20	-146.10	0.00	148.29	2.20	35.12	29.35	0
	$\mathbf{L}^{(min)} - \mathbf{G}^{(mid)}$	0	11.90	4.37	5.55	241.38	0.00	-237.01	5.55	56.14	32.89	0
	$\mathbf{L}^{(max)} - \mathbf{G}^{(mid)}$	0	7.59	1.25	1.21	116.69	0.00	-115.44	1.21	27.34	15.83	0
	$\mathbf{L}^{(min)} - \mathbf{G}^{(max)}$	0	16.99	31.60	232.04	601.13	0.00	-569.54	232.05	145.64	89.01	0
	$\mathbf{L}^{(max)} - \mathbf{G}^{(max)}$	0	14.32	18.03	133.97	474.05	0.00	-456.02	133.97	112.55	67.62	0
Rural	$\mathbf{L}^{(min)} - \mathbf{G}^{(min)}$	0	4.83	0.17	0.02	-23.54	0.00	23.71	0.02	14.04	4.96	0
	$\mathbf{L}^{(max)} - \mathbf{G}^{(min)}$	0	11.96	1.07	1.29	-66.24	0.00	67.31	1.29	39.86	12.40	0
	$\mathbf{L}^{(min)} - \mathbf{G}^{(mid)}$	0	13.10	4.01	28.92	110.56	0.00	-106.54	28.92	65.36	21.77	0
	$\mathbf{L}^{(max)} - \mathbf{G}^{(mid)}$	0	11.29	1.22	3.76	66.25	0.00	-65.03	3.76	38.57	11.76	0
	$\mathbf{L}^{(min)} - \mathbf{G}^{(max)}$	0	19.15	26.15	124.40	260.56	0.00	-234.42	124.40	157.11	54.49	0
	$\mathbf{L}^{(max)} - \mathbf{G}^{(max)}$	0	17.13	17.61	95.20	216.10	0.00	-198.49	95.20	130.33	44.87	0
Indus-trial	$\mathbf{L}^{(min)} - \mathbf{G}^{(min)}$	0	12.25	5.03	7.16	-376.15	0.00	381.18	7.16	44.95	52.43	0
	$\mathbf{L}^{(max)} - \mathbf{G}^{(min)}$	0	13.78	6.64	9.59	-434.73	0.00	441.37	9.59	52.05	58.26	0
	$\mathbf{L}^{(min)} - \mathbf{G}^{(mid)}$	0	20.16	4.02	1.08	-52.04	0.00	56.07	1.08	6.61	52.41	0
	$\mathbf{L}^{(max)} - \mathbf{G}^{(mid)}$	0	20.81	3.93	1.42	-111.45	0.00	115.38	1.42	13.60	58.24	0
	$\mathbf{L}^{(min)} - \mathbf{G}^{(max)}$	2	21.48	25.52	170.97	306.20	0.00	-280.67	170.97	38.75	94.70	0
	$\mathbf{L}^{(max)} - \mathbf{G}^{(max)}$	2	21.41	21.75	150.47	245.92	0.00	-224.17	150.47	31.83	89.21	0

Table 6.10.: Summarised simulation results of the real Link-Grids with $L(U)$-controlled LV-Grid-Links and Q-autarkic customers without overvoltage protections

tricity production, i.e. where the control coils do not absorb a significant amount of reactive power, the combination of $L(U)$-controlled LV-Link-Grids and Q-autarkic customers improves the real Link-Grids' performances by reducing the active power losses, the reactive power exchange between the MV- and the LV-grid and the equipment loading. In those scenarios with much distributed electricity production, the control coils maintain their local voltages by absorbing reactive power while reducing the number of upper voltage violations as well as the voltage spreading and while increasing the active power losses, the reactive power exchange between the MV- and the LV-grid and the equipment loading. But in some cases, i.e. in those cases where without any control on the LV-Grid, CP-Grid, CP-Producer-Link chain a large amount of reactive power is consumed by customers located at feeders which don't reach the control coils' voltage set points[1], the combination of $L(U)$-controlled LV-Link-Grids and Q-autarkic customers reduces the reactive power exchange between the MV- and the LV-grid and the transformer loading even during high distributed electricity production periods.

Regarding the Large Urban Link-Grid, the $L(U)$-control with Q-autarkic customers manages to maintain all node-voltages within the admissible voltage range. With a maximum maximal line loading of 76.02 % in the "min load, max production"-scenario, the Large Urban Link-Grid with $L(U)$-control and Q-autarkic customers is able to host more than 5 kWp of installed photovoltaic rating per customer if the distribution transformer is exchanged.

Regarding the Small Urban Link-Grid, the $L(U)$-control with Q-autarkic customers manages to maintain all node-voltages within the admissible voltage range. With a maximum maximal line loading of 89.01 % in the "min load, max production"-scenario, the Small Urban Link-Grid with $L(U)$-control and Q-autarkic customers is able to host more than 8 kWp of installed photovoltaic rating per customer if the distribution transformer is exchanged.

Regarding the Rural Link-Grid, the $L(U)$-control with Q-autarkic customers manages to maintain all

---

[1]i.e. the "max load, max production"-scenario of the Large Urban Link-Grid and both "max production"-scenarios of the Industrial Link-Grid.

node-voltages within the admissible voltage range. With a maximum maximal line loading of 54.49 % in the "min load, max production"-scenario, the Rural Link-Grid with *L(U)*-control and *Q*-autarkic customers is able to host more than 5 kWp of installed photovoltaic rating per customer if the distribution transformer is exchanged.

Regarding the Industrial Link-Grid, the *L(U)*-control with *Q*-autarkic customers doesn't manage to maintain all node-voltages within the admissible voltage range. In both "max production"-scenarios, two node-voltage still exceed the upper voltage limitation. This may be avoided by different settings of the *L(U)*-control (voltage set point or location in the grid). With a maximum maximal line loading of 94.70 % in the "min load, max production"-scenario, the Industrial Link-Grid with *L(U)*-control and *Q*-autarkic customers is not able to host significantly more than 45 kWp of installed photovoltaic rating per customer.

Table 7.10 in the appendix lists the individual control coils' reactive power consumption for the simulations summarised in table 6.10.

6.7. Comparison of the investigated control strategies

Based on the above presented simulation results of the theoretical Link-Grid this section provides a comparison of the different active power curtailment strategies, i.e. the *P(U)*-control and the overvoltage protection, and of the different reactive power control strategies, i.e. the *Q(U)*-, the *cosφ(P)*- and the *L(U)*-control with and without *Q*-autarkic customers. For comparing the reactive power control strategies only the simulation results without or with inactive voltage protections are considered.

6.7.1. Active power curtailment strategies

In the "min load, min production"- and the "max load, min production"-scenarios neither the overvoltage protections nor the *P(U)*-controls of the inverters take actions. Their behaviour is similar in these scenarios.

Table 6.11 lists the simulation results of the theoretical Link-Grid for the "min load, max production"-scenario for the investigated active power curtailment strategies. According to figure 6.5a, the voltages of

Scenario	Control strategy	Volt. prot.	Viol. idx.	$\Delta U^{(sdg)}$ [V]	$P^{(loss)}$ [kW]	$Q^{(ex)}$ [kvar]	$\mathcal{L}^{(tr)}$ [%]	$\mathcal{L}_{max}^{(sgm)}$ [%]	$P^{(ctl)}$ [kW]
$L^{(min)} - G^{(max)}$	**Without control**	$\times$	48	64.92	15.79	38.59	77.24	39.38	0.00
	Without control	$\sqrt{}$	0	15.29	1.05	20.42	25.00	7.53	180.00
	P(U)	$(\sqrt{})$	0	27.99	2.27	22.59	24.10	18.20	106.37

Table 6.11.: Summarised simulation results of the theoretical Link-Grid for the "min load, max production"-scenario for the investigated active power curtailment strategies

the feeders C1 and L1 have to be decreased to maintain acceptable voltages. The overvoltage protections disconnect the affected PV-arrays located at feeders C1 and L1 and thus prevents them from injecting any active power, resulting in an active power curtailment of 90 kW at the cable-feeder C1 and 90 kW at the overhead line-feeder L1 but an improved performance by means of voltage spreading, active power losses, reactive power exchange between the MV- and the LV-grid and equipment loading. The *P(U)*-control reduces the active power injection of the affected PV-arrays located at feeders C1 and L1, resulting in an active power curtailment of 48.27 kW at the cable-feeder C1 and 58.09 kW at the overhead line-feeder L1 but an improved performance by means of voltage spreading, active power losses, reactive power exchange between the MV- and the LV-grid and equipment loading. Due to its higher resistance, less active power can be injected into the overhead line-feeder L1 without exceeding the upper voltage limit, and thus more active power has to be curtailed by the inverters located at the overhead line-feeder than by those located at the cable-feeder.

Table 6.12 lists the simulation results of the theoretical Link-Grid for the "max load, max production"-scenario for the investigated active power curtailment strategies. According to figure 6.6a, the voltages of the overhead line-feeder L1 have to be decreased to maintain acceptable voltages. The overvoltage protections disconnect the affected PV-arrays located at feeder L1 and thus prevents them from injecting

Scenario	Control strategy	Volt. prot.	Viol. idx.	$\Delta U^{(sdg)}$ [V]	$P^{(loss)}$ [kW]	$Q^{(ex)}$ [kvar]	$\mathcal{L}^{(tr)}$ [%]	$\mathcal{L}^{(sgm)}_{max}$ [%]	$P^{(ctl)}$ [kW]
	Without control	$\times$	6	70.56	14.23	50.89	55.93	35.44	0.00
$L^{(max)} - G^{(max)}$	Without control	$\checkmark$	0	62.62	9.93	44.67	43.77	35.43	25.00
	$P(U)$	$(\checkmark)$	0	63.21	12.43	48.59	51.67	34.51	8.88

Table 6.12.: Summarised simulation results of the theoretical Link-Grid for the "max load, max production"-scenario for the investigated active power curtailment strategies

any active power, resulting in an active power curtailment of 25 kW but an improved performance by means of voltage spreading, active power losses, reactive power exchange between the MV- and the LV-grid and equipment loading. The $P(U)$-control reduces the active power injection of the affected PV-arrays located at feeders C1 and L1, resulting in an active power curtailment of 2.12 kW at the cable-feeder C1 and 6.77 kW at the overhead line-feeder L1 but an improved performance by means of voltage spreading, active power losses, reactive power exchange between the MV- and the LV-grid and equipment loading. in this scenario, the $P(U)$-control unnecessarily curtails active power at the cable-feeder C1, but nevertheless less active power is curtailed by the $P(U)$-controls than by the overvoltage protections.

6.7.2. Reactive power control strategies

Table 6.13 lists the simulation results of the theoretical Link-Grid for the "min load, min production"-scenario for the investigated reactive power control strategies. According to figure 6.4a, no actions are

Scenario	Control strategy	Viol. idx.	$\Delta U^{(sdg)}$ [V]	$P^{(loss)}$ [kW]	$Q^{(ex)}$ [kvar]	$\mathcal{L}^{(tr)}$ [%]	$\mathcal{L}^{(sgm)}_{max}$ [%]
	Without control	0	15.18	1.32	17.92	36.19	7.58
	$Q(U)$	0	15.18	1.23	-4.91	34.68	8.35
$L^{(min)} - G^{(min)}$	$cos\varphi(P)$	0	15.18	1.32	17.92	36.19	7.58
	$L(U)$	0	15.18	1.32	17.92	36.19	7.58
	$L(U)$ & Q-autarky	0	11.44	1.19	1.33	34.39	7.24

Table 6.13.: Summarised simulation results of the theoretical Link-Grid for the "min load, min production"-scenario for the investigated reactive power control strategies

required to maintain acceptable voltages. But anyway, the $Q(U)$-controlled inverters increase their local voltages by injecting reactive power, resulting in reduced reactive power flows and thus in reduced active power losses, a reduced transformer loading and a reduced reactive power exchange between the MV- and the LV-grid. In this scenario, the inverters located at the cable-feeder C1 inject 12.24 kvar and those located at the overhead line-feeder L1 inject 10.93 kvar. The $cos\varphi(P)$-control and the $L(U)$-control take no actions and thus avoid an unnecessary impairment of the grid's performance. Combining the $L(U)$-control with Q-autarkic customers additionally improves the grid's performance by means of voltage spreading, the active power losses, the reactive power exchange between the MV- and the LV-grid and the equipment loading. The missing downstream reactive power flows exert a greater impact on the overhead line-feeder's voltage profile than on the cable-feeder's (due to its higher reactance).

Table 6.14 lists the simulation results of the theoretical Link-Grid for the "max load, min production"-scenario for the investigated reactive power control strategies. According to figure 6.4b, the voltages of the overhead line-feeders L1 and L2 have to be increased to maintain acceptable voltages. The $Q(U)$-controlled inverters located at feeder L1 and C1 increase their local voltages by injecting reactive power and thus decrease the number of lower voltage limit violations from 48 to 11. In this scenario, the inverters located at the cable-feeder C1 inject 48.29 kvar and those located at the overhead line-feeder L1 also inject 34.99 kvar. This reactive power injection exerts a greater impact on the overhead line-feeder's voltage profile than on the cable-feeder's (due to its higher reactance). The additional reactive power flows within the grid increase the voltage spreading, the reactive power exchange between the MV- and the LV-grid, the equipment loading and the active power losses. The $cos\varphi(P)$-control and the $L(U)$-control take no

Scenario	Control strategy	Viol. idx.	$\Delta U^{(sdg)}$ [V]	$P^{(loss)}$ [kW]	$Q^{(ex)}$ [kvar]	$\mathcal{L}^{(tr)}$ [%]	$\mathcal{L}^{(sgm)}_{max}$ [%]
	Without control	48	31.03	5.43	36.44	73.94	15.43
	Q(U)	11	30.92	8.29	-42.62	78.54	26.58
$L^{(max)} - G^{(min)}$	$cos\varphi(P)$	48	31.03	5.43	36.44	73.94	15.43
	L(U)	48	31.03	5.43	36.44	73.94	15.43
	L(U) & Q-autarky	18	23.77	4.93	6.22	70.35	14.75

Table 6.14.: Summarised simulation results of the theoretical Link-Grid for the "max load, min production"-scenario for the investigated reactive power control strategies

actions and thus they don't decrease the number of lower voltage limit violations, but they also don't impair the grid's performance by means of voltage spreading, active power losses, reactive power exchange between the MV- and the LV-grid and equipment loading. In this scenario, the customers' Q-autarky reduces the number of lower voltage limit violations from 48 to 18 and decreases the voltage spreading, the active power losses, the reactive power exchange between the MV- and the LV-grid and the equipment loading and thus improve the grid's performance. The missing downstream reactive power flows exert a greater impact on the overhead line-feeder's voltage profile than on the cable-feeder's (due to its higher reactance).

Table 6.15 lists the simulation results of the theoretical Link-Grid for the "min load, max production"-scenario for the investigated control reactive power strategies. According to figure 6.5a, the voltages of

Scenario	Control strategy	Viol. idx.	$\Delta U^{(sdg)}$ [V]	$P^{(loss)}$ [kW]	$Q^{(ex)}$ [kvar]	$\mathcal{L}^{(tr)}$ [%]	$\mathcal{L}^{(sgm)}_{max}$ [%]
	Without control	48	64.92	15.79	38.59	77.24	39.38
	Q(U)	9	44.13	25.98	143.30	109.25	48.65
$L^{(min)} - G^{(max)}$	$cos\varphi(P)$	9	44.14	26.27	145.16	110.00	48.67
	L(U)	0	38.18	25.36	122.38	100.07	49.52
	L(U) & Q-autarky	0	33.98	25.53	111.57	95.41	49.44

Table 6.15.: Summarised simulation results of the theoretical Link-Grid for the "min load, max production"-scenario for the investigated reactive power control strategies

the feeders C1 and L1 have to be decreased to maintain acceptable voltages. The $Q(U)$- and the $cos\varphi(P)$-controlled inverters decrease their local voltages by absorbing reactive power and thus decrease the number of upper voltage limit violations from 48 to 9. In this scenario, the $Q(U)$-controlled inverters located at the cable-feeder C1 absorb 48.82 kvar and those located at the overhead line-feeder L1 absorb 47.31 kvar. The $cos\varphi(P)$-controlled inverters located at the cable-feeder C1 absorb 48.82 kvar and those located at the overhead line-feeder L1 also absorb 48.82 kvar. In this scenario, the $Q(U)$- and the $cos\varphi(P)$-controlled inverters located at L1 absorb more reactive power than necessary to prevent upper voltage limit violations of the overhead line-feeder, but those located at C1 absorb to less reactive power to prevent upper voltage limitations of the cable-feeder. The additional reactive power flows within the grid due to the $Q(U)$- or $cos\varphi(P)$-control decrease the voltage spreading and increase the reactive power exchange between the MV- and the LV-grid, the equipment loading and the active power losses. The $L(U)$-control decreases the grid's node-voltages by absorbing reactive power at the end of feeders C1 and L1 and thus decreases the number of upper voltage limit violations from 48 to 0. In this scenario, the $L(U)$-controlled coil located at the cable-feeder C1 absorbs 54.67 kvar and that located at the overhead line-feeder L1 absorbs 23.50 kvar. Although without control especially the overhead line-feeder L1 excessively exceeds the upper voltage limitation, less reactive power has to be absorbed by the control-coil located at the overhead line-feeder L1 to prevent upper voltage limitations (due to its higher reactance). The additional reactive power flows within the grid due to the $L(U)$-control decrease the voltage spreading and increase the reactive power exchange between the MV- and the LV-grid, the equipment loading and the active power losses. Combining the $L(U)$-control with Q-autarkic customers additionally improves the performance by means of voltage spreading, reactive power exchange between the MV- and the LV-grid and equipment loading while the

control coils have to absorb more reactive power to prevent upper voltage limit violations. Slightly higher active power losses emerge in this combination.

Table 6.16 lists the simulation results of the theoretical Link-Grid for the "max load, max production"-scenario for the investigated reactive power control strategies. According to figure 6.6a, the voltages of

Scenario	Control strategy	Viol. idx.	$\Delta U^{(sdg)}$ [V]	$P^{(loss)}$ [kW]	$Q^{(ex)}$ [kvar]	$\mathcal{L}^{(tr)}$ [%]	$\mathcal{L}^{(sgm)}_{max}$ [%]
	without control	6	70.56	14.23	50.89	55.93	35.44
	Q(U)	0	55.36	19.86	110.53	81.48	42.69
$L^{(max)} - G^{(max)}$	$cos\varphi(P)$	4	54.10	27.46	159.25	106.66	47.63
	L(U)	0	66.36	14.71	54.61	57.14	35.46
	L(U) & Q-autarky	0	57.01	14.08	27.01	48.84	34.69

Table 6.16.: Summarised simulation results of the theoretical Link-Grid for the "max load, max production"-scenario for the investigated reactive power control strategies

the overhead line-feeder L1 have to be decreased to maintain acceptable voltages. The *Q(U)*-controlled inverters located at feeder L1 decrease their local voltages by absorbing (21.40 kvar) of reactive power and thus decrease the number of upper voltage limit violations from 48 to 0. Those located at feeder C1 also decrease their local voltages by absorbing (35.11 kvar) of reactive power and thus lead to unnecessary reactive power flows and to low voltages at feeders C2 and L2. The *Q(U)*-control manages to maintain acceptable voltages but strongly impairs the grid's performance by means of active power losses, reactive power exchange between the MV- and the LV-grid and equipment loading. The *cosφ(P)*-controlled inverters located at feeder L1 decrease their local voltages by absorbing (48.82 kvar) of reactive power and thus decrease the number of upper voltage limit violations from 48 to 0. Those located at feeder C1 also decrease their local voltages by absorbing (48.82 kvar) of reactive power and thus lead to unnecessary reactive power flows and to violations of the lower voltage limitation at feeder L2. The *cosφ(P)*-control doesn't manage to maintain acceptable voltages and strongly impairs the grid's performance by means of active power losses, reactive power exchange between the MV- and the LV-grid and equipment loading. The *L(U)*-control decreases the grid's node-voltages by absorbing reactive power at the end of feeder L1 and thus decreases the number of upper voltage limit violations from 48 to 0. In this scenario, the *L(U)*-controlled coil located at the overhead line-feeder L1 absorbs 3.38 kvar. No reactive power is unnecessarily absorbed at the cable-feeder C1. The *L(U)*-control manages to maintain acceptable voltages but slightly impairs the grid's performance by means of active power losses, reactive power exchange between the MV- and the LV-grid and equipment loading. Combining the *L(U)*-control with *Q*-autarkic customers additionally improves the grid's performance by means of voltage spreading, active power losses, reactive power exchange between the MV- and the LV-grid and equipment loading while the control coils have to absorb more reactive power to prevent upper voltage limit violations.

7. Conclusion

7.1. Responsibility for voltage control

The investigated control strategies can be categorised according to the control responsibility. While the $L(U)$-control is performed by the DSO and the corresponding control devices are located within the LV-Grid-Link, the $P(U)$-, $Q(U)$- and $cos\varphi(P)$-control as well as the customers' Q-autarky is performed by the customers and the corresponding control devices are located within the CP-Producer-Links. All these control strategies can be performed as a local control, where only locally available data and thus no data exchange between different market players is required to perform voltage control, and as a coordinated control, where data is exchanged between different devices through a communication system to optimally control the overall system.

Local $P(U)$- and $Q(U)$-controls of customer owned PV-inverters lead to a discrimination between customers since the customers are differently located within the grid and thus provide system services to a different extent, in fact without remuneration. Local $cos\varphi(P)$-controls of customer owned PV-inverters do not lead to a discrimination between customers since the amount of reactive power they absorb is independent from their location in the grid. A coordinated voltage control strategy based on customer-owned PV-inverters requires a data exchange between the customers and the DSO which jeopardises the customers' data privacy. Without communicating with the customers, the DSO cannot influence the customers' Q-contribution and thus he cannot control the Q-behaviour of his low voltage grid (only indirectly by changing the voltages and thus the loads' and generators' behaviour).

With a local $L(U)$-control the customers aren't requested to provide system services and thus they are prevented from being discriminated. A coordinated voltage control strategy based on DSO-owned reactive power devices doesn't require a data exchange between the customers and the DSO and thus maintains the customers' data privacy. Without communicating with the customers, the DSO can influence the control-coils' but not the customers' Q-contribution and thus he can partly control the Q-behaviour of his low voltage grid.

With a local $L(U)$-control with Q-autarkic customers, the customers only cover their own Q-demand and thus they are prevented from being discriminated. A coordinated voltage control strategy based on DSO-owned reactive power devices and Q-autarkic customers doesn't require a data exchange between the customers and the DSO and thus maintains the customers' data privacy. Without communicating with the customers, the DSO can influence the control-coils' Q-contribution and thus he can completely control the Q-behaviour of his low voltage grid.

7.2. Impacts of local P- and Q-controls on the voltage profiles of low voltage grids

Manipulating the P- and Q-contribution of a CP-Grid-Link or the Q-contribution of a reactive power device by a local control strategy impacts not only the voltage profile of the related feeder (described as the "local effect" in [13]) but also the distribution transformer's secondary voltage and thus the voltage profiles of all other feeders connected to the LV-grid (described as the "global effect" in [13]). Compared to active power control strategies, reactive power control strategies produce a bigger global effect due to the low R/X-ratio of European distribution transformers. The local effect of a P-control depends on the resistance while the local effect of a Q-control depends on the inductance between the control device and the transformer's secondary side. A local effect emerges not only in the node where the power is injected or absorbed, but also in all nodes of the related feeder. A certain Q-absorption of a control device exerts the

greatest impact on a feeder's voltage profile if it is located at the end of the feeder. The local R/X-ratio increases along a feeder, especially in case of a cable-feeder. This means that prosumers located at the end of the feeder have to inject/absorb active power with a lower power factor to achieve the same relative compensation of the resulting voltage rise/drop than prosumers located at the beginning of the feeder. In the investigated low voltage grids, the overhead lines have higher resistances and much higher reactances than the cables so that their voltage profiles are more sensitive to active and especially reactive power flows. The simulations show that less reactive power has to be consumed at an overhead line-feeder to achieve a certain voltage reduction than at a cable-feeder. This means that there is a large potential to increase the hosting capacity of grids with long overhead line-feeders, e.g. in rural areas, with a reactive power control strategy.

7.3. Impacts of the investigated local control strategies on the performance of a theoretical LV-grid

The investigated local active and reactive power control strategies differently impact the performance of a low voltage grid in terms of the resulting voltage profile, active power losses, reactive power exchange with the overlaid MV-grid and equipment loading. This section compares the impacts of the investigated control strategies on the LV-grid's performance based on the simulation results of the theoretical Link-Grid.

7.3.1. Local active power control

Regarding the investigated active power curtailment strategies, i.e. the $P(U)$-control for PV-inverters and the disconnection of the PV-arrays by their overvoltage protections, both curtailment strategies are able to prevent violations of the upper voltage limitation while reducing the active power losses, the reactive power exchange between the MV- and the LV-grid and the equipment loading, but in return, active power is curtailed and thus wasted. Compared to overvoltage protections, $P(U)$-controlled inverters curtail less active power in total, but in some cases even though no upper voltage limit violations would occur without control.

7.3.2. Local reactive power control

Regarding the investigated reactive power control strategies, i.e. the $Q(U)$- and $cos\varphi(P)$-control of PV-inverters and the $L(U)$-control of control-coils located at the end of the feeders, all these control strategies are able to decrease the voltages within the LV-grid while increasing the active power losses, the reactive power exchange between the MV- and the LV-grid and the equipment loading, but in return, no active power is curtailed.

A. $Q(U)$-control

The $Q(U)$-controlled inverters inject or absorb reactive power in a wide voltage range, i.e. everywhere outside the configured dead band. During acceptable voltage conditions, the $Q(U)$-controlled inverters may unnecessarily inject/absorb reactive power and thus increase active power losses. In one of the investigated load/production-scenarios, this behaviour reduced the reactive power exchange between the MV- and the LV-grid. During overvoltage conditions at the feeders with distributed electricity production, the $Q(U)$-controlled inverters decrease their local voltages, but in many cases either to less or to much. Decreasing the voltages too less results in remaining violations of the upper voltage limitation; decreasing the voltages too much results in unnecessary high active power losses, Q-exchanges between the MV- and the LV-grid and equipment loadings. During undervoltage conditions, the $Q(U)$-controlled inverters increase their local voltages, but in many cases either to less or to much. Increasing the voltages too less results in remaining violations of the lower voltage limitation; increasing the voltages too much results in unnecessary high active power losses, Q-exchanges between the MV- and the LV-grid and equipment loadings. Figure 7.1 shows the spider chart of the $Q(U)$-control. While reducing the number of voltage
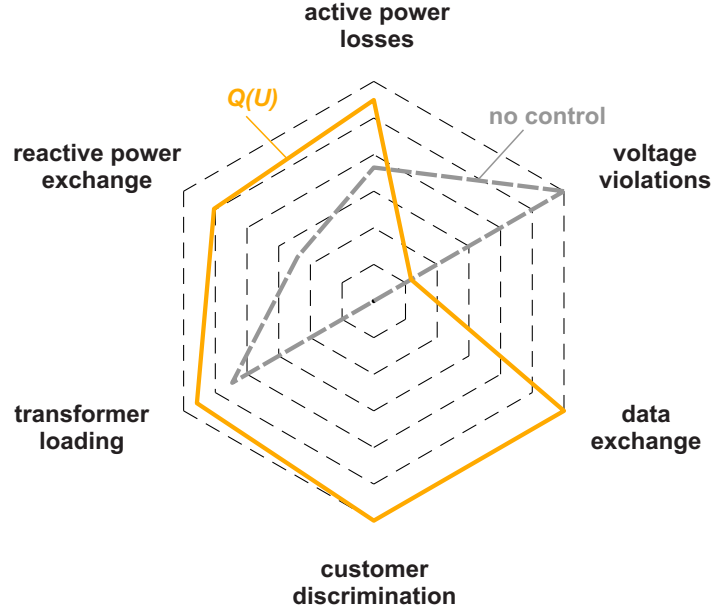
Figure 7.1.: Spider chart of the *Q(U)*-control

limit violations, the *Q(U)*-control causes large active power losses, reactive power exchanges between the MV- and the LV-grid and transformer loadings. Furthermore, the customers are discriminated and a data exchange between the customers and the DSO is required to enable a coordinated *Q*-control.

B. cosφ(P)-control

The $cos\varphi(P)$-controlled inverters absorb reactive power while injecting active power without considering the actual network situation (voltage). If the PV-arrays don't produce any active power, the $cos\varphi(P)$-controlled PV-inverters don't absorb any reactive power and thus don't increase the active power losses and the Q-exchange between the MV- and the LV-grid, but also don't alleviate lower voltage limit violations during undervoltage conditions. If the PV-arrays produce active power, the $cos\varphi(P)$-controlled PV-inverters absorb reactive power and thus increase the active power losses and the Q-exchange between the MV- and the LV-grid. During overvoltage conditions, the $cos\varphi(P)$-controlled inverters decrease their local voltages, but in many cases either to less or to much. Decreasing the voltages too less results in remaining violations of the upper voltage limitation; decreasing the voltages too much results in unnecessary high active power losses, Q-exchanges between the MV- and the LV-grid and equipment loadings. Figure 7.2 shows the spider chart of the $cos\varphi(P)$-control. While reducing the number of voltage limit violations, the $cos\varphi(P)$-control causes large active power losses, reactive power exchanges between the MV- and the LV-grid and transformer loadings. Furthermore, the customers are discriminated and a data exchange between the customers and the DSO is required to enable a coordinated Q-control.
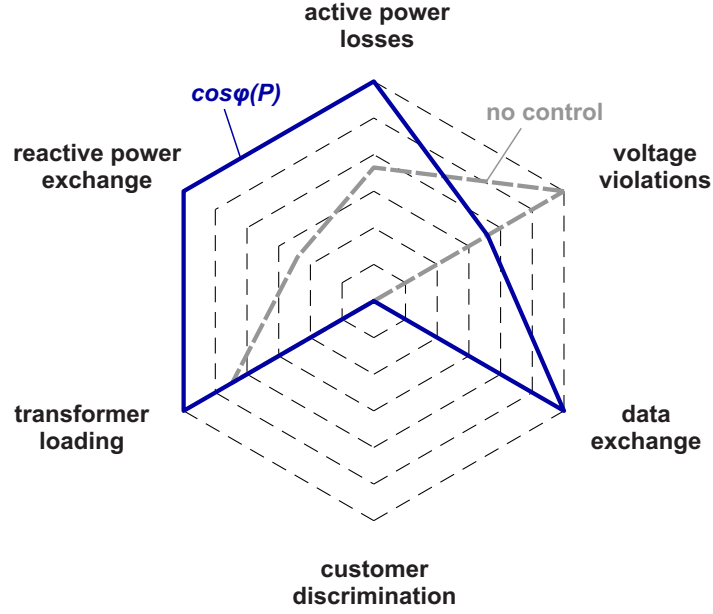
Figure 7.2.: Spider chart of the $cos\varphi(P)$-control

C. *L(U)*-control

The $L(U)$-controlled coils only absorb reactive power if their local voltages exceed the configured voltage set point and thus only increase the active power losses, the Q-exchange between the MV- and the LV-grid and the equipment loading during overvoltage conditions at the controlled feeders. If the control coils are sufficiently dimensioned they consume exactly the amount of reactive power which is required to maintain their local voltages, i.e. the voltages at the end of the feeders, at the configured voltage set point. During undervoltage conditions, the $L(U)$-control is not able to increase the voltages. Regarding the simulated scenarios with high distributed electricity production, the $L(U)$-control of a low voltage grid yields lower active power losses, a lower Q-exchange between the MV- and the LV-grid and lower equipment loadings than the $Q(U)$- and $cos\varphi(P)$-control of the P-injecting inverters does, while preventing upper voltage limit violations more reliably. Figure 7.3 shows the spider chart of the $L(U)$-control. While reducing the number
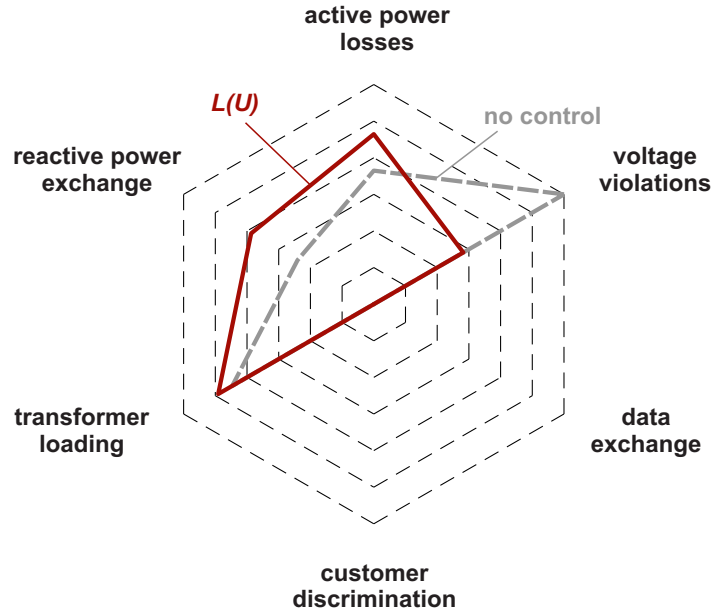
Figure 7.3.: Spider chart of the *L(U)*-control

of voltage limit violations, the $L(U)$-control causes some additional active power losses, reactive power exchanges between the MV- and the LV-grid and transformer loadings. The customers aren't discriminated and no data exchange between the customers and the DSO is required to enable a coordinated Q-control.

D. $L(U)$-control with Q-autarkic customers

Combining the $L(U)$-control with Q-autarkic customers improves the performance by reducing the voltage drop along feeders without distributed electricity production, the active power losses, the reactive power exchange between the MV- and the LV-grid and the equipment loading. During high distributed electricity production periods, the combination of $L(U)$-control and Q-autarkic customers results in slightly higher active power losses than a simple $L(U)$-control without Q-autarkic customers. Figure 7.3 shows the spider chart of the $L(U)$-control with Q-autarkic customers. While reducing the number of voltage limit
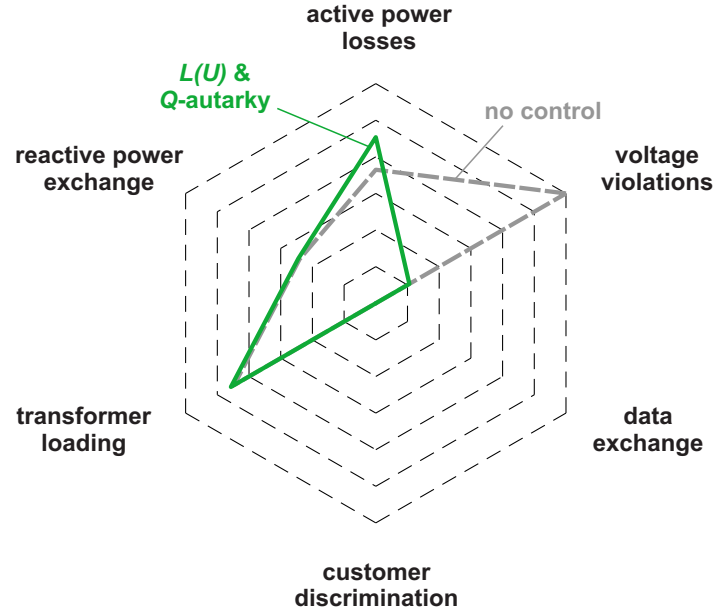
Figure 7.4.: Spider chart of the $L(U)$-control with Q-autarkic customers

violations, the $L(U)$-control with Q-autarkic customers causes some additional active power losses but does not substantially impact the reactive power exchanges between the MV- and the LV-grid and transformer loadings. The customers aren't discriminated and no data exchange between the customers and the DSO is required to enable a coordinated Q-control.

E. Overview of the investigated reactive power control strategies

Figure 7.5 shows the spider chart of all investigated control strategies. It can clearly be seen that the *L(U)*-
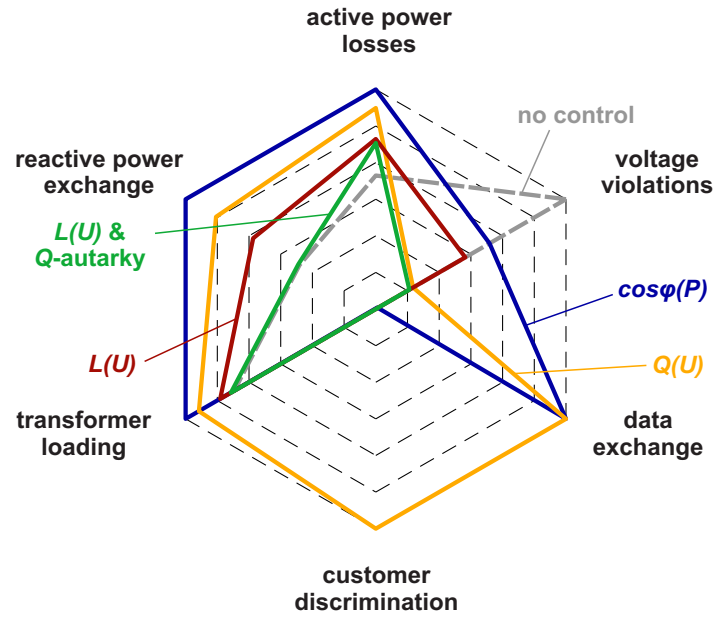
Figure 7.5.: Spider chart of all investigated control strategies

control with *Q*-autarkic customers shows the best performance for all defined evaluation criteria. Also the *L(U)*-control without *Q*-autarkic customers shows a better performance in average than the inverter controls, *Q(U)* and *cosφ(P)*. Only in case of lower voltage limit violations the *L(U)*-control is not able to improve the voltage profile, in contrast to the *Q(U)*-control. Compared to the *L(U)*-control strategies, the local inverter controls cause excessive active power losses, reactive power exchanges between the MV- and the LV-grid and transformer loadings, while a coordinated inverter control requires a data exchange between the customers and the DSO. Furthermore, the customers are discriminated with a local inverter control. The *cosφ(P)*-control may lead to lower voltage limit violations during high load/high production periods.

7.4. Impacts of the *L(U)*-control with and without *Q*-autarkic customers on the performances of realistic LV-grids

This section discusses the impacts of the *L(U)*-control on realistic low voltage grids based on the simulation results of the real Link-Grids. The simulations showed that the hosting capacities of the rural and urban low voltage grids are restricted by the voltage rise and the transformer loading and not by the thermal limits of the overhead lines and cables. A large potential to increase the urban and rural grids' hosting capacities without reinforcing the lines is available which can be exploited by using an appropriate reactive power based voltage control strategy. Less potential is available to increase the hosting capacity of the industrial grid, since due to the industrial customers' large reactive power demand the lines are almost fully loaded ($> 80\,\%$) for a distributed electricity production which leads to upper voltage violations.

The simulations with the urban and rural low voltage grids showed that the *L(U)*-control with a voltage set point at $1.09\,$p.u. manages to prevent upper voltage violations for all investigated PV-penetration scenarios. In the Industrial Link-Grid the *L(U)*-control with a voltage set point at $1.09\,$p.u. doesn't manage to prevent all voltage violations; the simulations of the maximum PV-penetration scenarios show that one network node still exceeds the upper voltage limitation. Furthermore, due to the small inductance between the distribution transformer and the control-coil (two parallel cables), a relatively large amount of reactive power has to be consumed by the coil to achieve a relatively low voltage reduction. For the simulated real Link-Grids, the control related *Q*-flows always increase the active power losses, the *Q*-exchange between the MV- and the LV-grid and the equipment loading.

Combining the *L(U)*-control with *Q*-autarkic customers improves the performance by reducing the reactive power exchange between the MV- and the LV-grid and the transformer loading in all simulated scenarios. The active power losses are slightly decreased during low and medium distributed electricity production periods and slightly increased during high distributed electricity production periods.

References

[1] *Commission renewable energy progress report*. European Commission. June 23, 2017. URL: http://eur-lex.europa.eu/legal-content/EN/TXT/PDF/?uri=CELEX:52017DC0057&qid=1488449105433&from=EN.

[2] *Enhancement of the network hosting capacity - clearing space for/with PV*. 25th European Photovoltaic Energy Conference and Exhibition / 5th World Conference on Photovoltaic Energy Conversion. Valencia, Spain, Sept. 2010.

[3] F. Marten et al. "Analysis of a reactive power exchange between distribution and transmission grids". In: *2013 IEEE International Workshop on Inteligent Energy Systems (IWIES)*. Nov. 2013, pp. 52–57. DOI: 10.1109/IWIES.2013.6698561.

[4] P. Schaefer et al. "Analysis of Strategies limiting the Reactive Power Flow between Power Distribution and Transmission Networks". In: *International ETG Congress 2015; Die Energiewende - Blueprints for the new energy age*. Nov. 2015, pp. 1–7.

[5] F. Katiraei and J. R. Aguero. "Solar PV Integration Challenges". In: *IEEE Power and Energy Magazine* 9.3 (May 2011), pp. 62–71. ISSN: 1540-7977. DOI: 10.1109/MPE.2011.940579.

[6] M. Zerva and M. Geidl. "Contribution of active distribution grids to the coordinated voltage control of the swiss transmission system". In: *2014 Power Systems Computation Conference*. Aug. 2014, pp. 1–8. DOI: 10.1109/PSCC.2014.7038467.

[7] *Cost-effective integration of photovoltaics in existing distribution grids: results and recommendations*. Apr. 14, 2017. URL: http://www.metapv.eu/sites/default/files/MetaPV_Final_Report_Results_and_Recommendations_FP.pdf.

[8] E. Demirok et al. "Local Reactive Power Control Methods for Overvoltage Prevention of Distributed Solar Inverters in Low-Voltage Grids". In: *IEEE Journal of Photovoltaics* 1.2 (Oct. 2011), pp. 174–182. ISSN: 2156-3381. DOI: 10.1109/JPHOTOV.2011.2174821.

[9] "Platz für 30 Gigawatt". In: *Photon magazin* (Feb. 2008).

[10] *Active Grid Integration of Distributed Generation utilizing existing infrastructure more efficiently*. 5th International Conference on the European Electricity Market. Lisbon, Portugal, May 2008.

[11] *Gesetz für den Ausbau erneuerbarer Energien (Erneuerbare-Energien-Gesetz - EEG 2017): § 12 Erweiterung der Netzkapazität*. URL: https://www.gesetze-im-internet.de/eeg_2014/__12.html (visited on 02/09/2017).

[12] A. Ilo. ""Link" - The smart grid paradigm for a secure decentralized operation architecture". In: *Electric Power Systems Research* 131 (2016), pp. 116–125.

[13] A. Ilo. "Effects of the Reactive Power Injection on the Grid—The Rise of the Volt/var Interaction Chain". In: *Smart Grid and Renewable Energy* 7 (2016), pp. 217–232. DOI: 10.4236/sgre.2016.77017.

[14] W. Gawlik. *Energieübertragung und Hochspannungstechnik*. ESEA - TU Wien, Sept. 29, 2014.

[15] K. Turitsyn et al. "Options for Control of Reactive Power by Distributed Photovoltaic Generators". In: *Proceedings of the IEEE* 99.6 (June 2011), pp. 1063–1073. ISSN: 0018-9219. DOI: 10.1109/JPROC.2011.2116750.

[16] *Benchmark Systems for Network Integration of Renewable and Distributed Energy Resources - Task Force C6.04.02*. May 15, 2013.

[17] *Technische und organisatorische Regeln für Betreiber und Benutzer von Netzen. Hauptabschnitt C: Technische Regeln für Netze mit Nennspannung < 110 kV*. 2009.

[18] *Harnessing PV inverter controls for increased hosting capacities of smart low voltage grids. Recent results from Austrian research and demonstration projects*. 4th Solar Integration Workshop. (Nov. 10, 2014).

[19] M. Rossi et al. "Analysis of active power curtailment strategies for renewable distributed generation". In: *2016 AEIT International Annual Conference (AEIT)*. Oct. 2016, pp. 1–6. DOI: 10.23919/AEIT.2016.7892744.

[20] E. Ghiani and F. Pilo. "Investigation on unintentional disconnection of photovoltaic plants in LV distribution networks". In: *2014 16th International Conference on Harmonics and Quality of Power (ICHQP)*. May 2014, pp. 39–43. DOI: 10.1109/ICHQP.2014.6842853.

[21] *Technische und organisatorische Regeln für Betreiber und Benutzer von Netzen. Hauptabschnitt D4: Parallelbetrieb von Erzeugungsanlagen mit Verteilernetzen*. July 1, 2016.

[22] A. Bokhari et al. "Experimental Determination of the ZIP Coefficients for Modern Residential, Commercial, and Industrial Loads". In: *IEEE Transactions on Power Delivery* 29.3 (June 2014), pp. 1372–1381. ISSN: 0885-8977. DOI: 10.1109/TPWRD.2013.2285096.

[23] URL: https://www.powersys-link.com/ (visited on 09/04/2017).

[24] *Statistik Austria*. Apr. 5, 2017. URL: http://www.statistik.at/web_de/statistiken/energie_umwelt_innovation_mobilitaet/energie_und_umwelt/energie/energieeinsatz_der_haushalte/022680.html.

List of Figures

List of Tables

Appendix

Busbar	$P_{f,n}^{(init,load)}$ [kW]	$Q_{f,n}^{(init,load)}$ [kvar]	Customer classification	Busbar	$P_{f,n}^{(init,load)}$ [kW]	$Q_{f,n}^{(init,load)}$ [kvar]	Customer classification
(1,1)	4.4720	1.4699	residential	(1,9)	4.0248	1.9493	commercial
(1,2)	7.0434	3.4113	industrial	(1,10)	5.0310	2.4367	industrial
(1,3)	4.0248	1.9493	industrial	(1,11)	40.2480	19.4930	industrial
(1,4)	4.0248	1.9493	industrial	(2,1)	11.1800	3.6747	residential
(1,5)	37.2294	18.0311	industrial	(2,2)	20.1240	9.7465	commercial
(1,6)	4.0248	1.9493	industrial	(2,3)	25.1550	12.1831	commercial
(1,7)	1.0062	0.4874	industrial	(2,4)	12.0744	5.8479	commercial
(1,8)	10.0620	4.8732	industrial	(3,1)	201.2400	97.4650	industrial

Table 7.1.: Minimum load scenario of the Industrial Link-Grid

Customer class	Sub class	Z_P	I_P	P_P	Z_Q	I_Q	P_Q
Residential	type A	1.31	-1.94	1.63	9.2	-15.27	7.07
	type B	0.96	-1.17	1.21	6.28	-10.16	4.88
	type C	1.18	-1.64	1.47	8.29	-13.67	6.38
Commercial	Drug store	0.27	-0.33	1.06	5.48	-9.7	5.22
	Restaurant	0.69	0.04	0.27	1.82	-2.24	1,43
	Laundromat	0.77	-0.84	1.07	8.09	-13.65	6.56
	Optics	0.55	0.24	0.21	0.55	-0.09	0.54
Industrial		1.21	-1.61	1.41	4.35	-7.08	3.72

Table 7.2.: ZIP coefficients of different load classes during summer period

Link-Grid	Sub class
Theoretical	type B
Large urban	type B
Small urban	type C
Rural	type B
Industrial	type A

Table 7.3.: Assignment of ZIP-coefficients to the residents connected to the individual network models

Node	ZIP model
(1,9)	drug store
(2,3)	restaurant
(2,4)	laundromat
(2,1)	optics

Table 7.4.: ZIP coefficients of the commercial customers in the Industrial Link-Grid

Control strategy	$u_{f,n}$	$P_{f,n}^{(pv)}/P_{f,n}^{(r,pv)}$	$P_{f,n}^{(inv)}/P_{f,n}^{(pv)}$	$\cos(\varphi)_{f,n}^{(inv)}$	$Q_{f,n}^{(inv)}/S_{f,n}^{(r,inv)}$
Uncontrolled **operation**	0.900	-	1	-	-
	1.100	-	1	-	-
	1.100	-	0	-	-
	1.150	-	0	-	-
P(U)	0.900	-	1	-	-
	1.074	-	1	-	-
	1.100	-	0	-	-
	1.150	-	0	-	-
cosφ(**P**)	-	0.0	-	1.0	-
	-	0.5	-	1.0	-
	-	1.0	-	0.9	-
Q(U)	0.900	-	-	-	0.4359
	0.955	-	-	-	0.4359
	0.985	-	-	-	0.0000
	1.015	-	-	-	0.0000
	1.045	-	-	-	-0.4395
	1.100	-	-	-	-0.4395

Table 7.5.: Inverter control characteristics

Short cut	A [mm²]	I_{th} [A]	R' [Ω/km]	X'_L [Ω/km]	C' [μF/km]	R'/X'_L
C-AL	25	100	1.2000	0.0890	0.550	13.48
	50	145	0.6410	0.0850	0.720	7.54
	95	215	0.3200	0.0820	0.950	3.90
	150	275	0.2060	0.0800	1.040	2.58
	240	360	0.1250	0.0800	1.200	1.56
C-CU	16	100	1.1500	0.0890	0.500	12.92
	25	130	0.7270	0.0880	0.550	8.26
	35	155	0.5240	0.0850	0.630	6.16
OL-AL	50	210	0.6152	0.3764	0.000	1.63
	95	320	0.3264	0.3557	0.000	0.92

Table 7.6.: Data of the cables and overhead lines within the network models

Link-Grid	$S^{(r,tr)}$ [kVA]	$U^{(r,tr,p)}$ [kV]	$U^{(r,tr,s)}$ [kV]	u_k [%]	u_r [%]	Vector group
Theoretical	160	20.00	0.40	4.04	1.00	Yzn5
Large Urban	630	20.00	0.40	4.00	1.00	Dyn5
Small Urban	400	21.00	0.42	3.70	1.00	Dyn5
Rural	160	20.00	0.40	4.04	1.00	Yzn5
Industrial	800	20.00	0.40	4.00	1.00	Dyn5

Table 7.7.: Data of the distribution transformers within the network models

Link-Grid	Feeder	$N_f^{(res)}$	$N_f^{(com)}$	$N_f^{(ind)}$	$P_f^{(r,pv)}$ [kW]	Cable share [% of km]	Max feeder length [km]
Theoretical	**C1**	20	-	-	100	100.00	1.630
	C2	20	-	-	0	100.00	1.630
	L1	20	-	-	100	0.00	1.630
	L2	20	-	-	0	0.00	1.630
Large Urban	**1**	35	-	-	18	77.68	0.740
	2	7	-	-	10	100.00	1.230
	3	26	-	-	89	100.00	0.380
	4	2	-	-	0	100.00	0.305
	5	17	-	-	31	100.00	0.505
	6	19	-	-	20	100.00	0.915
	7	17	-	-	0	93.19	0.767
	8	21	-	-	0	100.00	1.270
	9	31	-	-	0	100.00	0.640
Small Urban	**1**	26	-	-	12	51.92	0.485
	2	4	-	-	15	100.00	0.150
	3	18	-	-	5	100.00	0.435
	4	23	-	-	43	93.55	0.610
	5	7	-	-	16	100.00	0.265
	6	13	-	-	10	61.36	0.610
Rural	**1**	21	-	-	5	100.00	1.630
	2	22	-	-	15	31.23	0.880
	3	4	-	-	0	14.63	0.565
	4	14	-	-	0	32.76	0.690
Industrial	**1**	2	1	9	25	100.00	0.715
	2	5	3	0	5	100.00	0.220
	3	0	0	1	0	100.00	0.025

Table 7.8.: Feeder specific overview of the network models

Link-Grid	Scenario	Q_{L1} [kvar]	Q_{L1a} [kvar]	Q_{L1b} [kvar]	Q_{L2} [kvar]	Q_{L3} [kvar]	Q_{L4} [kvar]	Q_{L6} [kvar]	Q_{L7} [kvar]	Q_{L8a} [kvar]	Q_{L8b} [kvar]	Q_{L9} [kvar]
Large Urban	$L^{(min)} - G^{(min)}$	-	0	0	-	-	-	0	0	0	0	0
	$L^{(max)} - G^{(min)}$	-	0	0	-	-	-	0	0	0	0	0
	$L^{(min)} - G^{(mid)}$	-	0	0	-	-	-	0	0	0	0	0
	$L^{(max)} - G^{(mid)}$	-	0	0	-	-	-	0	0	0	0	0
	$L^{(min)} - G^{(max)}$	-	53.7	9.43	-	-	-	42.64	15.13	39.36	16.35	21.75
	$L^{(max)} - G^{(max)}$	-	8.88	0.34	-	-	-	9.64	0	20.49	2.35	0
Small Urban	$L^{(min)} - G^{(min)}$	-	0	0	-	0	0	0	-	-	-	-
	$L^{(max)} - G^{(min)}$	-	0	0	-	0	0	0	-	-	-	-
	$L^{(min)} - G^{(mid)}$	-	0	0	-	0	0	0	-	-	-	-
	$L^{(max)} - G^{(mid)}$	-	0	0	-	0	0	0	-	-	-	-
	$L^{(min)} - G^{(max)}$	-	16.35	35.93	-	32.75	62.03	3.77	-	-	-	-
	$L^{(max)} - G^{(max)}$	-	6.19	0	-	0	24.53	0	-	-	-	-
Rural	$L^{(min)} - G^{(min)}$	0	-	-	0	-	-	-	-	-	-	-
	$L^{(max)} - G^{(min)}$	0	-	-	0	-	-	-	-	-	-	-
	$L^{(min)} - G^{(mid)}$	16.12	-	-	0	-	-	-	-	-	-	-
	$L^{(max)} - G^{(mid)}$	0	-	-	0	-	-	-	-	-	-	-
	$L^{(min)} - G^{(max)}$	68.41	-	-	18.17	-	-	-	-	-	-	-
	$L^{(max)} - G^{(max)}$	48.64	-	-	7.32	-	-	-	-	-	-	-
Industrial	$L^{(min)} - G^{(min)}$	0	-	-	-	-	-	-	-	-	-	-
	$L^{(max)} - G^{(min)}$	0	-	-	-	-	-	-	-	-	-	-
	$L^{(min)} - G^{(mid)}$	0	-	-	-	-	-	-	-	-	-	-
	$L^{(max)} - G^{(mid)}$	0	-	-	-	-	-	-	-	-	-	-
	$L^{(min)} - G^{(max)}$	82.47	-	-	-	-	-	-	-	-	-	-
	$L^{(max)} - G^{(max)}$	54.62	-	-	-	-	-	-	-	-	-	-

Table 7.9.: Q-consumption of the control coils of the real Link-Grids with $L(U)$-controlled LV-Grid-Links and without any control on the CP-Grid-, CP-Producer-Link chain and without overvoltage protections

Link-Grid	Scenario	Q_{L1} [kvar]	Q_{L1a} [kvar]	Q_{L1b} [kvar]	Q_{L2} [kvar]	Q_{L3} [kvar]	Q_{L4} [kvar]	Q_{L6} [kvar]	Q_{L7} [kvar]	Q_{L8a} [kvar]	Q_{L8b} [kvar]	Q_{L9} [kvar]
Large Urban	$L^{(min)} - G^{(min)}$	-	0	0	-	-	-	0	0	0	0	0
	$L^{(max)} - G^{(min)}$	-	0	0	-	-	-	0	0	0	0	0
	$L^{(min)} - G^{(mid)}$	-	0	0.02	-	-	-	0	0	0	0	0
	$L^{(max)} - G^{(mid)}$	-	0	0	-	-	-	0	0	0	0	0
	$L^{(min)} - G^{(max)}$	-	65.02	12.48	-	-	-	51.17	23.85	43.64	20.64	30.83
	$L^{(max)} - G^{(max)}$	-	34.79	6.95	-	-	-	28.94	5.20	29.75	11.86	8.77
Small Urban	$L^{(min)} - G^{(min)}$	-	0	0	-	0	0	0	-	-	-	-
	$L^{(max)} - G^{(min)}$	-	0	0	-	0	0	0	-	-	-	-
	$L^{(min)} - G^{(mid)}$	-	0	0	-	0	0.06	0	-	-	-	-
	$L^{(max)} - G^{(mid)}$	-	0	0	-	0	0	0	-	-	-	-
	$L^{(min)} - G^{(max)}$	-	20.13	48.66	-	43.49	72.57	8.09	-	-	-	-
	$L^{(max)} - G^{(max)}$	-	14.64	23.02	-	22.17	47.76	3.34	-	-	-	-
Rural	$L^{(min)} - G^{(min)}$	0	-	-	0	-	-	-	-	-	-	-
	$L^{(max)} - G^{(min)}$	0	-	-	0	-	-	-	-	-	-	-
	$L^{(min)} - G^{(mid)}$	22.41	-	-	2.10	-	-	-	-	-	-	-
	$L^{(max)} - G^{(mid)}$	2.41	-	-	0	-	-	-	-	-	-	-
	$L^{(min)} - G^{(max)}$	73.73	-	-	23.01	-	-	-	-	-	-	-
	$L^{(max)} - G^{(max)}$	59.43	-	-	16.99	-	-	-	-	-	-	-
Industrial	$L^{(min)} - G^{(min)}$	0	-	-	-	-	-	-	-	-	-	-
	$L^{(max)} - G^{(min)}$	0	-	-	-	-	-	-	-	-	-	-
	$L^{(min)} - G^{(mid)}$	0	-	-	-	-	-	-	-	-	-	-
	$L^{(max)} - G^{(mid)}$	0	-	-	-	-	-	-	-	-	-	-
	$L^{(min)} - G^{(max)}$	157.51	-	-	-	-	-	-	-	-	-	-
	$L^{(max)} - G^{(max)}$	139.77	-	-	-	-	-	-	-	-	-	-

Table 7.10.: Q-consumption of the control coils of the real Link-Grids with $L(U)$-controlled LV-Grid-Links and Q-autarkic customers without overvoltage protections
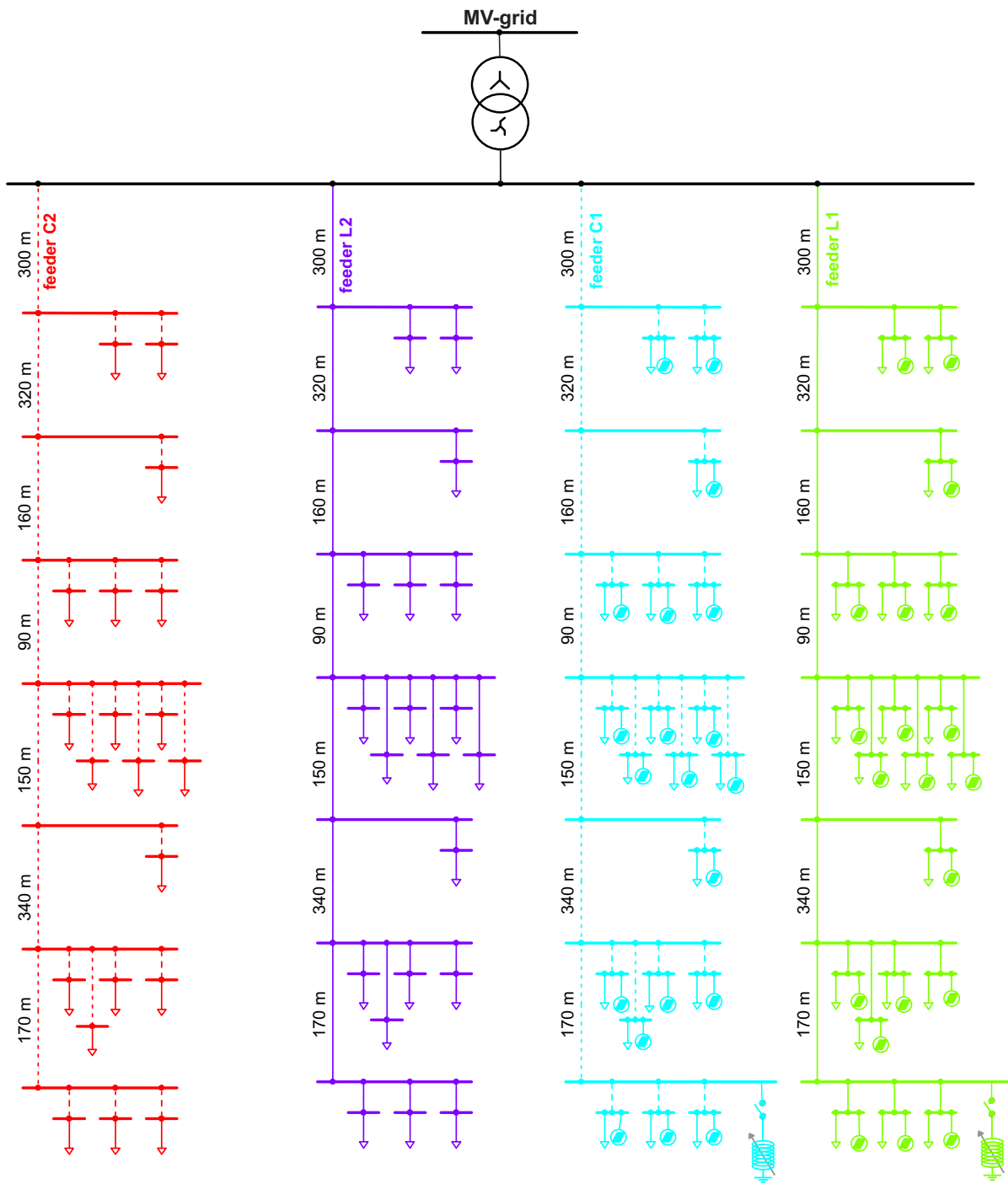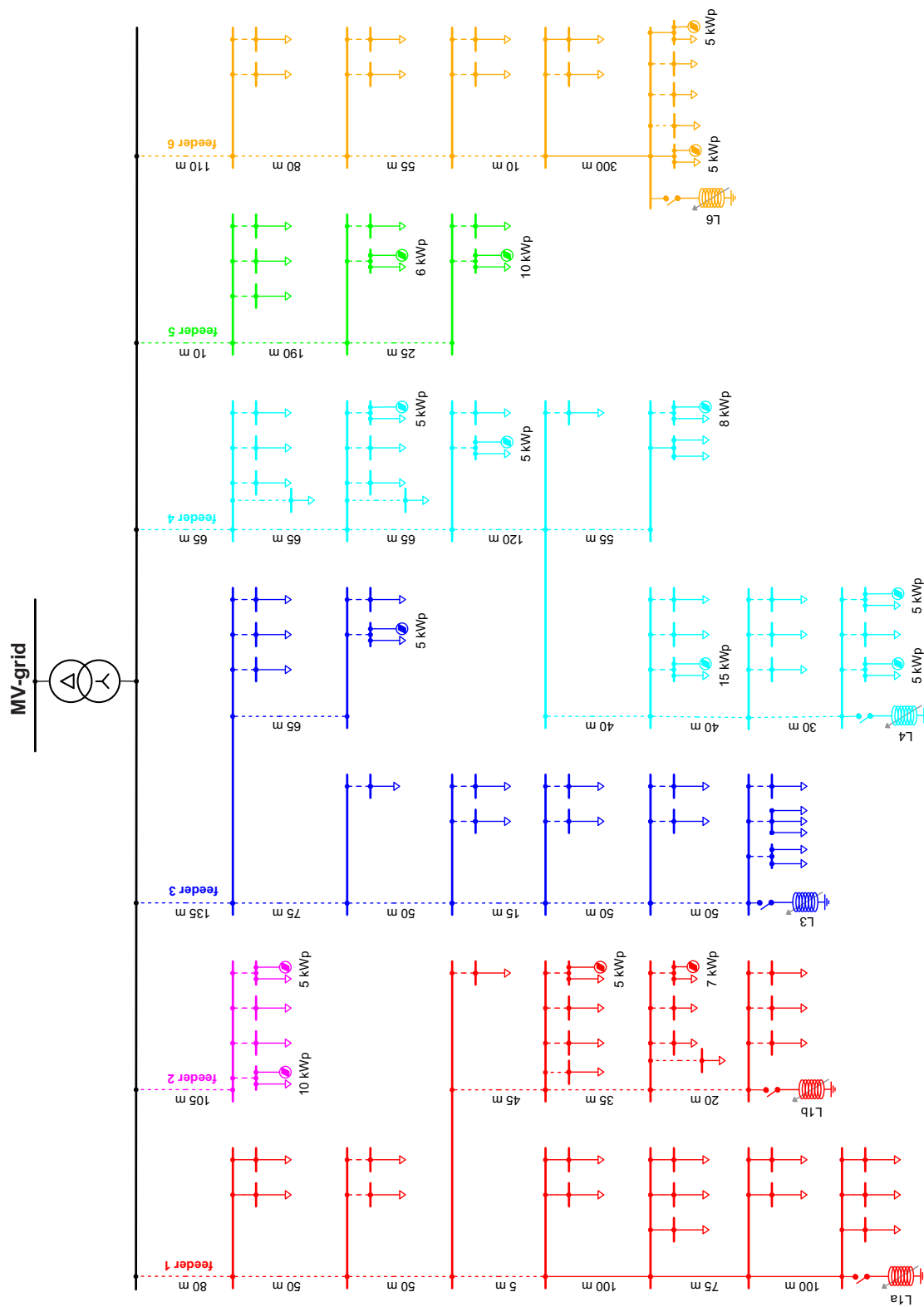
Figure 7.1.: Theoretical Link-Grid

116

Figure 7.2.: Large Urban Link-Grid
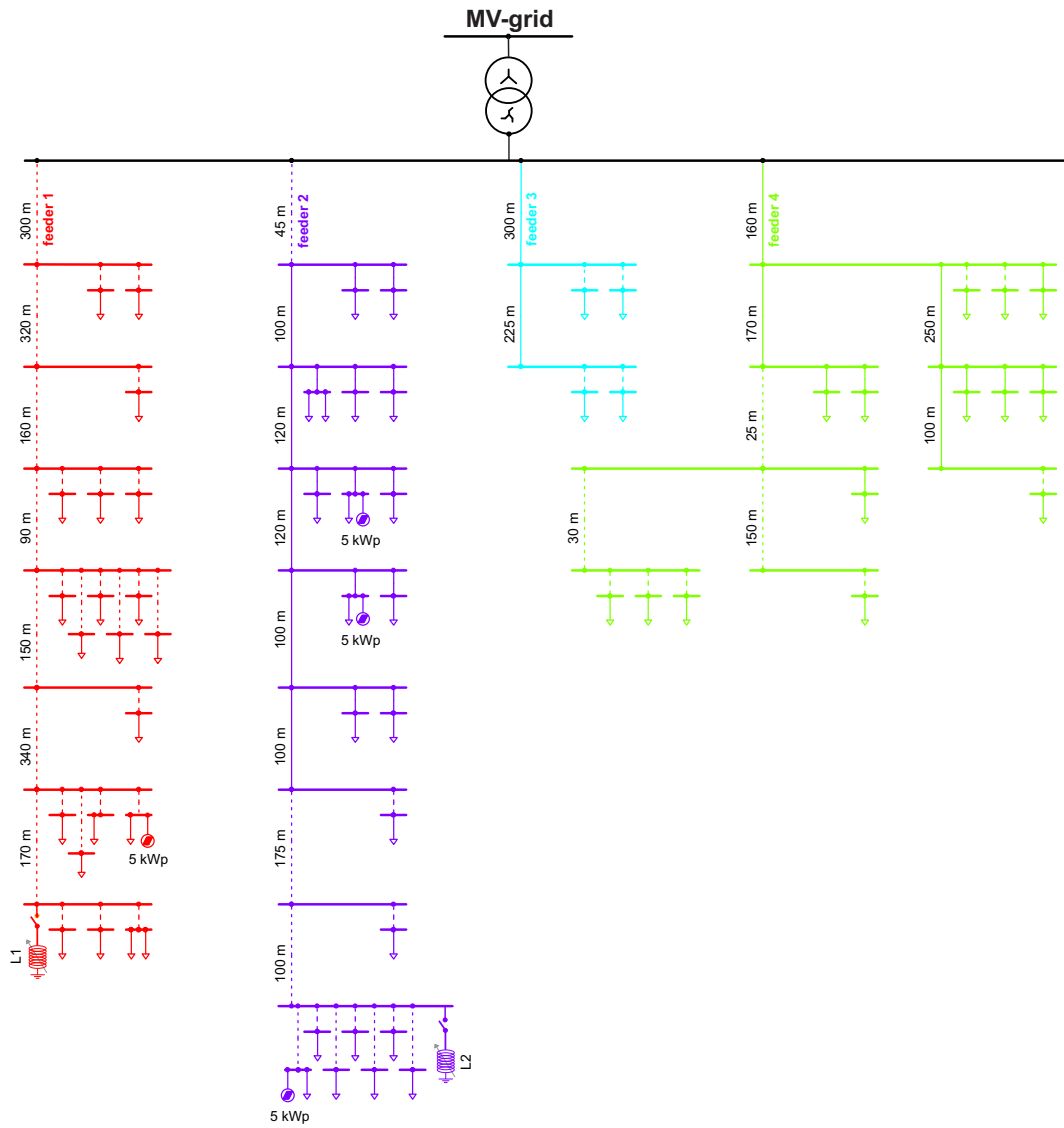
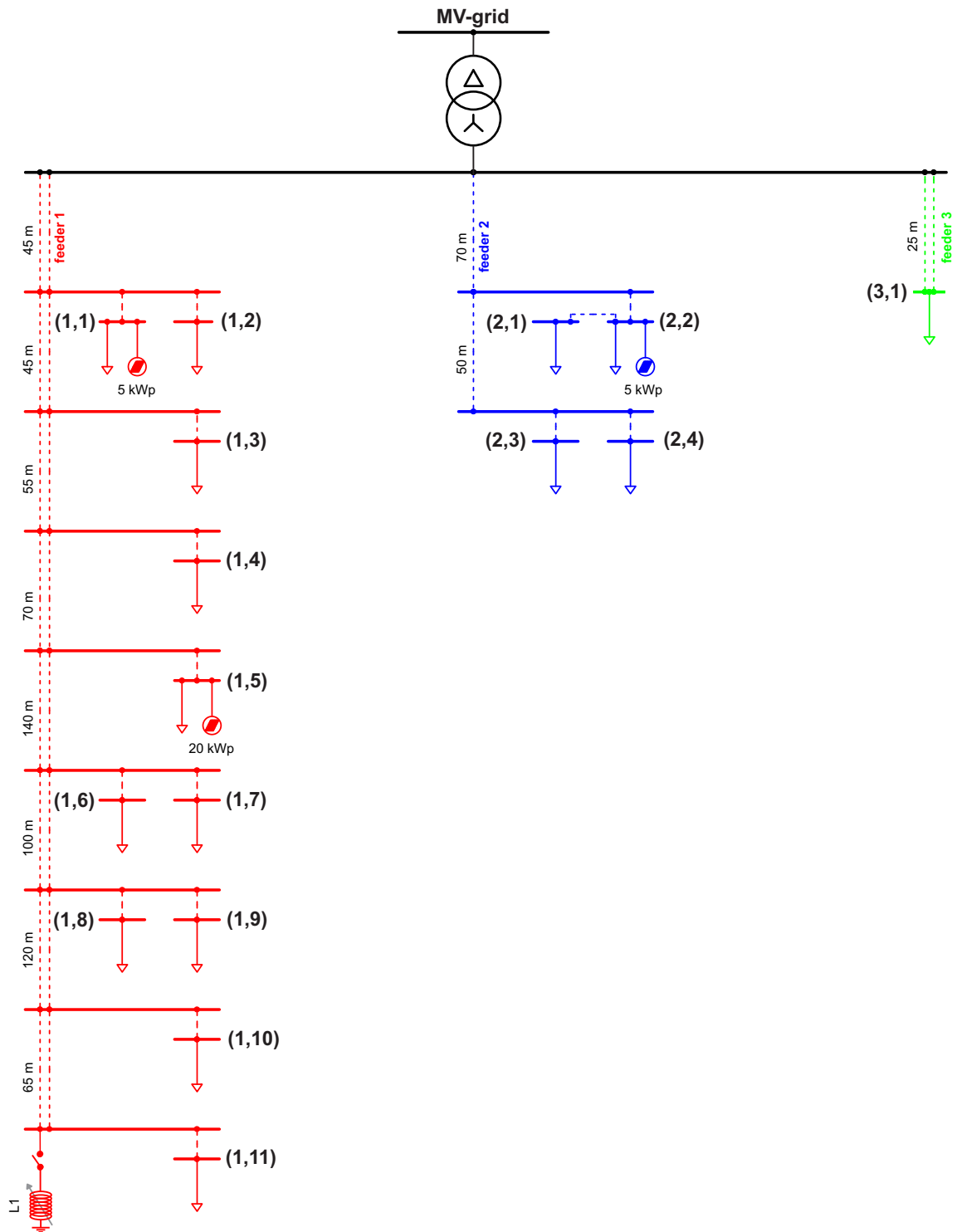Figure 7.3.: Small Urban Link-Grid

Figure 7.4.: Rural Link-Grid

Figure 7.5.: Industrial Link-Grid

120

Eidesstattliche Erklärung

Hiermit erkläre ich, dass die vorliegende Arbeit gemäß dem Code of Conduct – Regeln zur Sicherung guter wissenschaftlicher Praxis (in der aktuellen Fassung des jeweiligen Mitteilungsblattes der TU Wien), insbesondere ohne unzulässige Hilfe Dritter und ohne Benutzung anderer als der angegebenen Hilfsmittel, angefertigt wurde. Die aus anderen Quellen direkt oder indirekt übernommenen Daten und Konzepte sind unter Angabe der Quelle gekennzeichnet.

Die Arbeit wurde bisher weder im In– noch im Ausland in gleicher oder in ähnlicher Form in anderen Prüfungsverfahren vorgelegt.

Wien, im November 2017

_____
Daniel-Leon Schultis, BSc